

REPORT DOCUMENTATION PAGE

Form Approved
OMB No. 0704-0188

Public reporting burden for this collection of information is estimated to average 1 hour per response, including the time for reviewing instructions, reading appear data sources, generated, and maintaining the data needed, and completing and reviewing the collection of information. Send comments regarding this burden estimate or any other aspects of this collection of information, including suggestions for reducing this burden, to Washington Headquarters Services, Directorate of Information Operations and Reports, 1216 Jefferson Davis highway, Suite 1204, Arlington, VA 22202-4302, and to the Office of Management and Budget, Reduction Project (0704-0185), Washington, DC 20355

1. AGENCY USE ONLY (Leave Blank)		2. REPORT DATE 23 JUNE 00	3. REPORT TYPE AND DATES COVERED FINAL 06/18/97 - 06/30/00	
4. TITLE AND SUBTITLE Superhard Nanophase Cutter Materials for Rock Drilling Applications			5. FUNDING NUMBERS DE-FG02-96ER82154	
6. AUTHOR(S) Contributing authors: O. Voronov, G.Tompa, R. Sadangi, B. Kear, C. Wilson, P. Yan				
7. PERFORMING ORGANIZATION NAME(S) AND ADDRESS(ES) Diamond Materials Inc. 120 Centennial Ave. Piscataway, NJ 08854 V. (732) 885-0805 F. (732) 885-5910			8. PERFORMING ORGANIZATION REPORT NUMBER DMI-41018-FINAL	
9. SPONSORING/MONITORING AGENCY NAME(S) AND ADDRESS(ES) U.S. Department of Energy Paul Grabowski EE-12 Washington, DC 20585			10. SPONSORING/MONITORING AGENCY REPORT NUMBER	
11. SUPPLEMENTARY NOTES				
12a. DISTRIBUTION/AVAILABILITY STATEMENT See DoDD5230.24, "Distribution/Availability statements on Technical Documents"			12b. DISTRIBUTION CODE	
13. ABSTRACT (Maximum 200 words) The Low Pressure-High Temperature (LPHT) System has been developed for sintering of nanophase cutter and anvil materials. Microstructured and nanostructured cutters were sintered and studied for rock drilling applications. The WC/Co anvils were sintered and used for development of High Pressure-High Temperature (HPHT) Systems. Binderless diamond and superhard nanophase cutter materials were manufactured with help of HPHT Systems. The diamond materials were studied for rock machining and drilling applications. Binderless Polycrystalline Diamonds (BPCD) have high thermal stability and can be used in geothermal drilling of hard rock formations. Nanophase Polycrystalline Diamonds (NPCD) are under study in precision machining of optical lenses. Triphasic Diamond/Carbide/Metal Composites (TDCC) will be commercialized in drilling and machining applications.				
14. SUBJECT TERMS diamond ceramics, diamond compacts, high pressure, PCD, diamond, nanodiamond			15. NUMBER OF PAGES 96	
			16. PRICE CODE	
17. SECURITY CLASSIFICATION OF REPORT UNCLASSIFIED	18. SECURITY CLASSIFICATION OF THIS PAGE UNCLASSIFIED	19. SECURITY CLASSIFICATION OF ABSTRACT UNCLASSIFIED	20. LIMITATION OF ABSTRACT SAR	

DISCLAIMER

This report was prepared as an account of work sponsored by an agency of the United States Government. Neither the United States Government nor any agency thereof, nor any of their employees, makes any warranty, express or implied, or assumes any legal liability or responsibility for the accuracy, completeness, or usefulness of any information, apparatus, product, or process disclosed, or represents that its use would not infringe privately owned rights. Reference herein to any specific commercial product, process, or service by trade name, trademark, manufacturer, or otherwise does not necessarily constitute or imply its endorsement, recommendation, or favoring by the United States Government or any agency thereof. The views and opinions of authors expressed herein do not necessarily state or reflect those of the United States Government or any agency thereof.

DISCLAIMER

Portions of this document may be illegible in electronic image products. Images are produced from the best available original document.

1. Project Summary

The Low Pressure-High Temperature (LPHT) System has been developed for sintering of nanophase cutter and anvil materials. Microstructured and nanostructured cutters were sintered and studied for rock drilling applications. The WC/Co anvils were sintered and used for development of High Pressure-High Temperature (HPHT) Systems. Binderless diamond and superhard nanophase cutter materials were manufactured with help of HPHT Systems. The diamond materials were studied for rock machining and drilling applications. Binderless Polycrystalline Diamonds (BPCD) have high thermal stability and can be used in geothermal drilling of hard rock formations. Nanophase Polycrystalline Diamonds (NPCD) are under study in precision machining of optical lenses. Triphasic Diamond/Carbide/Metal Composites (TDCC) will be commercialized in drilling and machining applications.

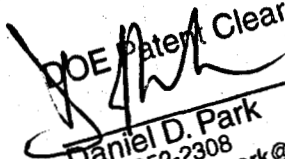

DOE Patent Clearance Granted
2/27/02
Date
Daniel D. Park
(630) 252-2308
E-mail: daniel.park@ch.doe.gov
Office of Intellectual Property Law
DOE Chicago Operations Office

TABLE OF CONTENTS

1. Project Summary	2
2.0 TABLE OF CONTENTS	3
3.0 Accomplishments of Phase II Objectives	4
3.1 Apparatus and methodology	6
3.2 Manufacturing of conventional and nanoscale WC/Co anvils	9
3.2.1 Raw materials selection	9
3.2.2 Characterization of the WC/Co sintered samples	15
3.2.3 WC/Co anvil design and fabrication	17
3.2.4 Concept of apparatus	30
3.3. Sintering of diamond ceramic	36
3.3.1 Sintering of diamond powder	37
3.3.2 Three different strategies for sintering of powders	37
3.4. Characterization of diamond powders and ceramics	39
3.5. Testing BPCD samples	56
3.5.1 Testing methodology	56
3.5.2 Testing results	59
3.6. Methods for BPCD and NPCD manufacturing	63
3.6.1 Principles of polycrystalline diamond materials manufacturing	63
3.6.2 Automation of BPCD and NPCD manufacturing	67
3.6.3 Requirements for pilot manufacturing and scale up methods for the fabrication of 8 - 13 mm diameter BPCD compacts	71
3.7 Design of diamond tool with BPCD and NPCD	72
3.7.1 Diamond cutter design	72
3.7.2 Diamond drill bits	73
3.8 The idea of a self-sharpening cutter	80
4.0 Phase III commercialization plan	85
5.0 References	87
6.0 Publications, reports and provisional patent applications during the project	88
7.0 Appendix	90

3.0 Accomplishments of Phase II Objectives

The main goal has been achieved through realization of the following specific technical objectives:

1. Improve density and fracture toughness of Binderless Polycrystalline Diamond (BPCD) by sintering at HPHT. We use nanograined WC/Co anvils to obtain pressures up to 15 GPa- *accomplished*; The WC/Co of different profiles have been sintered with help of Low Pressure High Temperature (LPHT) System. The reaction cell for 15 GPa has been developed. The set of BPCD has been sintered.
2. Further improve properties and performance of BPCD by reducing grain size down to nanoscale dimensions- *accomplished*; The nanophase diamonds (NPCD) with extremely small grain size down to ~1 nm were sintered from fullerene soot. The performance of NPCD is high in machining of Al-Si and Al-Si-C alloys. It is under study in machining of glass.
3. Develop cost-effective industrial methods for the fabrication of 8-13 mm diameter BPCD compacts- *accomplished*; this method was developed with help of prototype HPHT System and with application of 300-ton high rate semi-automated press. The samples of 1-6 mm diameter were manufactured. The designed automated HPHT System will use 3000-ton hydraulic press, DC Power Supply and Computerized Controller.
4. Develop cost-effective methods for brazing BPCD to WC/Co substrate and integrate into drag bit cutters of various designs- *accomplished*; Low Pressure-High Temperature Systems were developed for brazing of BPCD to WC/Co and other substrates. The samples were brazed by titanium alloys in argon and show no decrease of strength after cooling down.
5. Evaluate single cutter performances in granite turning and vertical lathe tests with detailed instrumentation to record cutter temperature and loading forces- *accomplished*; Single cutter performances were evaluated in granite machining with detailed instrumentation and recording of cutters temperatures and loading forces. This evaluation has been done for "sharp" cutters and for "dull" cutters. In addition the machining of hot granite logs (to 500°C) by diamond cutters were studied with good results.
6. Fabricate drill bits with multiple cutters and test their performance in hard rock drilling applications. Compare performance of BPCD with conventional PDC and TSP inserts- *accomplished*; The core drill bits performance with BPCD cutters of Ø1 mm, 2 mm and 3 mm were studied for medium and hard rocks on vertical lathe and in field. The samples of 1 and 2 mm sizes were produced from cylinders of Ø4 mm and Ø6 mm by laser cutting. The Ø3-mm samples were used as sintered. The

performance is high and steady for 1-mm pins. The performance of 3-mm cutters depends on bit design and decreases with "dulling" of cutters.

7. Develop detailed Phase III commercialization plan- *accomplished*; The Phase III commercialization plan was developed and submitted.
8. This document constitutes the final report, documenting the results of this effort.

3.1 Apparatus and methodology

3.1.1 Sintering Methods

The simplest and most efficient way to produce maximum stresses in the solid state is to use high pressure anvils. We used a design invented by V.P. Bridgeman early in the century, in which he used flat anvils and a cylindrical container that was modified and improved by H.T. Hall in the USA and by L.F. Vereshchagin in the USSR [1-3]. We used "profiled" anvils of WC/6%Co with Vickers hardness of 11 GPa and with cavity diameter of 15 mm. All supporting rings were made from 4340-H steel (which is the best for this purpose), hardened to $HR_c=46-58$. Figure 3.1-1 shows design and dimensions of the reaction cells used for sintering at high pressure high temperature conditions. A profiled container of plastic stone is located between the anvils. Polycrystalline Calcite (limestone or lithographic stone are the other names for this material) with a hardness of 3 on Mohs scale is good for this purpose. We achieved 9 GPa using a limestone container and 8 GPa using a steatite container (see Fig. 3.1-2). Steatite (or soapstone or lava stone) is a rock consisting almost wholly of polycrystalline talc, it is 1 on Mohs scale softer than lithographic stone.

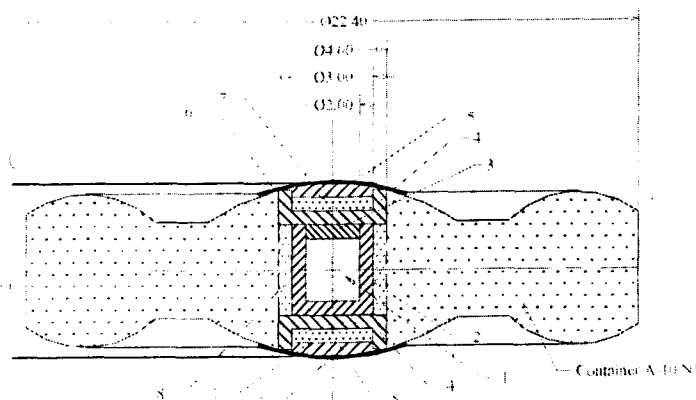


Figure 3.1-1. Reaction Cell A-10 for high pressure-high temperature sintering.

When the loading force is constant, the temperature increases, and the experiment occurs at a constant container volume of V_0 . The loading force F_0 may be described by:

$$F_0 = 2\pi \int_0^{r_0} P(r) r dr$$

where $P(r)$ is pressure in plastic stone (it is better to use tensor of stress instead of parameter P for correct calculations) and r_0 is radius of anvils. When the loading force is fixed, the temperature begins to increase. We used a Clifton model hydraulic press with maximum loading of 1000 tons to obtain F_0 . The transformations occur at constant volume V_k , where V_k is the volume of cavity at constant force F_0 . If the temperature changes and the phase transition takes place in a volume δV , which constitutes part of the container volume V_k , then the change in pressure is

$$\Delta P = \frac{1}{\alpha V} \int_V \left\{ \beta(\bar{r}) \Delta T(\bar{r}) - \frac{\Delta \rho(\bar{r})}{\rho(\bar{r})} \right\} \delta V$$

where $V_k = V + \delta V$, α is compressibility, β is thermal expansion, ρ is density, $\Delta\rho$ is change of density at the phase transformation, ΔT represents the temperature change as a function of position in the container. The calculation shows that ΔP is very large if $\Delta\rho/\rho \sim 1$. For HPHT technical understanding, it should be noted that: 1. $\Delta\rho/\rho \sim 0.29$ for transformation: compressed graphite-diamond; 2. $\Delta\rho/\rho \sim 0.78$ for transformation: compressed naphthalene-diamond. If $\Delta\rho/\rho > 1$, ΔP may have the value of P , which is the beginning of heating at 8 GPa and ending at ambient pressure. The initial "cold" pressure may be as high as 8 GPa, but the pressure at high temperatures may be as "low" as 0.0001 GPa.

Figure 3.1-2 represents the pressure calibration curves. We developed the processing regime for the High Pressure/High Temperature (HPHT) sintering that led to the formation of Binderless PCD (BPCD) and Nanograin PCD (NPCD) material. We conducted experiments on BPCD and NPCD sintering at a range of pressure/temperature conditions and exposure time.

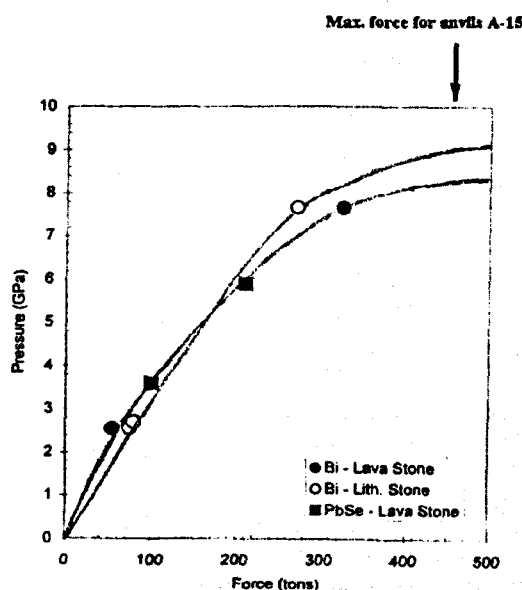


Figure 3.1-2. Cold pressure calibration. The anvils of WC6%Co with cavity diameter of 15 mm (A-15). Calibration is done by transitions in Bi and PbSe for two containers: calcite (lithographic stone) and talc (lava stone).



Figure 3.1-3. DMI's 300 ton press

Using the described techniques and equipment, we successfully produced an array of materials. DMI's unique High Pressure High Temperature systems are housed in the Department of Ceramic Engineering at Rutgers University and at DMI's facility in Piscataway, New Jersey. DMI operates the Rutgers facility under a CRADA between DMI and Rutgers. The principal equipment for obtaining high static pressure is an industrial-scale press with a loading force of 1000 tons. It weighs about 4 tons and has a working volume of 17in \times 17in \times 22in with a frame width and height of 48in. and 90in., respectively. DMI also acquired a project press with a loading force of 300 tons (see Figure 3.1-3). This press was designed according to DMI's specifications. It has a minimum of 10 sec. and maximum 24 hours of loading-unloading automatic production

cycle. It allows pilot scale Phase III production of new materials as well as quick turnaround experimentation needed for process optimization.

The high temperatures in the system are generated by resistively heating the reaction cell. We have installed two Hewlett Packard 6464C DC power supplies, each of which is capable of delivering 1000 amperes of current at 10 volts. These units need input power of three phase 208V and 60 A (per phase). The two power supplies may be used in either parallel or series mode depending on higher current or higher voltage requirements. We installed also Lambda EMI 10 kW DC power supply. The proprietary system described above allows DMI to reach "cold" pressures up to 80% of the Vickers Hardness of WC/Co materials that are used for anvils manufacturing. For conventional micrograin (3-7 μ m) powders of WC/Co-6% sintered anvils had HV=11.0 GPa. Thus, using this material, we can reach in our shaped anvils HPA cold pressures up to 9 GPa. Nanograined WC/Co10% with grain size 0.3-0.7 μ m will probably have HV=15GPa and thus will allow us to reach cold pressures up to 12 GPa using the same design of HPA.

3.1.2 Sintering regimes

Sintering of diamond material is accomplished at high pressure/high temperature. The pressure and temperatures achieved in high pressure cell should be sufficient for full transformation of carbon into polycrystalline diamond. In Figure 14 we show the Carbon phase diagram. Data in the 3000 to 5000 $^{\circ}$ C temperature range are not reliable. The line separating Graphite and Diamond phases indicate conditions at which Gibb's thermodynamic potentials of bulk forms of these phases of Carbon are equal. (Rossini and Jessup called them Free energies) This diagram is based on experimental and theoretical studies of Rossini and Jessup and theoretical calculations that extrapolated these results reported by Leipunski.

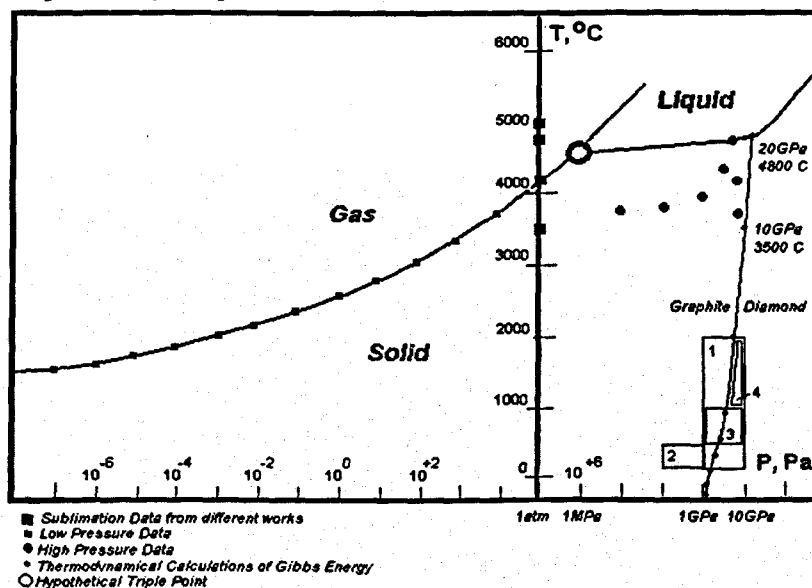


Figure 3.1-4. Carbon temperature-pressure state diagram

1. HPHT region where DMI is working at Present time;
2. HP impregnation;
3. Sintering of fullerene soot;
4. HPHT transformation of sintered fullerene soot into polycrystalline diamond in presence of Co, Fe, Ni.

When we talk about the P-T region of thermodynamic stability for diamond we consider the region in the diagram that is bound from the left by the curve indicating Graphite/Diamond thermodynamic equilibrium and from the top by the curve indicating melting conditions for carbon materials.

In the current study we transformed diamond powders and fullerene soot, into polycrystalline diamond at P-T conditions where diamond is thermodynamically stable. The experiments were conducted at 7 to 9 GPa pressures, 1000 to 2000°C temperatures, and using 10 to 100 sec exposure time to these conditions.

3.2 Manufacturing of conventional and nanoscale WC/Co anvils

DMI dedicated substantial time and resources to sintering WC/Co anvils. Sintering of high quality WC/Co anvils that allow high pressures in the reactor cell is the key to development of effective diamond sintering technology. Among all currently known materials, WC/Co has the best combination of high compressive strength and high hardness. In conventional sintering methods for PCD with metal binder the sintering pressures are in 5 to 7 GPa range. Since sintering of Binderless PCD requires higher pressures, the focus of our effort was development of WC/Co sintering methodology that will lead to production of anvils that are suitable for use for diamond sintering at reaction cell pressures higher than 7 GPa [specifically, with a goal of achieving 15GPa in this work].

3.2.1 Raw materials selection

We selected a number of micron and submicron grain size WC/Co powders to be used for sintering WC/Co anvils with 6-12% wt. of Co. The powders can be divided in three classes:

1. Nanograned WC/Co produced by chemical processing of precursor materials in a patented process by Nanodyne Inc.
2. Submicron grained WC/Co produced by super fine mechanical milling of conventional powder by a number of manufacturers.
3. Micron grained WC/Co produced by mechanical milling.

The Nanodyne material is produced in a chemical process where WC is chemically bound to cobalt [6]. The final step of WC/Co powder processing is spray drying, which result in powder consisting of hollow porous spheres 1 to 100 μm in diameter with wall thickens of 0.5 to 5 μm . The grain size of this material is typically smaller than 0.1 μm . The Nanodyne material has the smallest grain size for the WC/Co powders and has the highest potential for application as anvil material. However this material is not sold in the form useful for compaction of green bodies and processing of raw powders is a multi step process that generally required the following:

1. Mechanical grinding of hollow spheres;
2. Mixing with paraffin diluted in hexane (about 2% paraffin by weight of WC/Co is used);
3. Drying and granulation of the WC/Co-paraffin mixture;
4. Separation granulated particles by size.

Most of the samples were made from the Nanodyne powder and significant effort was dedicated to improvement of the described above processing steps. However in laboratory conditions dealing with small samples of material and having resource and time limitations it was difficult to optimize preprocessing of Nanodyne powders. Thus our results suffered from ambiguities of powder preprocessing.

In order to improve consistency in production of WC/Co anvils and focus on green body sintering and anvils fabrication we decided to use commercially produced submicron size WC/Co powders that are sold in sintering ready form. One of these powders were purchased from American National Carbide. It had grain size smaller than $0.8 \mu\text{m}$. This powder is formed by 0.3 to $0.5 \mu\text{m}$ particles that are pre-mixed with a plastificator. Use of ready to sinter powders significantly improved consistency of our sintering experiments.

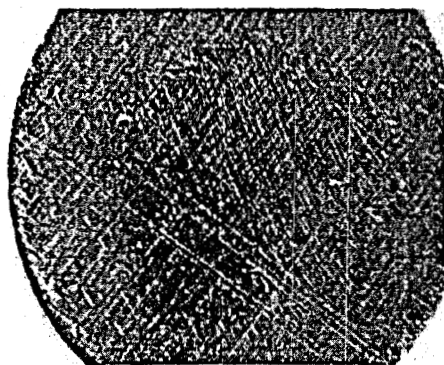


Figure 3.2-1. Fully dense WC/Co cylindrical sample produced from nanograined WC/Co powder.

We designed and fabricated a number of custom dies that allowed sintering cylindrical 4 to 50 mm diameter green bodies of WC/Co/wax with various height. The green bodies were made at pressures of 0.5 to 500 MPa. Green bodies were made using a 10 ton manual press, and pressure was measured using a set of pressure and force gauges. The sintering ready powder that contains about 2% paraffin (wax) will have apparent density of 3.85 g/cc .

We have determined that by using 50 MPa pressure we could form green bodies that can be sintered into fully dense

WC/Co samples with $\rho = 14 \text{ g/cc}$. A sample of fully dense WC/Co cylinder made from nanoscale WC/Co powder is shown in Figure 3.2-1.

Two vacuum chambers were used for the sample sintering. A miniature vacuum chamber shown in Figure 3.2-2 allowed sintering of a single small samples that were usually dewaxed in a separate chamber. The large vacuum chamber shown in Figure 3.2-3 allowed sintering at temperatures of Co liquid phase. This chamber is equipped with nine MoSi_2 heaters and argon source it is also equipped with graphite heaters. We have sintered WC/Co samples in argon atmosphere at 1.5 to 15 psi pressure. The large vacuum chamber allowed concurrent sintering of large number of samples and it has a working cycle of 12 hours. Dewaxing and sintering was conducted in either in one cycle or in two cycles.

Figure 3.2-4 shows a sintering diagram where dewaxing and sintering are accomplished in one cycle. A segment of heating at constant 400 C temperature corresponds to dewaxing stage.

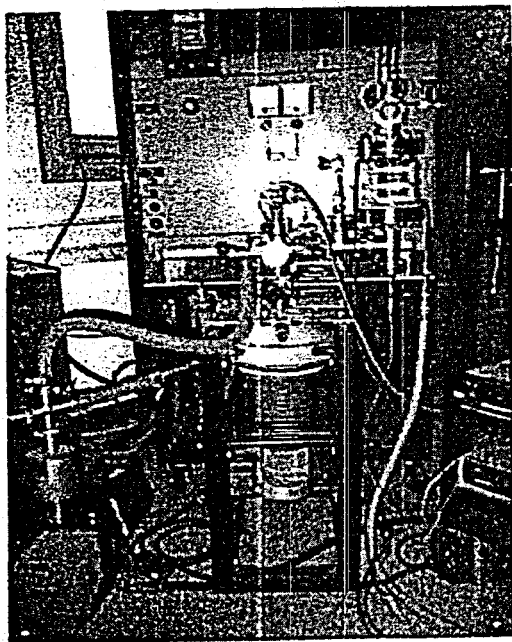


Figure 3.2-2. Miniature vacuum chamber used for small samples sintering

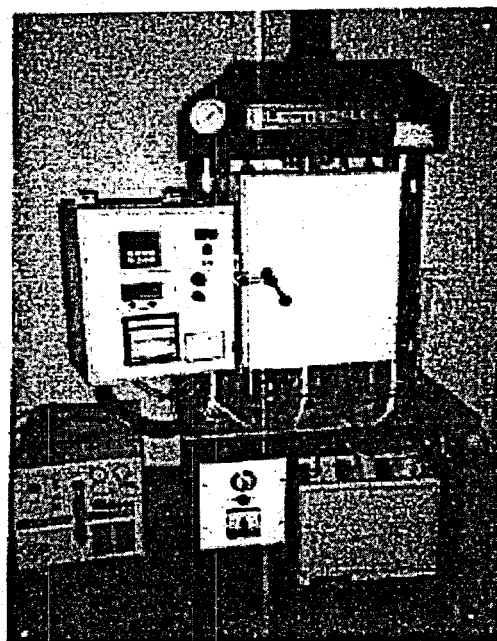


Figure 3.2-3. Large vacuum chamber used for anvils sintering

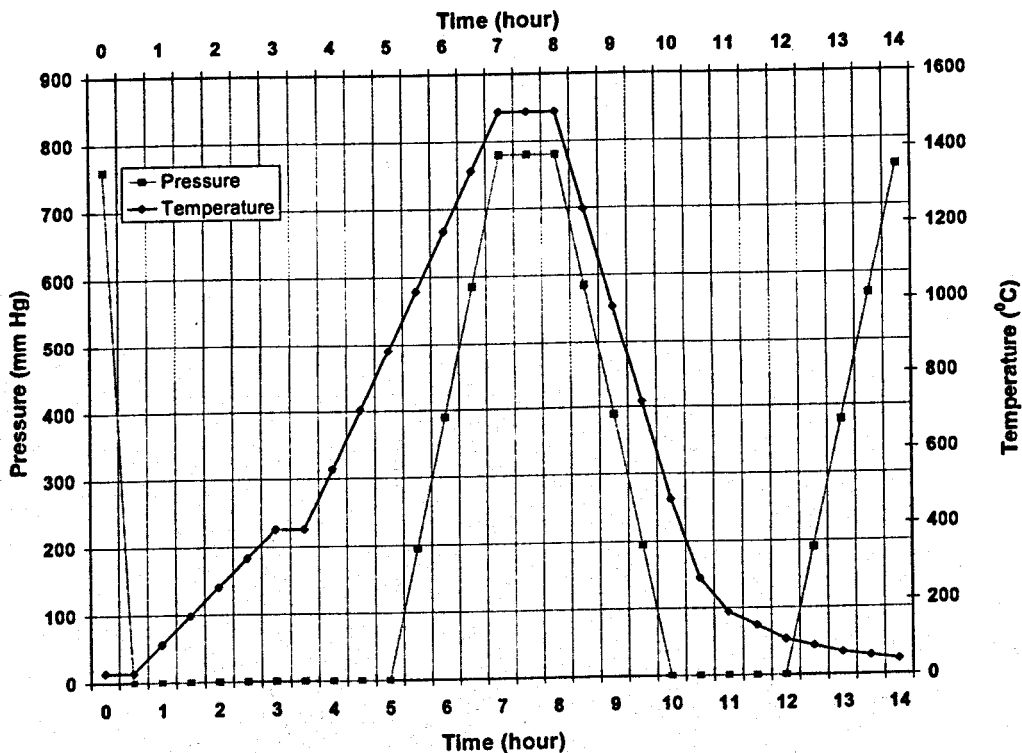


Figure 3.2-4. Typical diagram for one cycle dewaxing and sintering of WC/Co.

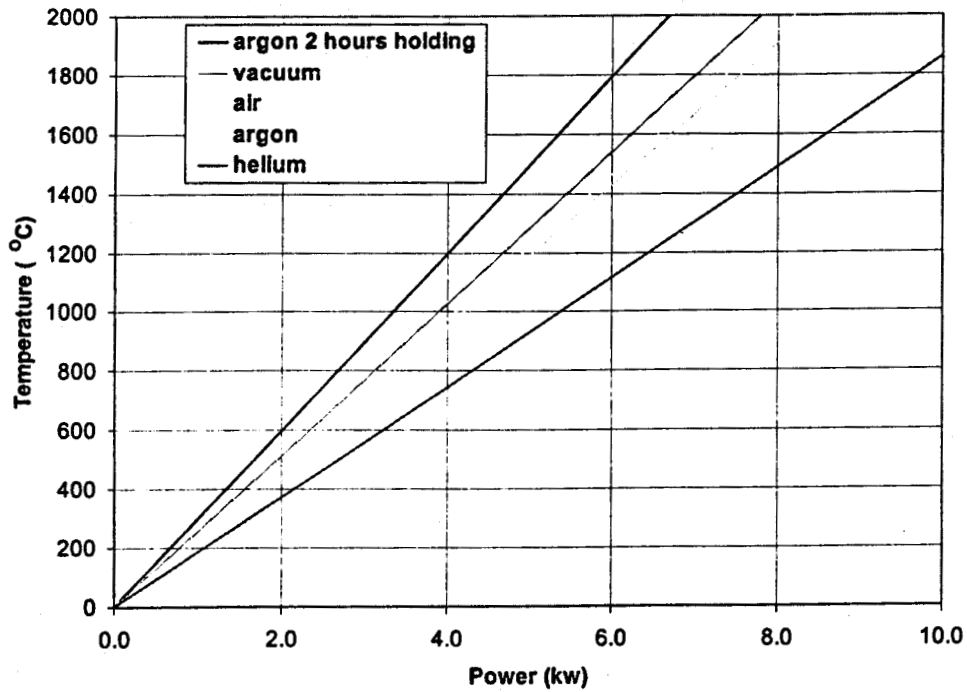


Figure 3.2-5a. Chamber temperature (estimated) as a function of power supply for vacuum, air, argon, and helium atmospheres (for MoSi₂ heating elements and alumina insulation).

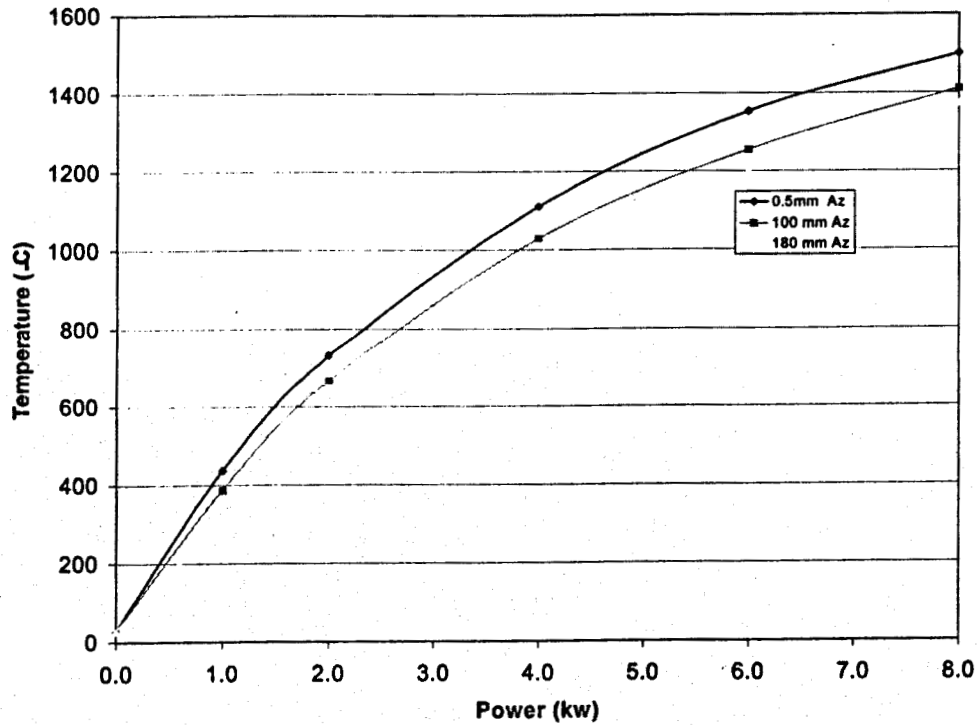


Figure 3.2-5b. Chamber temperature as a function of power, in argon, graphite ceramic heating elements and carbon insulation.

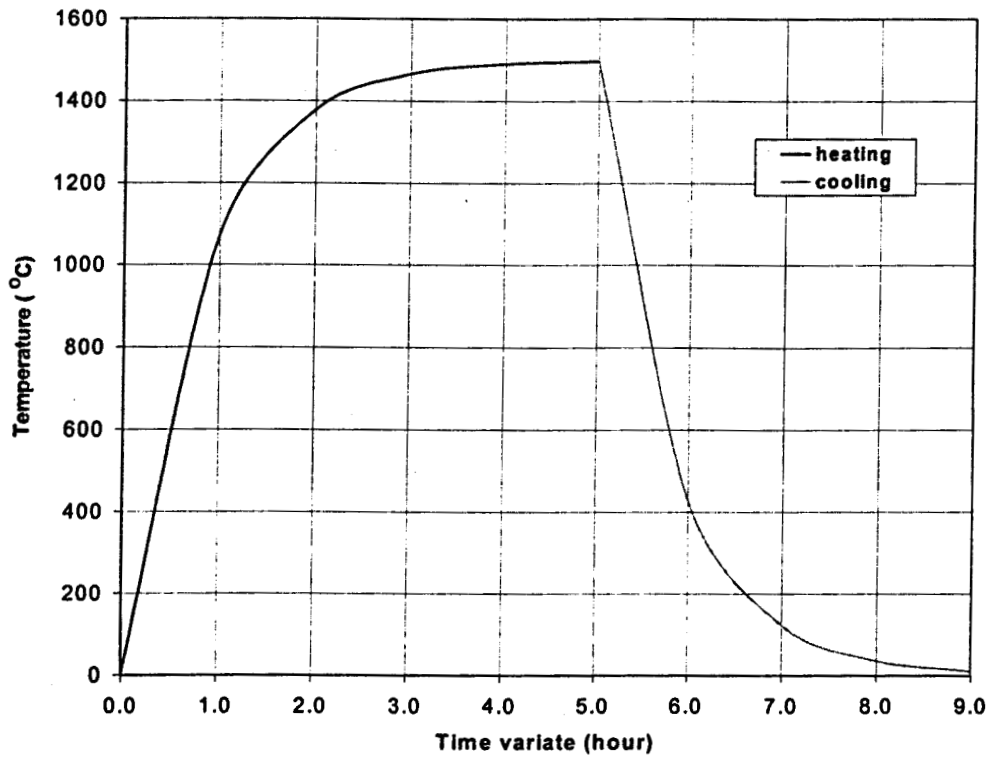


Figure 3.2-6a. Dynamics of vacuum chamber heating with MoSi₂ heating elements and alumina insulation at constant power supply (estimated by function).

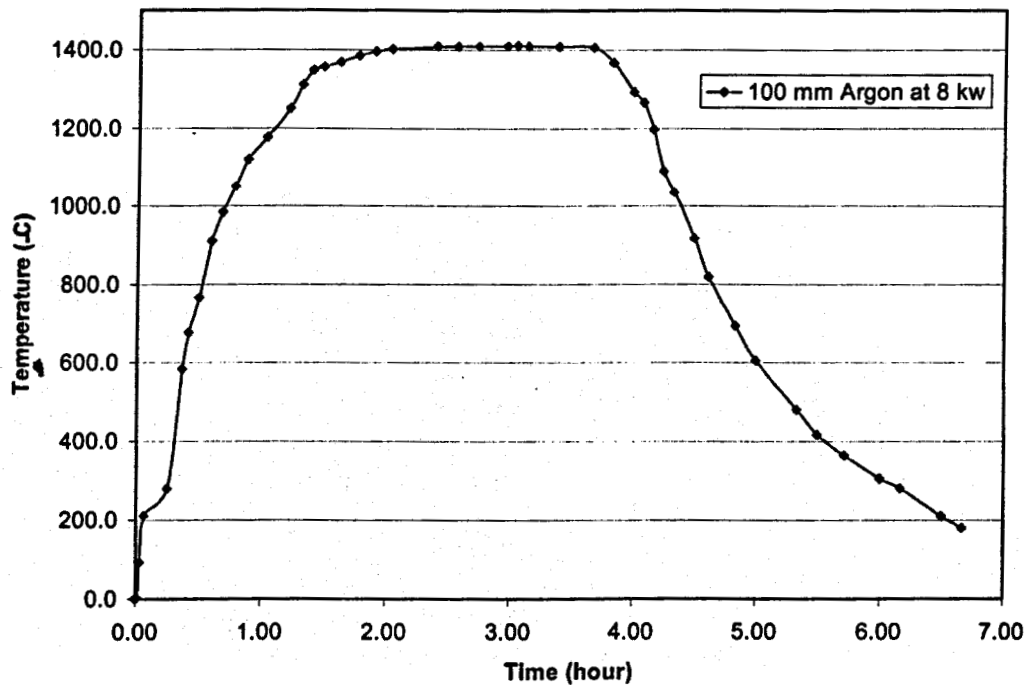


Fig. 3.2-6b. Dynamics of argon chamber with graphite ceramic heaters and carbon insulation.

The described method of WC/Co anvils sintering allowed full control over green body pressing and sintering conditions.

Figure 3.2-5 shows temperature in chamber as a function of power supply to the vacuum chamber in cases of processing in vacuum, air, argon, and helium. Figure 3.2-6 shows temperature as function of time for heating at constant power supply. The functions shown in Figures 3.2-5 and 3.2-6 illustrate the dynamic response of the vacuum chamber to power supply that should be taken into account while designing processing regimes for sample sintering.

Figure 3.2-7 illustrates steps involved in sintering of WC/Co anvils starting with milling of WC/Co materials and ending in grinding of the sintered samples to obtain required profiles and surface finish.

WC/Co ANVILS AND INSERTS PRODUCTION

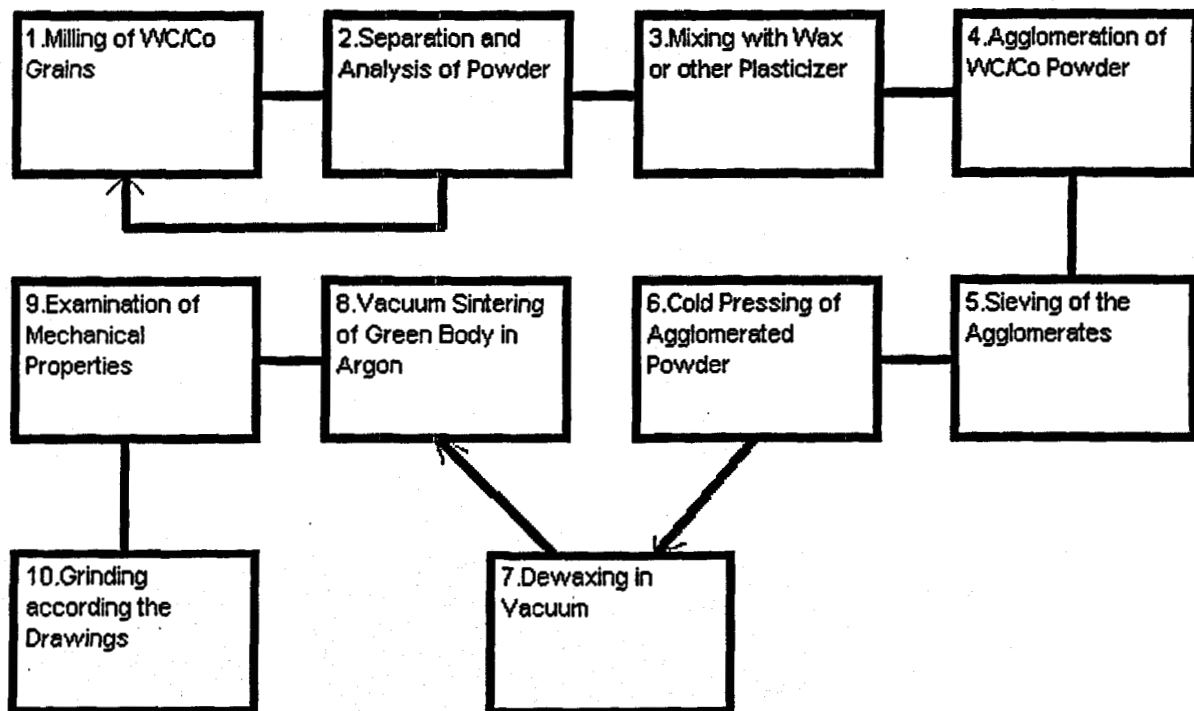


Figure 3.2-7. Stages of WC/Co parts manufacturing.

3.2.2 Characterization of the WC/Co sintered samples

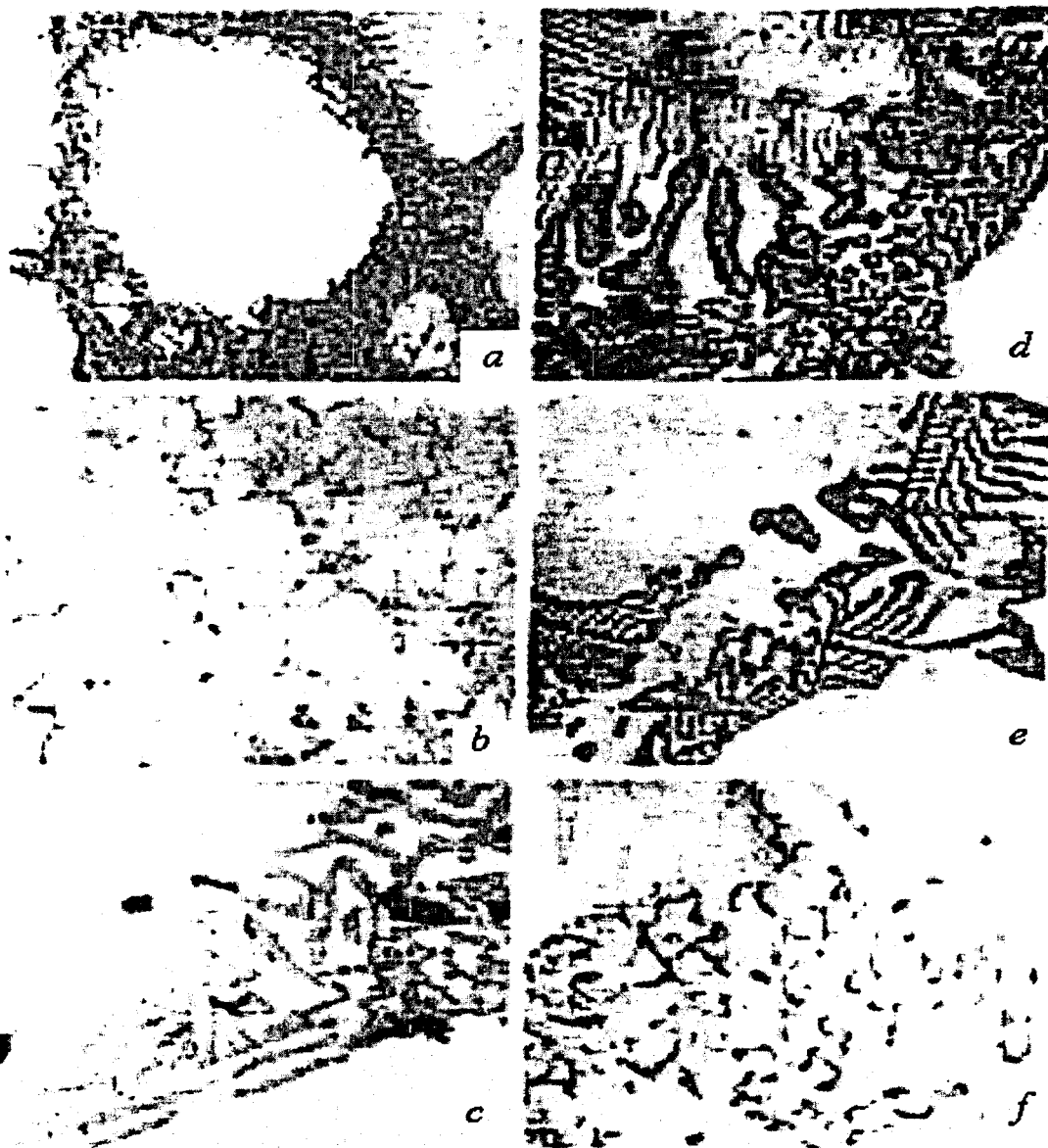


Figure 3.2-8. Structure of the WC/Co eutectic formations.

- a- stable eutectic WC+ γ surrounding by γ , x400
- b- stable eutectic WC+ γ +C, x100
- c- the same like b but with x1500
- d- stable eutectic WC+ γ + η_1 , x1500
- e- stable eutectic γ + η_1 between γ , x1500
- f- metastable eutectic γ + η_1 +C, x1500.

Synthesis of WC/Co composite can be analyzed using Co-WC phase diagram in cross-section. However more often in cases of excess or deficiency of carbon it is useful to analyze the W-C-Co system. The composite system will have metastable form of cobalt carbides Co_2C and Co_3C , and solid solution of carbon in cobalt that has a melting point of 1300 C. The W-C system can form two carbides WC and W_2C . Hexagonal phase of α -WC is stable up to temperatures of 2525 C at which point β -WC can form which has face centered cubic lattice. WC is soluble in cobalt and can form eutectic mixtures. The solid mixture of W and C in cobalt is responsible for most of the exceptional properties of WC/Co. When system has excess of carbon, crystallization can follow the standard path with formation of γ -phase, WC and graphite or following a metastable path with participation of γ and η phases and graphite. The triple eutectics of $\gamma + \text{WC} + \text{graphite}$ will melt at 1298 C and WC/Co composite will form at 1350 – 1450 C at 0.1 to 100 MPa pressure. Behavior and formation of the WC/Co system at high pressures is not well studied. In Figure 3.2-8 we show the structure of the eutectic formations. Table 3.2-1 shows how some key characteristics of the composite material that are changing as function of cobalt concentration and grain size.

Table 3.2-1 Properties of WC/Co composite as function of Co concentration and grain size.

Composition, %wt.		Physical Properties					Mechanical Properties							
WC	Co	Grain size of WC	Coercive force, oersted	Resistivity, micro ohm ² cm	Thermal expansion, at 20-800°C $\times 10^6$ degree ⁻¹	Thermal conductivity, cal/cm ² sec ⁰ C	Density, g/cm ³	Tensile strength kg/mm ² after grinding by dia mond wheel	Bending strength kg/mm ² after grinding by dia mond wheel	Comp resive strength kg/mm ² after grinding by dia mond wheel	Hardness		Modu lus of elasti city	Impact streng th, kg ^m /cm ²
											HRA	HV kg/mm ²		
97	3	1 1-2	250-280	19,3	4,10	—	15,0-15,3	—	130	473	91,0	1650	66,0	0,16
			170-200	19,0	—	0,12	15,0-15,3	59	140	427	89,0	1350	65,5	0,15
96	4	2-3 2-5	140-180	19,3	4,70	0,12	14,9-15,1	—	—	436	—	1360	65,0	0,16
			60-90	18,8	4,40	—	14,9-15,1	—	—	411	88,0	1160	65,0	0,20
94	6	1 1-2 2-5	200-250	23,4	4,40	0,16	14,8-15,1	—	150	491	90,0	1430	64,5	0,26
			130-160	19,2	4,90	0,15	14,6-15,0	73	165	439	88,5	1310	64,0	0,21
			75-100	18,8	4,70	0,13	14,6-15,0	—	—	368	87,5	1100	63,5	0,27
92	8	1-2 2-5	120-160	18,6	5,10	0,12	14,4-14,8	79	175	421	87,5	1240	61,0	0,30
			50-70	18,0	4,80	0,11	14,4-14,8	—	185	347	86,5	1050	60,0	0,35
90	10	1-2	80-100	18,4	5,20	0,13	14,2-14,6	110	195	412	87,0	1160	58,5	0,35
85	15	1-2	80-90	19,4	6,00	0,16	13,9-14,1	134	200	365	86,0	1040	57,0	0,38
80	20	1-2	75-90	19,5	5,70	0,10	13,4-13,7	140	220	340	84,5	950	49,0	0,48
75	25	1-2	60-80	—	—	0,09	12,9-13,2	145	250	303	83,0	900	48,0	0,51

From the above given description one can conclude that formation of the WC/Co is a very complex process, and accurate characterization of material sintered at different condition presents a very labor intensive task. Since the main task of our study was to establish conditions that will allow us to obtain high quality WC/Co anvils suitable for applications in BPCD production we limited characterization to measurement of the most fundamental properties such as hardness and sample density.

We measured hardness of the samples on Mohs, Rockwell, and Vickers scales. In Table 3.2-2 hardness and density results are given for samples sintered from nano and micrograined WC/Co powders.

Table 3.2-2. Hardness, density and fracture strength in compression for samples of ϕ 10 mm.

#	Area (cm ²)	Diameter (cm)	Height (cm)	Volume (cm ³)	Mass (g)	Density (g/cm ³)	Compression force (kg)	Fracture strength σ_f (kg/cm ²)	Hardness* (g/mm ²)
1	0.673	0.926	0.473	0.318	4.530	14.236	0		
2	0.676	0.928	0.478	0.323	4.604	14.254	0		
3	0.680	0.931	0.476	0.324	4.600	14.211	33.566	49.360	
4	0.673	0.926	0.470	0.316	4.498	14.242	27.869	41.467	
5	0.674	0.927	0.465	0.313	4.480	14.292	33.793	50.123	
A	0.675	0.927	0.472	0.319	4.543	14.247	31.751	47.014	1616
A is Average. The Argon pressure for this group of samples is 780 mmHg									
1	0.684	0.933	0.468	0.320	4.533	14.168	29.484	43.125	
2	0.676	0.928	0.484	0.327	4.683	14.321	34.019	50.297	
3	0.673	0.926	0.473	0.319	4.548	14.277	32.659	48.494	
4	0.673	0.926	0.480	0.323	4.599	14.228	29.484	43.779	
5	0.678	0.929	0.475	0.322	4.582	14.247	34.246	50.523	
A	0.677	0.928	0.476	0.322	4.589	14.248	31.978	47.238	1607
A is Average. The Argon pressure for this group of samples is 100 mmHg									
1	0.672	0.925	0.473	0.318	4.503	14.166	26.535	39.486	
2	0.667	0.922	0.477	0.318	4.549	14.300	32.432	48.629	
3	0.673	0.926	0.473	0.319	4.563	14.323	32.659	48.494	
4	0.676	0.928	0.477	0.323	4.590	14.226	29.484	43.591	
5	0.668	0.923	0.474	0.317	4.530	14.300	34.246	51.238	
A	0.671	0.925	0.475	0.319	4.547	14.263	31.071	46.276	1554
A is Average. The Argon pressure for this group of samples is 0.5 mmHg									
*Hardness is the average of the hardness of the medium samples for the same batch under loads of 300, 500, 1000, 2000 (g)									

3.2.3 WC/Co Anvils Design and Fabrication

Working volume (volume of the sintered sample) of the High Pressure Apparatus (HPA) is a function of the pressures and temperatures that one aims to achieve and the loading force produced by the press. In Figure 3.2-8. we show an example of working volume of the HPA as a function of pressure for three temperatures 300 K, 1000 K, and 2000 K. Also in this figure we indicate the initial working volumes for A-10, A-15, A-35, and A-50 anvils. A set of A-25 anvils was sintered for our new 300 tons press HPHT system. For the Phase I and Phase II research we have designed two type of anvils A-15 and A-10.

Their cross sections are shown in Figure 3.2-10. The design of the supporting rings (steel), and WC/Co inserts and supports allows use of these two different anvils without a change in the High Pressure / High Temperature (HPHT) assembly A-15 anvils, made from micrograined WC/Co, can be used for mass production of 0.5 to 2.0 carats of BPCD diamond compacts at 8-9 GPa pressures and 1500 -2000 °C temperatures. These anvils can be used to produce pressures up to 10 GPa in

experimental studies. A-10 anvils are designed for pressures in the 10-15 GPa range that reached using anvils made from n-WC/Co. It should be noted here that anvils with larger working volume will require a new support assembly.

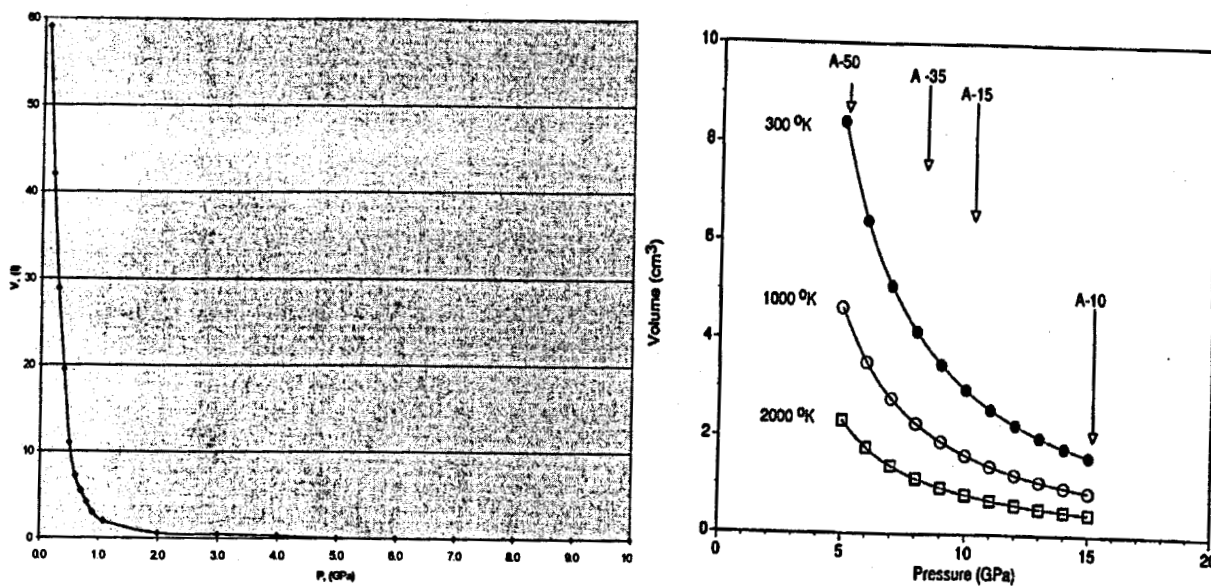


Figure 3.2-9 Working volume of the HPA as a function of required pressures and temperatures [4] for the 1000 ton press.

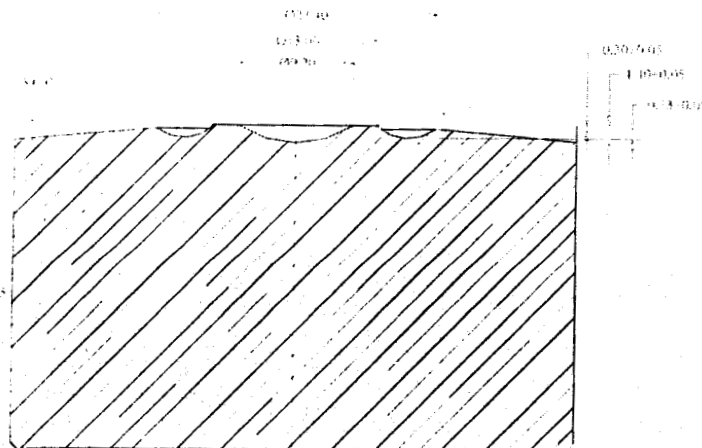


Figure 3.2-10 Cross sections of the A-10 anvils (designed for 8-15 GPa pressure range).

In the HPA, the anvils compress a container made of lithographic stone with a central volume that has a spheroidal shape. As shown in Figure 3.20 the internal volume of the lithographic container is filled by a reaction cell that is made of lithographic stone and graphite. Under pressure, the inner part of the reaction cell is lens shaped. The semi-hydrostatic pressure is constant in the reaction cell volume. The pressure decreases from the maximum value in the cell to ambient levels at the boundaries of the lithographic container. The approximate value of load that is required to reach a certain pressure can

be calculated by multiplying the pressure value and the cross section area of the central volume of the lithographic container: $F(\text{ton}) = P(\text{kbar}) \times \pi r^2(\text{cm}^2)$. This estimate holds up to pressures that are equal to the compressive strength of the anvil material.

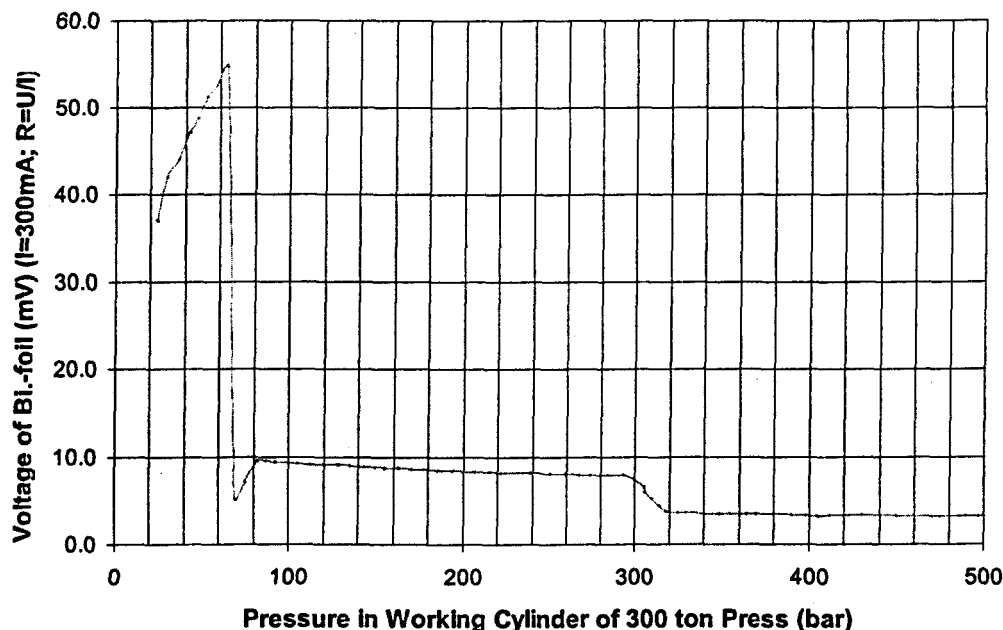


Fig 3.2-11. "Cold pressure" calibration by Bismuth's transitions
(for Anvils A-15, limestone container, press 300 ton)

The dependence of Bi-foil resistance on working cylinder pressure for 300 tons press is depicted in fig.3.2-11. The dependence of value of loading force on oil pressure inside working cylinder is shown on fig. 3.2-12. The resistance increases with increasing of loading force until pressure inside the reaction cell reaches ~ 2.5 GPa, then the first transition occurs. The middle point of transition corresponds to 2.55 ± 0.01 GPa. (Loading force increases in Bi-calibration experiments with the speed of 300 kgf/sec. from 0 to 300 tons). The resistance of second Bi phase is ten times less than the resistance of the first one. The middle point of the second transition corresponds to 2.69 ± 0.01 GPa. The resistivity of the third phase is two times higher than the resistivity of the second one. The resistance of sample insignificantly decreases in pressure range 2.8-7.3 GPa. The middle point of the third transition corresponds to the pressure of 7.7 ± 0.2 GPa. The resistance of sample in the fourth phase is 2.5 time less than the resistance in the third phase. (The values of resistivity might be measured very precisely, but we will use it just for calibration, so we will need only approximate values). The resistivity of the fourth phase insignificantly decreases when the pressure increases. The dependence of pressure in reaction cell of Lava-stone (pyrophyllite) container compressed between two profiled anvils with diameter of cavity of 15 mm sintered from microstructured (3-5 μm) WC/Co6 (6% wt. of Co) powder on loading force is shown in fig. 3.2-13.

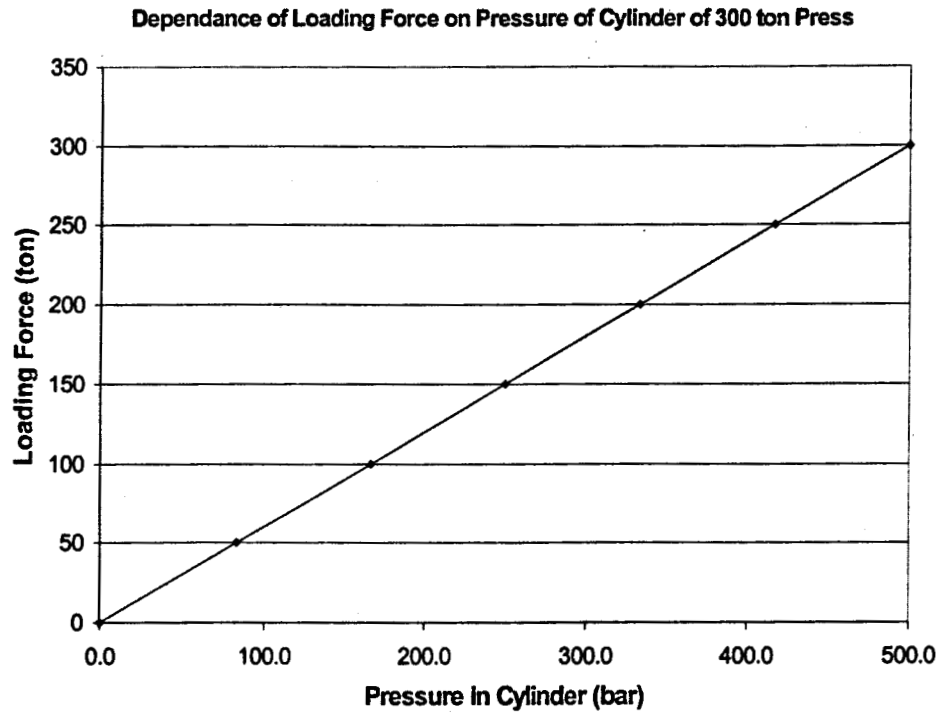


Fig. 3.2-12. Dependence of loading force on oil pressure inside working cylinder of press 300 ton

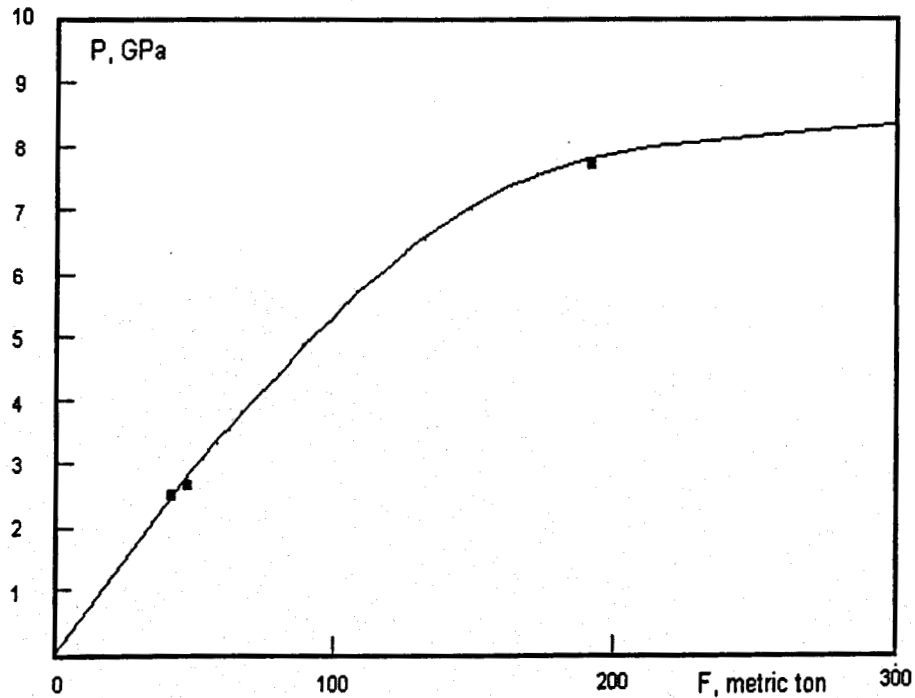


Fig 3.2-13. The dependence of pressure in reaction cell on loading force (A-15, limestone container, press 300 ton).

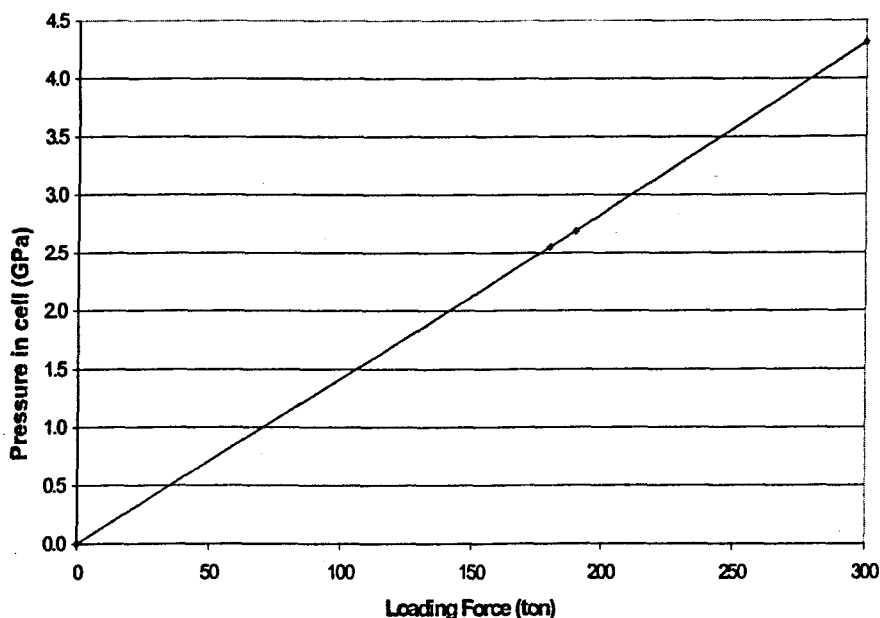


Fig 3.2-14. The dependence of pressure in reaction cell on loading force (with rubber ring) (A-15, limestone container, press 300 ton, ϕ 120 mm, h 6 mm rubber ring)

This dependence can be described by equation:

$$P = \frac{F}{S \cdot (1 - \alpha \cdot F^{1/2} + \beta \cdot F)}$$

where P is pressure in reaction cell, F is loading force, S is some average area, α and β are coefficients that represent hardness and strength of material of anvils and some area as well. (This equation will be explained in Final Report) The βS is $\sim 1/H_V$ where H_V is Vickers hardness of material of anvils. The drawing of anvils, container and cell for "cold pressure" calibration is depicted in fig. 3.2-15. and 3.2-16.

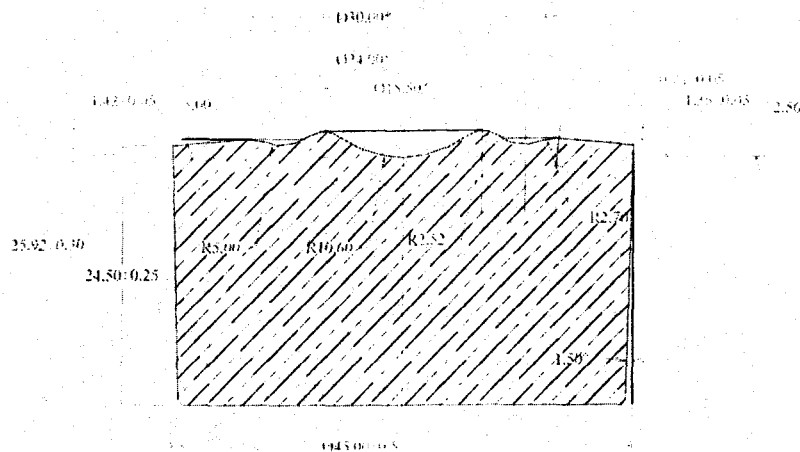


Fig 3.2-15. The drawing of anvil A-15 (designed for 5-9 GPa pressure range).

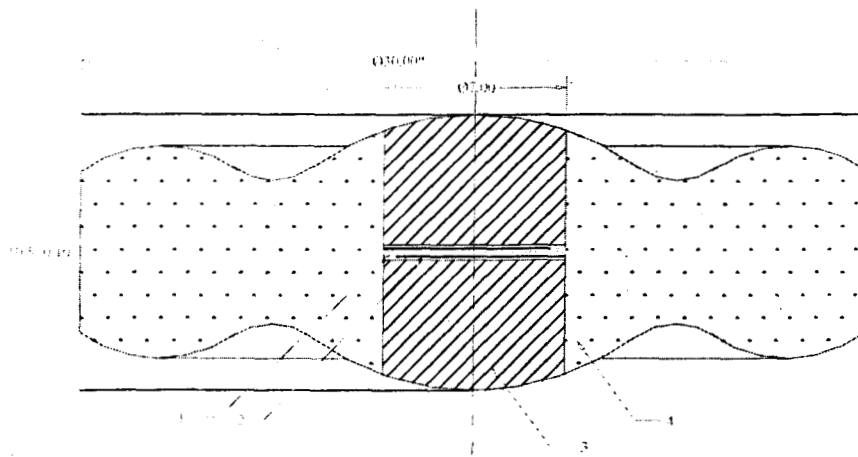


Fig 3.2-16. The drawing of container and cell (A-15) for "cold pressure" calibration by Bi-transition
Parts of cell: 1-Bi foil; 2- paper; 3-graphite ceramic; 4-lava-stone container

The first calibration of Fig. 3.2-11 has been obtained for this container with no rubber ring surrounding Lava-stone. These anvils and container were basically designed for polycrystalline diamond making. Good bulk polycrystalline diamond can be synthesized from graphite ceramic, glassy carbon or diamonite (that is fullerene-like carbon), if pressure exceeds 7.0 GPa, and the quality grows up in pressure range 7.0-10.0 GPa when "cold pressure" increases. To be sure about top-quality transformation of non-diamond carbon into bulk polycrystalline diamond we need always to see the third Bi-transition in cold pressure calibration. If HPHT System is designed so that if we do not see this transition, we can not be sure about quality of man-made polycrystalline diamond. Nevertheless in this particular Project we evaluated sintering the carbon soot in the pressure range 1.0-3.0 GPa, even in pressure range 0.1-1.0 GPa to make in future the large pieces of new carbon materials. Therefore it is desirable to have reaction cell that permits to work with the same gauges, presses, HPHT Systems in lower pressure range but with the same accuracy. To do that we have made the calibration of reaction cell with $\varnothing 120$ mm and 6 mm thick rubber ring (fig. 3.2-14). Rubber ring takes some part of loading force thus making calibration curve less steep and more even.

The anvils with diameter of cavity of 25 mm have been sintered from submicrostructured WC/Co10 powder with 10 %wt. of Co. Supporting steel rings for these anvils were made (Karl O. Mueller Machine & Tool Co., Inc.). The anvils with cavity diameter of 25 mm were used for making larger Diamonite parts (up to 15 mm in diameter) in pressure range 1.0-3.0 GPa. (see fig.3.2-17).

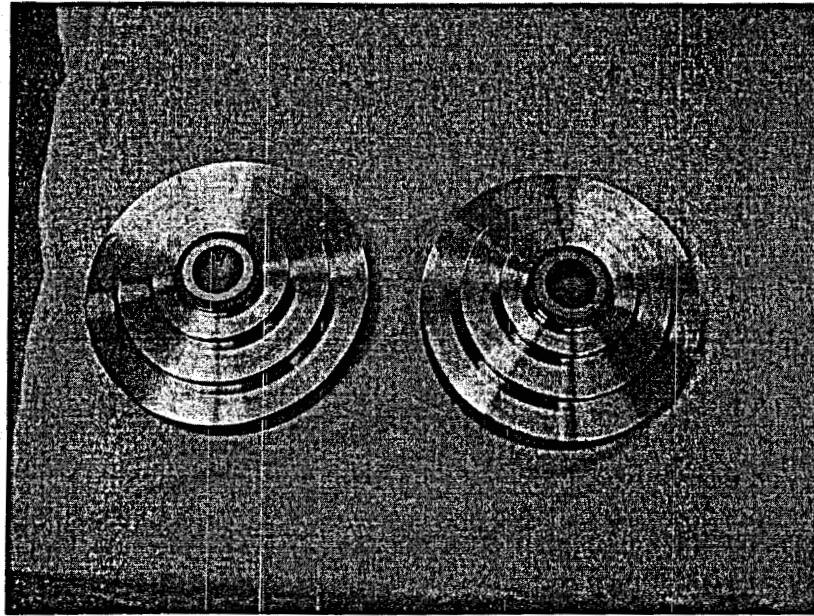


Fig 3.2-17 The photograph of submicrostructured WC/Co 10% anvils with 25 mm cavity and supporting steel rings before pressing together (designed for pressure range 1-6 GPa).

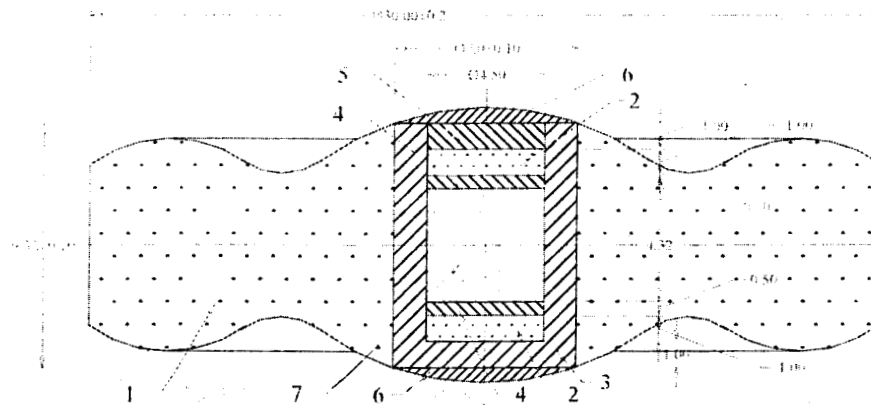


Fig 3.2-18. Reaction cell of Ø7mm with container A-15
Parts of cell: 1,2 - lava-stone; 3,4,5,6 - graphite ceramic; 7 - sample

The dependence of temperature on power and time can be described for reaction cell of Fig. 3.2-18 like:

$$T = 625 \cdot W \cdot \left(1 - e^{-t/1.3}\right) + 25 \quad \text{for heating up } (T < 2000^\circ\text{C})$$

$$T = 625 \cdot W \cdot e^{-t/1.3} + 50 \quad \text{for cooling down,}$$

where T is in $^\circ\text{C}$, W is in kW, t is in sec. and the power has been increased or decreased abruptly. When the time t is seven time more than the time of relaxation τ ($t=7\tau=9.1$ sec.) we have the 0.1% temperature stabilization. Since $\tau=1.3$ sec. is very small, the

temperature stabilization inside the reaction cell sets in within 10 second. The certain time is required in order to heat the center of the sample to a temperature close to that of its exterior surface, i.e. the walls of heater. This time ($\tau^{(0)}$) is proportional to the surface area of the sample:

$$\tau^{(0)} \approx \frac{1}{12\pi} \cdot \frac{c\rho}{\lambda} \cdot S_0$$

where c is thermal capacity, ρ is density, λ is thermal conductivity of sample, S_0 is surface area of sample. All values c , ρ , λ depend on pressure and temperature. Nevertheless roughly τ^0 may vary from 0.002 sec. for diamond to 20 sec. for amorphous carbon (which has 15000-time lower thermal conductivity than diamond at ambient pressure). As one can see, $\Delta t \sim 10$ sec. is not always enough long time to get the stable condition.

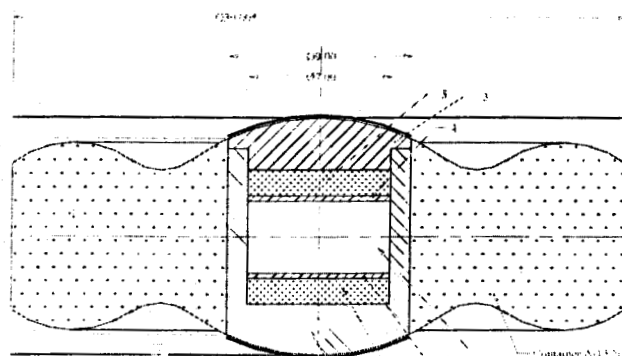


Fig 3.2-19a. Reaction cell of $\varnothing 9$ mm with container A-15
Parts of cell: 1- sample; 2,3,4 – graphite ceramic; 5 - lava-stone

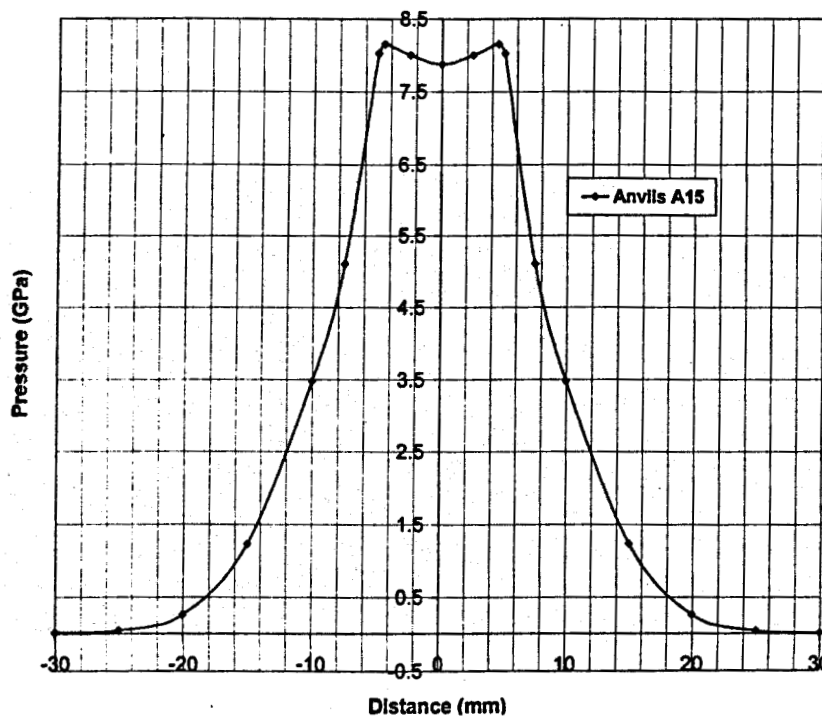


Fig. 3.2-19b. Dependence of pressure on distance in reaction cell A-15

Another reaction cell that is prepared for experiments is shown on Fig.3.2-19. The dependence of temperature on power and time can be described for this reaction cell by equations:

$$T = 417 \cdot W \cdot \left(1 - e^{-1/2.9}\right) + 25 \quad \text{for heating up}$$

$$T = 417 \cdot W \cdot e^{-1/2.9} + 50 \quad \text{for cooling down.}$$

This reaction cell is largest possible reaction cell for such a container and profiled anvils with diameter of cavity of 15 mm. We are planning to use this reaction cell to study the sintering of powders under pressure as well as to study the joining of carbon materials with metal parts under pressure (in pressure range 1.0-10.0 GPa). The dependence of temperature on power for this reaction cell in stable conditions is shown in Fig.3.2-20.

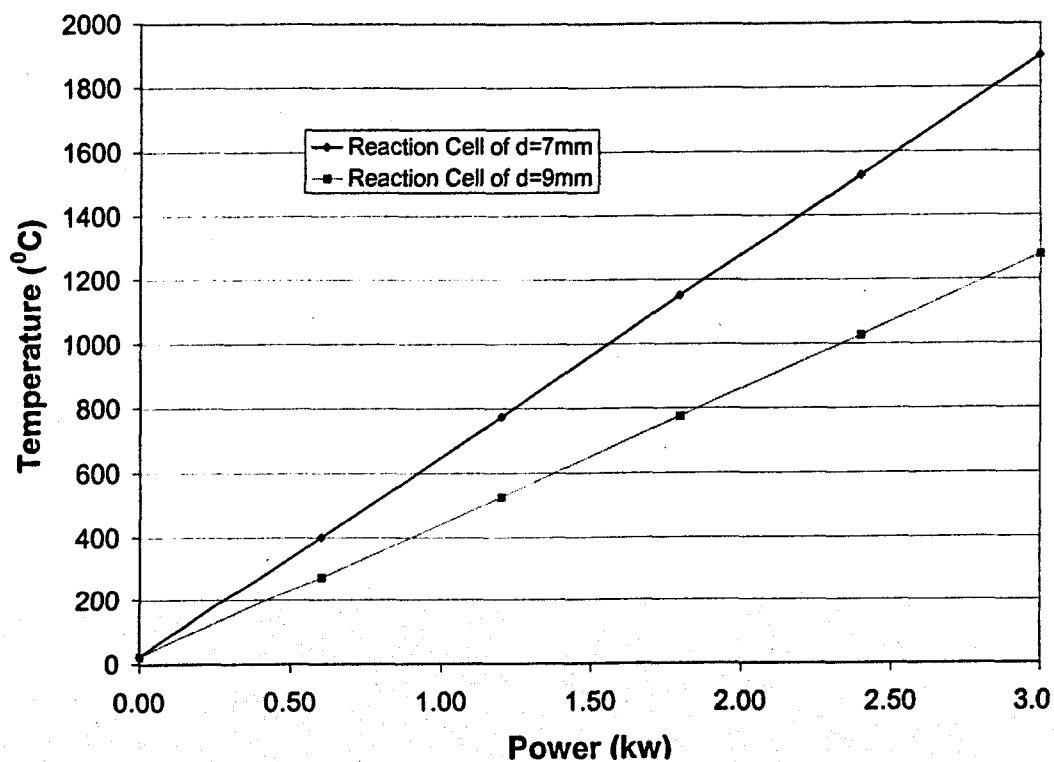


Fig 3.2-20. The Dependence of temperature on power in stable (static) state.

It is necessary to repeat "cold pressure" calibration after every 10 HPHT experiments to be sure that value of pressure is defined correctly. The dependence of heater resistance on temperature is shown on Fig.3.2-21 at loading force of 300 tons. The schematics of "cold pressure" control circuits and temperature control circuits of new HPHT System are shown on Fig. 3.2-22.

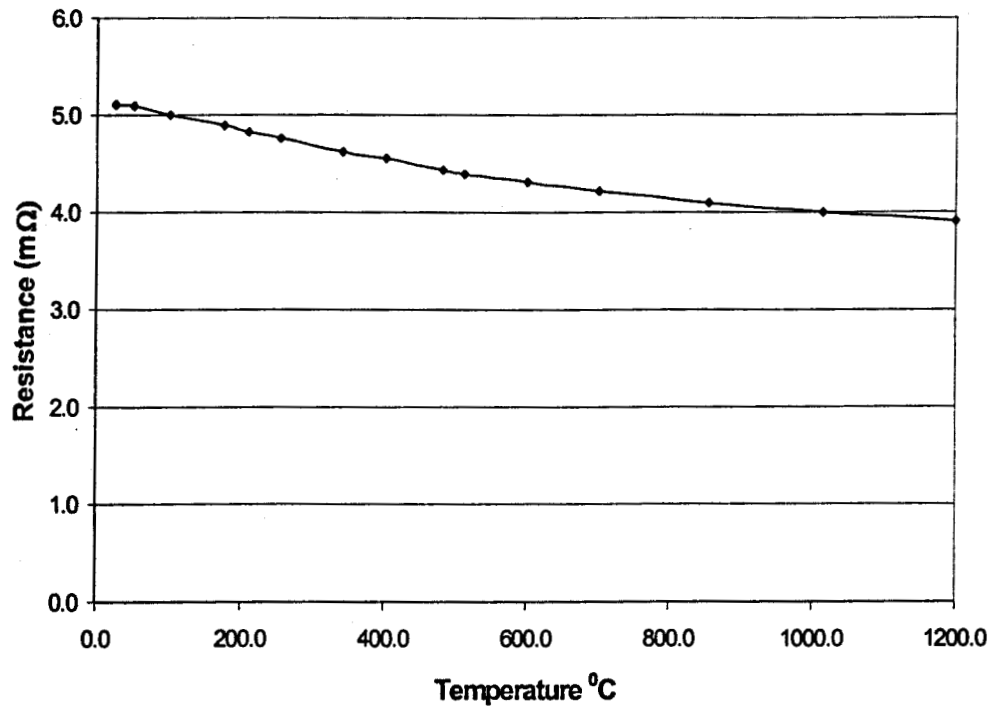


Fig 3.2-21. The dependence of heater resistance on temperature (for cell of $\varnothing 7\text{mm}$)

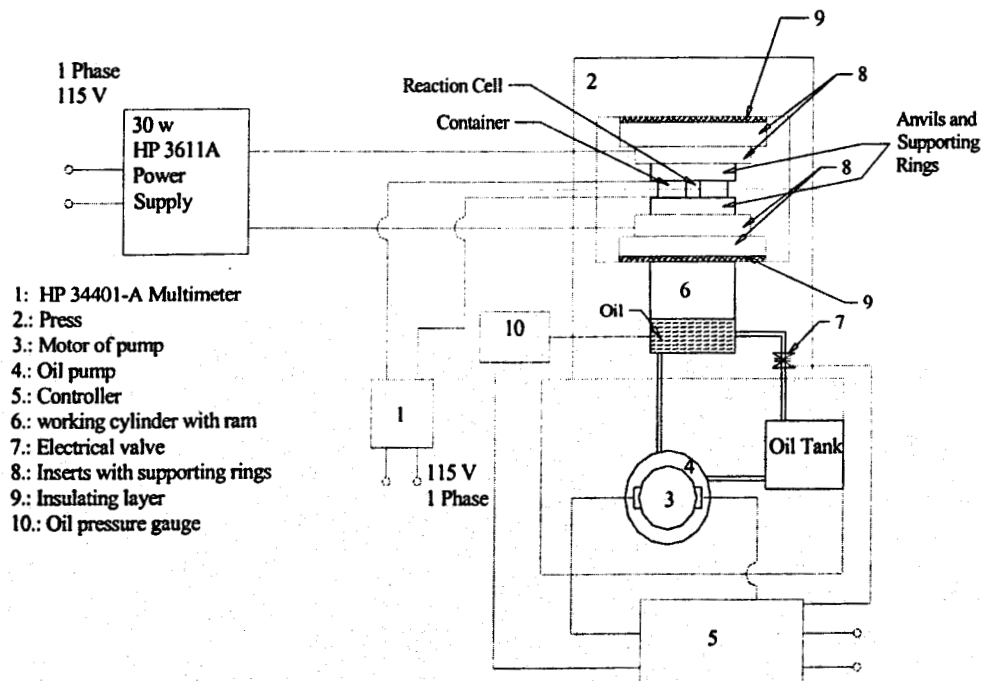


Fig 3.2-22a. The schematic of control circuit of "cold pressure" calibration by Bi

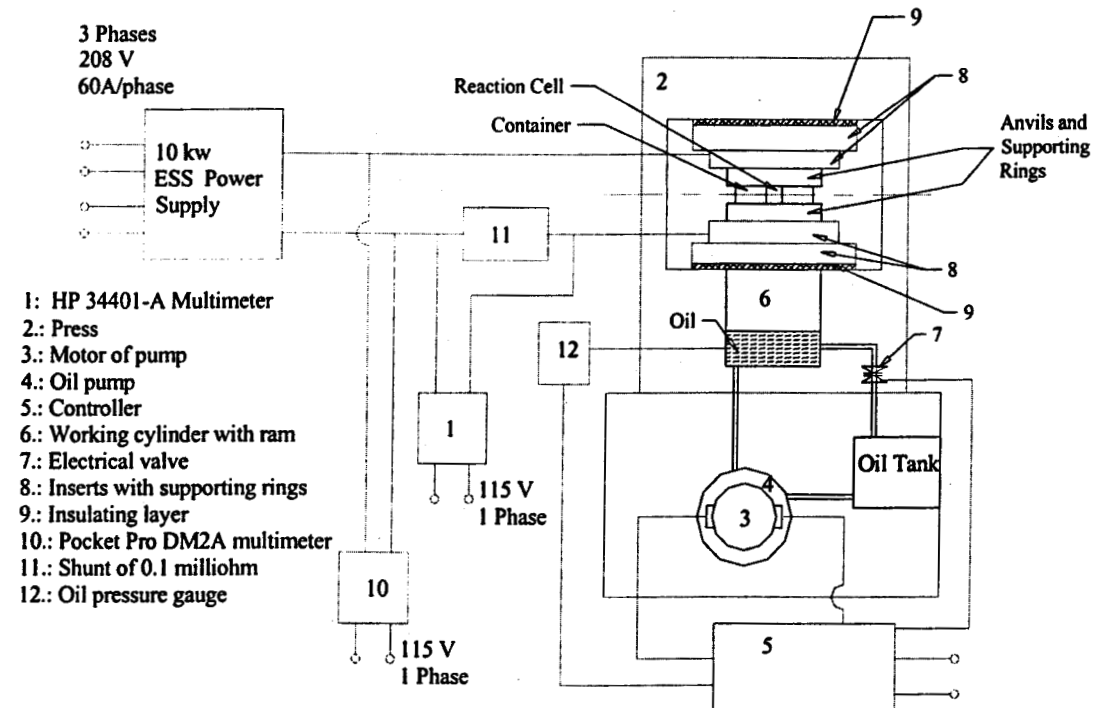


Fig 3.2-22b. The schematic of control circuit for high temperature heating under high pressure

DMI implemented the described above designs for a number of anvil configurations. We have also designed and fabricated a number of green body dies that allowed us to sinter WC/Co anvils from various WC/Co powder at a range of sintering conditions. In Figure 3.2-23 we show a photograph of a preform that is used for green body sintering. In Figure 3.2-24 a number of finished WC/C anvils are shown after sintering and polishing.

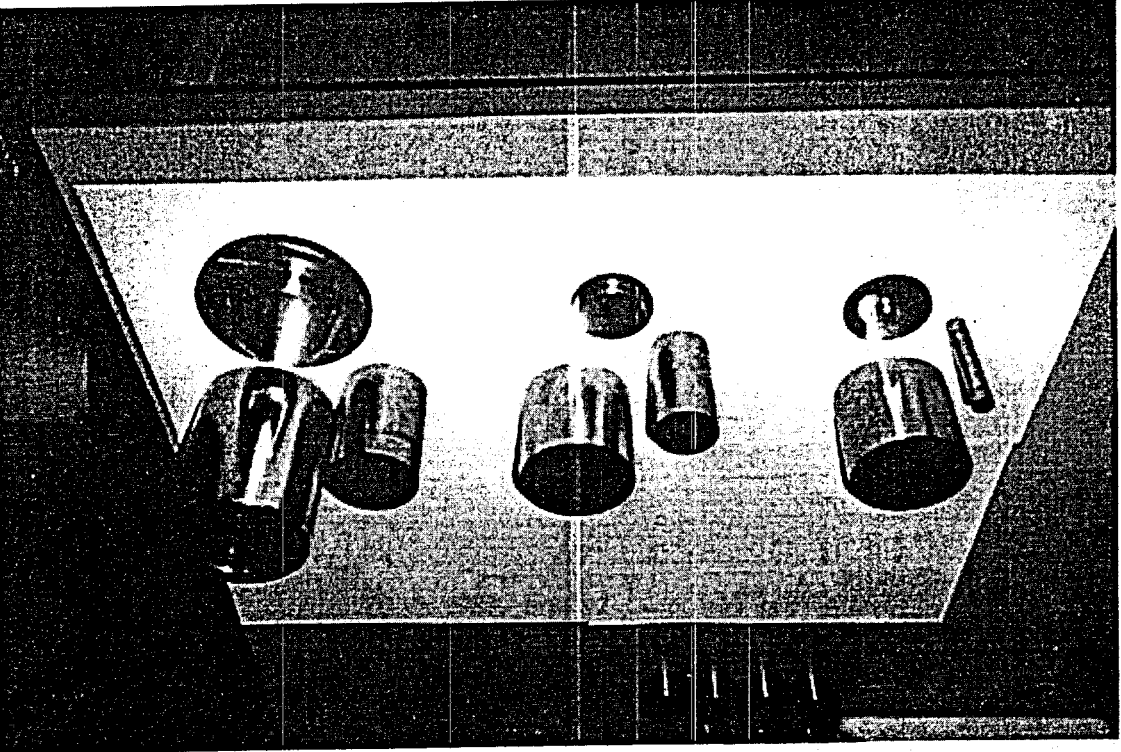


Fig. 3.2-23a Photo of dies for WC/Co compaction

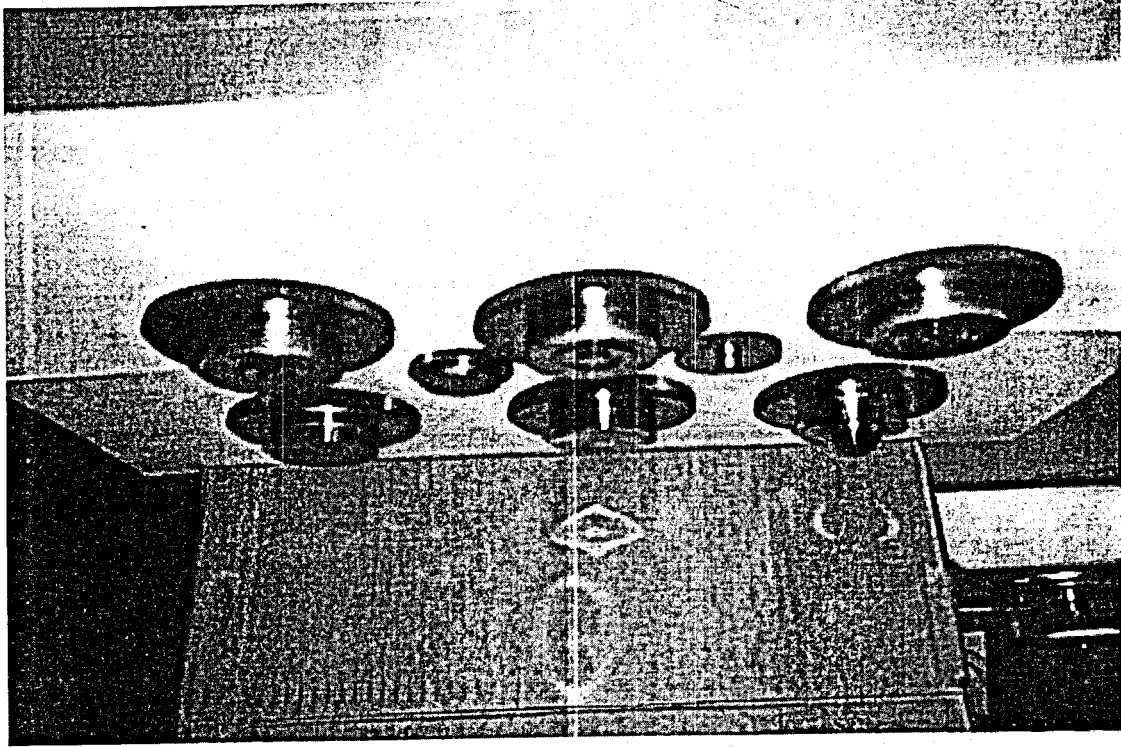


Fig. 3.2-23b. The collar step bearings of dies with different profiles.

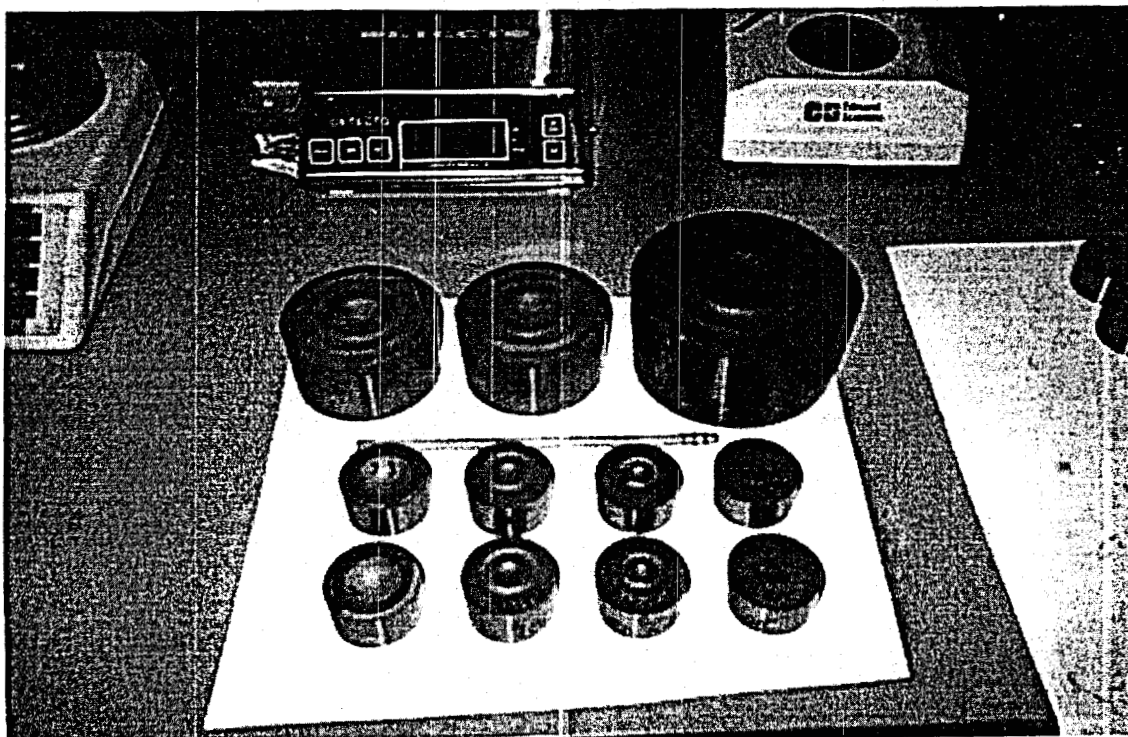


Figure 3.2-24 The WC/Co anvils are ready for sintering of BPCD.

3.2.4 Concept of apparatus for achieving super high static pressures and temperatures in relatively large volume.

The design of the high pressure apparatus (HPA) and reaction cell (RC) that permit the achievement of ~20 GPa pressure in ~1 cm³ volume and ~100 GPa pressure in ~1 mm³ volume is described in this section. The volume of the reaction cell to achieve ~2000^oC temperature will be ~100 mm³ and ~0.1 mm³ respectively; to achieve ~4000^oC, the temperature will be ~10 mm³ and ~0.01 mm³ respectively. These volumes could be considerably increased if using a press that has considerably larger loading force and working space volume (height, length and width of "press window").

A typical HPA and RC with hard alloy or diamond anvils can achieve ~15 GPa (for WC/Co) and ~100 GPa (for diamond) in a working volume of about 1 μm³. On the other hand, if the RC with a large working volume is available, it is possible to make pieces of diamond from the carbon melt during relatively small time intervals. These pieces are nanostructured or single crystalline, depending on the cool down rate.

It also may be possible to sinter a new carbon material that is harder than diamond. Previous experimental results and theoretical evaluations show that this might occur at ~20 GPa pressure and ~500-600^oC temperature in the case of a fullerene soot C₆₀ carbon precursor.

The HPA design that DMI is using at the present time is shown in fig.3.2.4-1 and the RC design is shown in fig.3.2.4-2. The HPA consists of two profiled anvils (1) and three supporting steel rings (2-4). The anvils compress a container (5) made from plastic stone and the reaction cell (6) inside the container. The inserts (7) and (8) are made from WC/Co6%wt, and are supported by steel rings. The hardness of the rings decreases from the center to the periphery. The RC (fig. 3.2.4-2) consists of a graphite crucible (1) that serves like a heater and sample (2). The container (3) is squeezed by the anvils (4). Supporting steel rings are needed to increase the load onto the anvils and inserts. They provide side-supporting pressure that increases the effective fracture strength of the anvils at compression. The set of rings is needed because the maximal supporting pressure that a multi-layer cylinder can bear is two times greater than the maximal pressure that can be achieved without distraction in mono layer cylinder:

$$P_{0(max)} \sim 2\sigma_{ts}/\sqrt{3} \quad (1)$$

where σ_{ts} is the ultimate tensile strength of steel at stretching [4] (~2.0 GPa for hardened steel). This allows us to achieve a maximal working pressure in the RC (P_{Wmax}) that is higher than the fracture compressive strength of the anvil material; however, this pressure is always less than the Vickers hardness (H_V) of the anvil material:

$$\sigma_{fs} \leq P_{Wmax} \leq H_V \quad (2)$$

The maximum working volume (V_{max}) in which this pressure could be achieved depends on σ_{fs} , maximal loading force (F_{max}) of the press, the size of the frame window (a_j) and the size of the anvils (V_a) used:

$$V_{max} = V_{max}(\sigma_{fs}, F_{max}, a_j, V_a) \quad (3)$$

According to theory, the fracture compressive strength of brittle (not plastic) materials is inversely proportional to the volume of sample:

$$\sigma_{fs} = \eta \sigma_{cs} V_a^{-\gamma} \quad (4)$$

where $\eta = \eta_0 V_{0a}^\gamma$ is constant, η_0 is dimensional constant that is typical for a given material, V_{0a} is the volume of a standard sample for measuring compressive strength (σ_{cs}), and exponent γ is a typical value for a given material ($\gamma \sim 1/15$ for regular WC/Co). The values of σ_{cs} and H_V in formula (2) are also interrelated. The H_V^{st} is $\sim 2.5 \sigma_{cs}^{st}$ for hardened steel that has some plasticity. The H_V^{cer} is $\sim 7 \sigma_{cs}^{cer}$ for brittle rocks, stones and ceramics. The H_V^{com} is ~ 3 to $5 \sigma_{cs}^{st}$ for composite materials having a brittle skeleton and plastic matrix, such as materials of WC/Co. The degree of sensitivity of fracture compressive strength to the volume of the sample that is defined by the value of γ depends on porosity, crystallite size (structurization) and value of side supporting pressure (P_{ss}):

$$\gamma = \gamma(\rho_A, d, P_{ss}) \quad (5)$$

where ρ_A is apparent density, and d is the typical size of crystallites.

Below, we review a HPA design that allows maximum high static pressures in the 10-100 GPa range. We will call this range "super high pressure". Higher pressure in a large working volume can be achieved with the help of dynamics methods or at conditions of gravitational squeezing. We will call that range ($P > 100$ GPa) "ultra high pressure".

Let us consider the achieving of high temperatures. High temperature (HT) can be achieved by electrical current passing through a heater made from graphite ceramic. The thermal regime of the reaction cell and container may be computed from the equation:

$$W dt = \int c \rho \cdot dT \cdot dV + (\int \lambda \cdot grad T \cdot dS) dt \quad (6)$$

where $W = q dV$ is power, q is power emitted in unit volume, c is specific heat capacity, ρ is density, λ is thermal conductivity. This equation in a static state looks like:

$$div(\lambda \cdot grad T) = 0 \quad (7)$$

The approximate solution of equation (6) for spherical thermal conductivity allows us to evaluate the thickness of thermal insulation and the relaxation time that is needed for the reaction cell to respond over power change and to get into the static state:

$$T = T_{max} (1 - e^{-\tau/t}) \quad (8)$$

$$\text{where } T_{max} = W/v; \quad \tau = \eta/v; \quad \eta = \int c \cdot \rho \psi(\mathbf{r}) dV; \quad v = \int div(\lambda grad \psi(\mathbf{r})) dV;$$

and $\psi(\mathbf{r})$ is a special function typical for one particular container. If the energy releases not overall volume of sample, some interval of time is necessary for heating of the center

of sample to a temperature close to the temperature of the heater T_{\max} . The typical relaxation time (τ_0) depends on the properties and the size of the sample:

$$\tau_0 = \frac{1}{3} \frac{c_0 \rho_0}{\lambda_0} r_0^2 \quad (9)$$

where c_0 , ρ_0 , λ_0 are heat capacity, density and thermal conductivity of the sample and r_0 is radius of the sample [4].

Carbon is the most infusible element. Temperatures in the region 100-2000°C are easily achievable using graphite heaters. Let us call this region "high temperatures" (HT), and the region where carbon does not still melt, but reacts with all elements and compounds with the exception of inert gases, "very high temperatures" (VHT). The top boundary of this region lies between 4000°C and 5000°C. The VHT region is difficult to achieve, especially at VHP, when the volume of thermal insulation is very limited. There are other difficulties in achieving VHT, except possible reaction of the sample with the heater and the heater with the container. Unlike the thermal conductivity of a single crystalline solid state that decreases in this region when temperature increases, the thermal conductivity of porous polycrystalline solid state increases with a rise in temperature. In addition, the part of thermal flow transferred by radiation significantly increases. Thermal flow from the heater by thermal conductivity is proportional to the first power of temperature, but thermal flow by radiation is proportional to the fourth power of temperature:

$$E_e = \sigma^{ST} \oint \beta_T(r) \alpha_T(r) T^4 dS dt \quad (10)$$

where α_T is blackness, σ^{ST} is Stefan-Boltzman constant, β_T is integral coefficient of reflection of electromagnetic waves from surface. The energy E_e added to the right part of (6) increases the heat transfer at VHT and leads to a situation where a small increase in temperature demands a large increment of heater power.

Below, we describe a facility that can achieve static SHP in combination with static VHT. This unit might be useful not only for making diamond materials, but also for gaining new knowledge and educating. The Earth is a gradient high pressure furnace. Pressure is generated by the force of gravity and increases from 1 atm. on the surface to 3,600,000 atm. at the center. The temperature gradient is determined by cooling core and energy release by radioactive isotopes nuclear decay. The temperature grows from 0°C on the surface to 5000°C at the center. That is why it is interesting to study experimentally, in laboratory conditions, the state of substances and reactions between them in this region.

The HPA design for SHP and VHT is shown in fig. 3.2.4-3. The anvil (1) and insert (2, 3) materials are chosen so that the hardness increases from the last insert to anvil. The insert made from hardened steel (3) rests on a plate of soft steel; the insert made from hard alloy (2) rests on an insert of hardened steel. The anvils (1) are manufactured either from diamond ($H_K=100$ GPa) or from carbide with a hardness of $H_V=30$ GPa (TiC or SiC). The inserts and anvil form a pyramid that decreases pressure from maximum inside the reaction cell to contact pressure of ~1GPa on a surface between the last insert and the plate of soft steel. The container (4) of plastic stone is located between two profiled anvils (1). Some part of the container flows out of a cavity

into clearance between anvils during the increase of loading force, thus determining the gradient of pressure from maximum inside the reaction cell to ambient outside of container. The clearance between the outer part of the anvils and supporting rings could be a vacuum, air (gas) or polymeric material with high compressibility (rubber). Such a rubber ring around the container can regulate the gradient of pressure. The plastic stone that makes up the container (4) is not a conductive material. The reaction cell (5) is located inside container (4).

Supporting rings (6-14) are made from hardened alloyed steel. The heat treatment of rings is done in such a way that hardness and ultimate tensile strength decreases from the central rings to the periphery, but plasticity of the rings increases. The calculation of stresses in rings is done so that all rings work in elastic range and maximal stresses in any ring do not exceed yield strength (σ_{ys}) of this ring material. Outside safety rings (15-17) are made from soft, not heat-treated steel. The centering rings (18-23) are made from non-conductive polymeric materials.

The HPA has a cylindrical axis of symmetry. The centering rings are used for precise coincidence of the axes of the top and bottom parts of HPA. The top and bottom parts of HPA are electrically insulated from press. The conductivity of the heater material is considerably higher than the conductivity of the container material. The heater is connected to the top and bottom parts of the HPA by contacting units. Electrical voltage is applied to top and bottom parts of HPA.

The design of the reaction cell is shown in fig. 3.2.4-4. A sample (10) of carbon material is located inside the heater (1), which is made of graphite ceramic. The heater is surrounded by a layer (2) of pure diamond powder that insulates the heater from the first screen (3). The screen (3) is insulated from the second screen (5) by carbide powder (4) that does not react with carbon within the temperature range existing between the two screens at static regime. The screen (5) is located inside the container (6), which is made of plastic stone. Copper foil (7) on the surface of the anvils (9) provides the electrical contact. A rubber ring (8) regulates the pressure gradient in the container.

As described, this reaction cell allows us to melt carbon under super high pressure in the static regime and in relatively large volume.

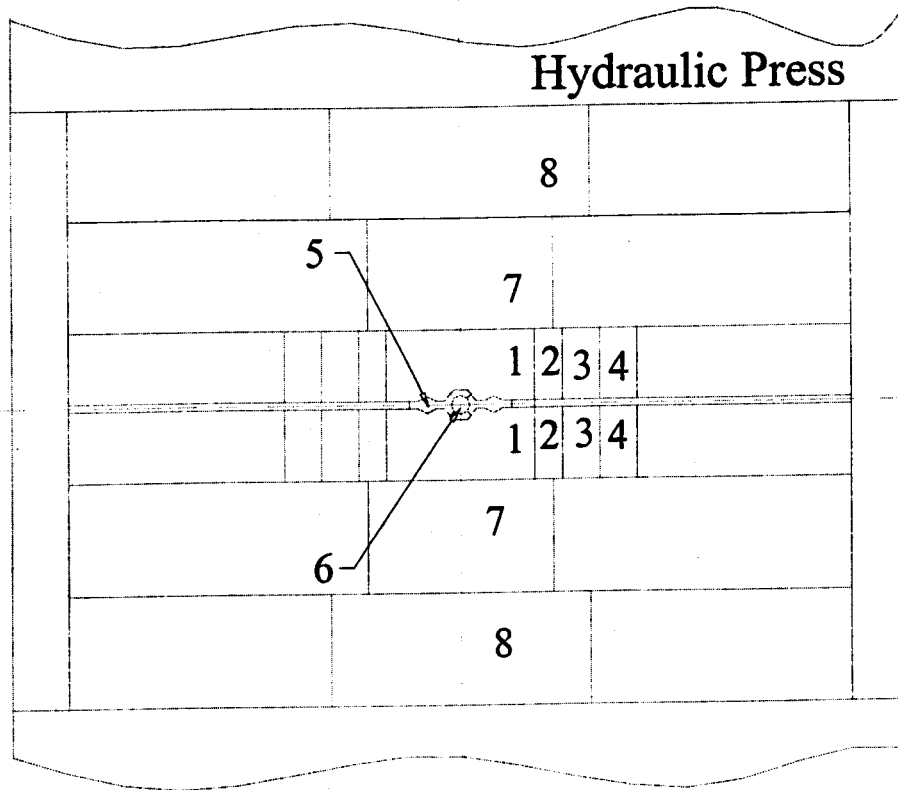


Fig 3.2.4-1. Prototype Schematic of DMI's High Pressure Apparatus

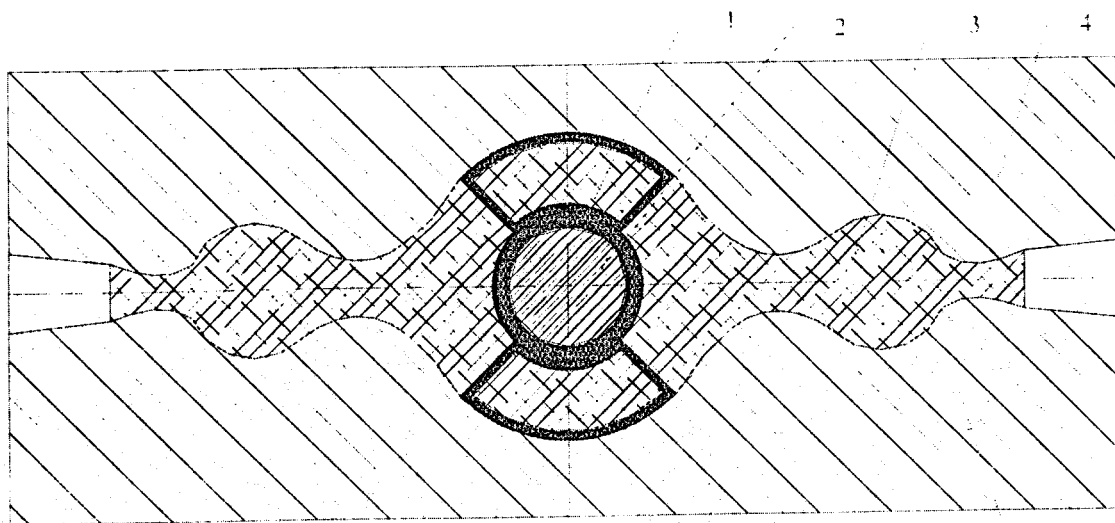


Fig 3.2.4-2. Prototype Reaction Cell for 20-2000 °C range

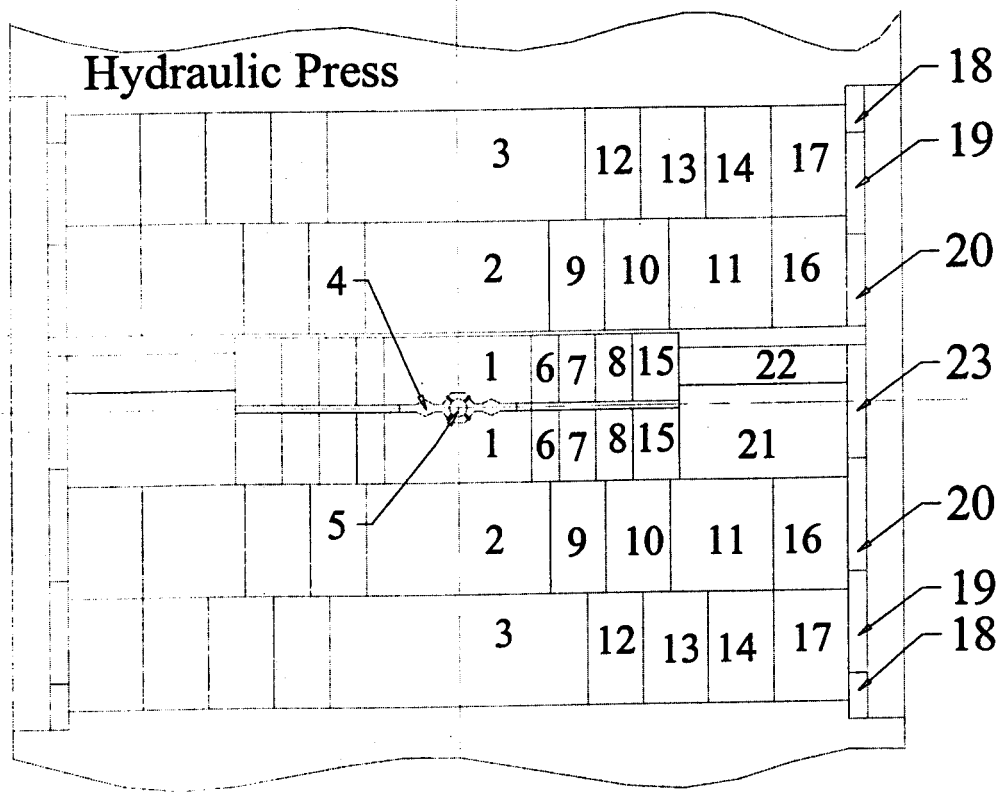


Fig 3.2.4-3. High Pressure Apparatus

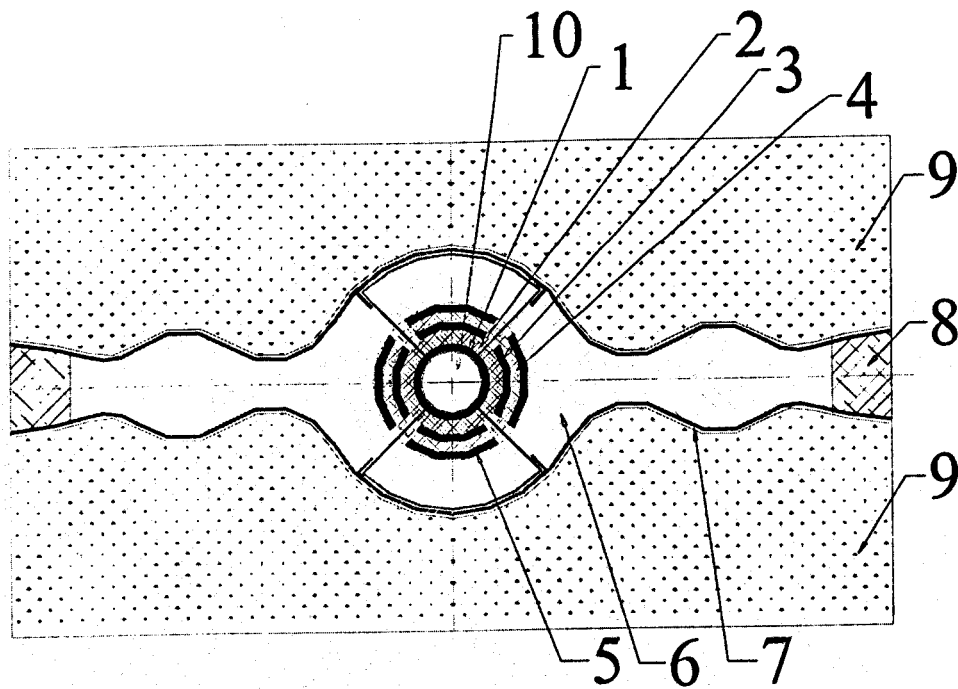


Fig 3.2.4-4. Reaction Cell for 20-5000 °C range

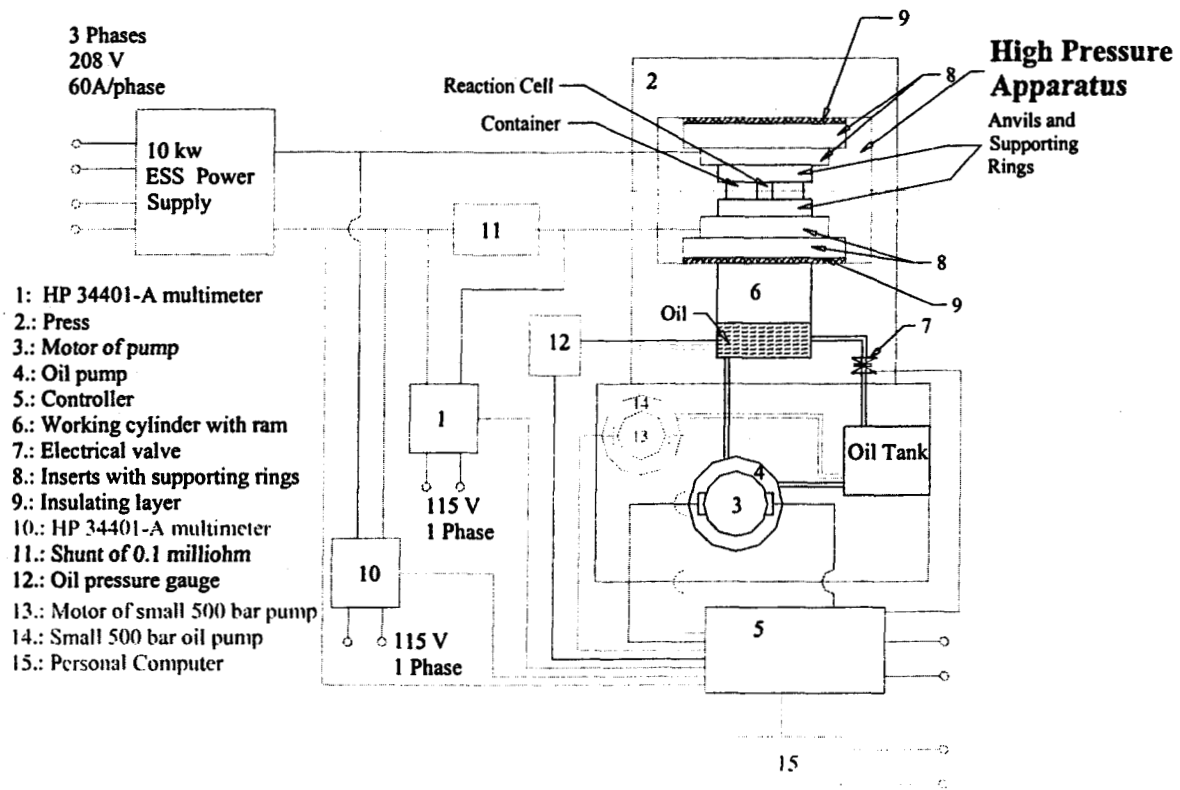


Fig 3.2.4-5. The design of automated High Pressure-High Temperature System

3.3. Sintering of diamond ceramics

Polycrystalline Diamond (PCD) materials can be synthesized from graphitic materials (graphite ceramics, glassy carbon, and others) and fullerite type materials or sintered from diamond powder at high pressure high temperature (HPHT) conditions [5,8]. To maintain the bulk shape of the sintered sample and assure strength of the PCD during sintering process, the initial cold pressure in the reaction cell should exceed 7 GPa. PCD can be synthesized using phase transformation of initial carbon materials in the presence of catalyst or via re-crystallization of carbon melt. Ni is one of the best catalysts for diamond synthesis since molten Ni is wetting very well and dissolves carbon without the formation of stable carbides. However, pure Ni can react explosively with carbon at certain conditions, thus it is more convenient to use nickel alloys as catalysts. Fe and Co are also catalysts for diamond synthesis. Transformation from other forms of carbon to diamond occurs at temperatures of 1000 to 2000°C in 10 to 100 sec. Higher pressure leads to a decrease in PCD grain size. The final grain size of the PCD material is also a function of the grain size of the initial carbon material used in the synthesis process. In order to melt carbon, the temperature must be higher than 4000°C; and to crystallize the carbon melt into diamond, the pressure must be higher than 20 GPa (see more detail in section 3.2.6, "Concept of Supercell"). The grain size of PCD material will

also depend on the cooling rate after sintering. Cooling the sample in less than 1 sec can lead to nanograin PCD. Slow cooling and long exposure to HPHT conditions will lead grain growth and can lead to formation of diamond monocrystals.

Well cleaned diamond powder can be sintered into PCD when exposed to 8-10 GPa pressure and 1800-2000°C temperature for 10 -100 sec. The quality of PCD material improves with increase of temperature. The most advantageous for sintering is the $\frac{3}{4} T_m$, where T_m is the melting temperature. For carbon, this corresponds to the 3000 to 4500 °C range. To maintain conditions for diamond phase on the carbon phase diagram, at these temperature one should maintain pressures in the 15 to 20 GPa range.

3.3.1 Sintering of diamond powder

Diamond powders with the grain size from 0.1 to 1 mm as well as larger size diamond fragments of 1-10 mm will fracture to smaller size pieces when subjected to very high pressures. We call pressures of 1-10 GPa "Very High Pressure," which corresponds to approximately 10,000-100,000 atm. Experimental techniques are different for pressure ranges 10-100 atm, 100-1,000 atm, 1,000-10,000 atm., and very high pressure. Thus, we can consider compression at high pressure as one of the methods of crushing powder into smaller grains. Mixing of these fragments with powders of 10-100 μm (0.1-0.01 mm) in a 50:50 ratio prevents cleavage of grains and breakage. Particle sizes in 10 to 100 μm range are most suitable for sintering of diamond powders as well as other brittle powders. Optimal for diamond sintering is powder with grain size of ~50 μm with uniform size and spherical shape of particles. These powders flow well and do not tend to sinter irregularly. Powders in the 50 to 100 μm are also more advantageous because they can be graded by size using simple sieving methods. These powders can have mono crystal or polycrystal grains. Polycrystals can have grain size from 1nm to 10 μm . PCD materials with grain size of 1 to 100 μm will be called microstructured, grain sizes in 0.1 to 1.0 μm will be called submicrostructured and grain sizes of 0.001 to 0.1 μm will be called nanostructured. Powders with 0.1 to 10 μm grain size tend to sinter irregularly, forming low density and high porosity PCD. Thus, these particles should be agglomerated before sintering. As a rule, the initial apparent density of agglomerated powder should be at least $\frac{1}{4}$ of the density of fully dense sintered material, and agglomerated powder under pressure should be $\frac{1}{2}$ of the density of fully dense polycrystal. Spherical particles with a clean, smooth surface are best suited for sintering (fig. 3.4-4 and 3.4-5).

The consideration described above will be true not only for diamond, but also for other brittle materials. However, sintering of PCD is technically challenging; thus, PCD is most sensitive to the best sintering conditions described above. A small deviation from these conditions can lead to significant decay in the quality of the sintered PCD materials. Inclusion of metal alloy binder significantly reduces sintering of diamond/metal composite, where metal is brazing diamond particles with diamond dissolving in metal and recrystallizing at the grain boundaries. These composites can be formed at 1 to 7 GPa pressure with quality of the composite improving with the increase of sintering pressure and reduction of metal content.

3.3.2 Three different strategies for sintering powders in three different ranges

1. Thus, let us suppose that we have pieces of diamond of 1-10 mm size or diamond powder of 0.1-1 mm range to sinter. How do we sinter those pieces together? Take 50%wt. of pieces, mix it properly with powder of 50 μm grain size and pour the mixture into the reaction cell. Sinter it using the HPHT System at as high a pressure and temperature as possible. The pressure should be $P > 8$ GPa, temperature should be $T > 1800^{\circ}\text{C}$, and duration should be $\Delta t > 10$ sec.
2. Sintering of 10-100 μm range powders. Take the powder with well-separated grains. Let us suppose that grains of powder are distributed in 50-60 μm range with maximum of distribution of 55 μm . Dry the powder, pour it into the graphite crucible, and sinter it using the HPHT System. The quality will depend on the shape and toughness of the grains, and the smoothness and purity of the grain surface. Use powder with spheroidal, smooth, tough grains.
3. The strategy for sintering micropowders with 1-10 μm grains, submicropowders with 0.1-1 μm grains and nanopowders with 0.001-0.1 μm grains is quite similar. Prepare the powder by milling or by another method. Separate the grains by size with help of liquid sedimentation or by another method. Make sure that the grains have a narrow size distribution and that they are at least 99% pure carbon. If not, lower the quantity of impurities by chemical treatment. Mix powder with organic liquid and agglomerate it. Ovalize the agglomerates and separate it by size. Preferable size distribution is 50-60 μm . Make "green body" by compressing at room temperature. Put a green body into the graphite crucible of reaction cell. Dry it up and dewax. Sinter it at pressure of $P > 8.0$ GPa, heating up to temperature of $T > 1800^{\circ}\text{C}$ with holding time of $\Delta t > 10$ seconds. If there are cracks, mix with micro-powder and sinter again.

These three different strategies are suitable not only for diamond, but for all powders of brittle ceramics. The value of pressure for other materials should not be so high.

3.4. Characterization of diamond powders and ceramics

DMI used the following methods for characterizing diamond powders prepared for sintering of BPCD.

1. The distribution of grain size was studied by liquid sedimentation (fig.3.4-1) and by SEM.
2. The shape of grains and structure of the surface has been studied using an optical microscope (fig.3.4-2, fig.3.4-3) and with help of SEM-imaging (fig.3.4-4, 3.4-5)
3. The purity of the powder was studied by x-ray structural analysis (fig.3.4-6), by the x-ray energy dispersive analysis, by weighting the ash, by x-ray diffraction analysis of the ash, TEM and x-ray energy dispersive analysis of ash (fig.3.4-7, 3.4-8)

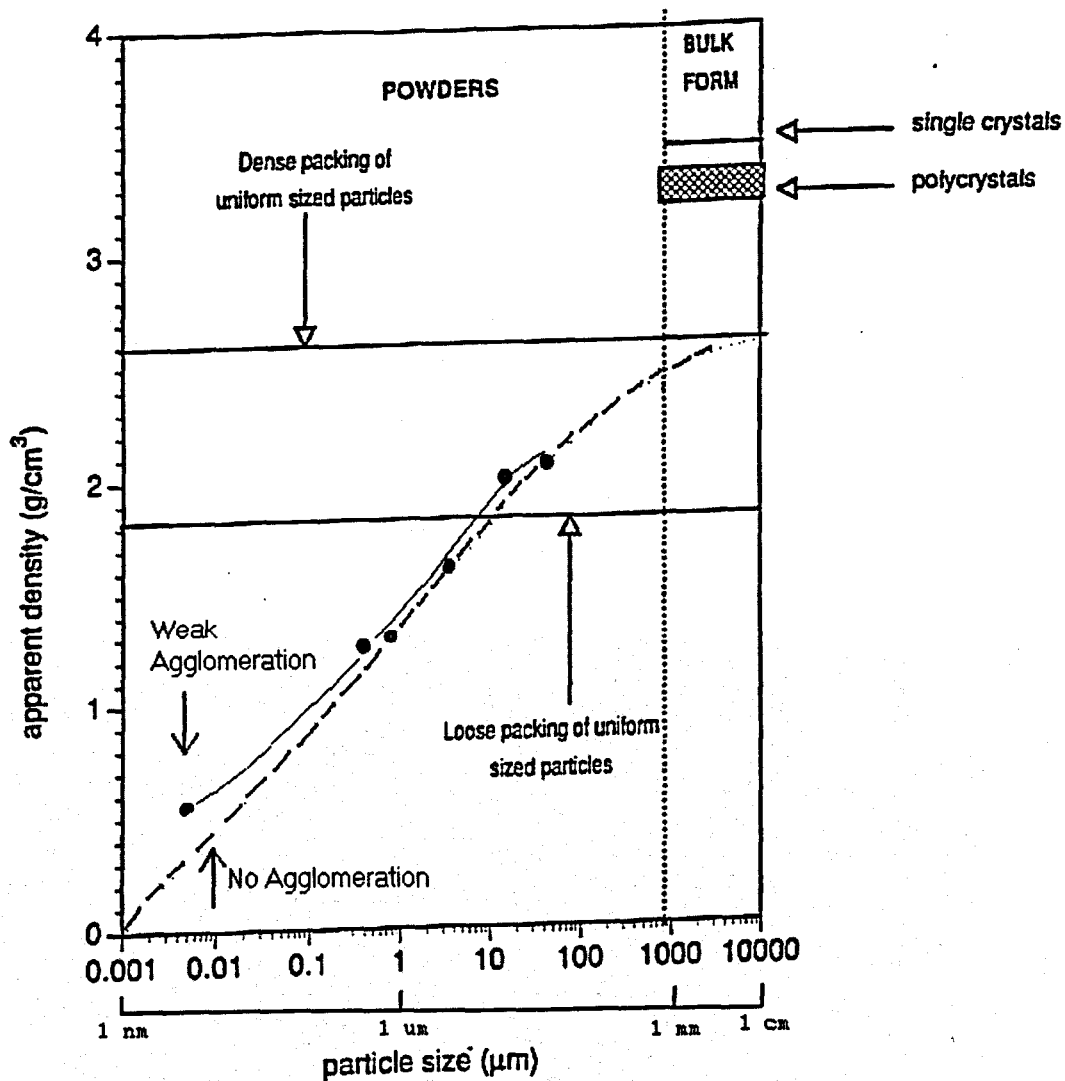


Fig. 3.4.0-1. Dependence of density as poured on grain size of diamond powders.

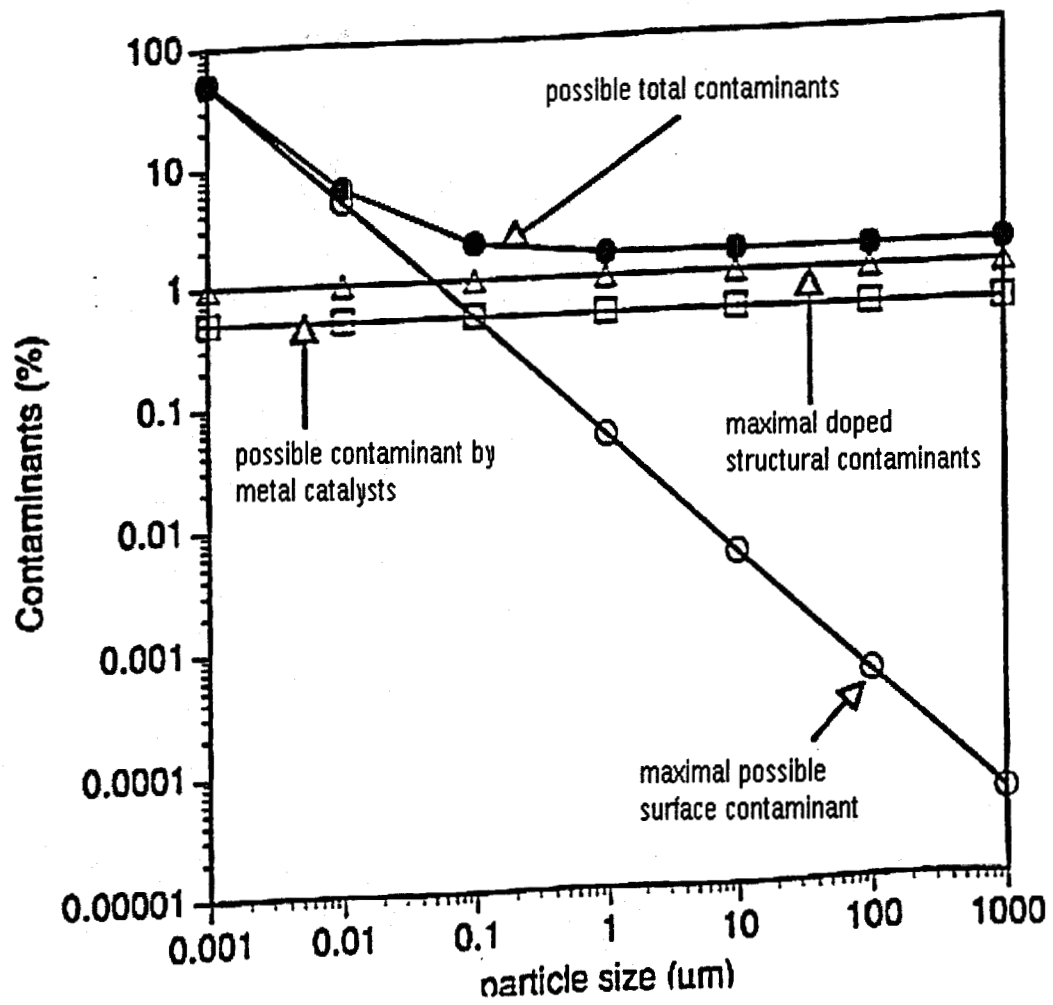


Fig. 3.4.0-2. Dependence of quantity of possible contamination on grain size.

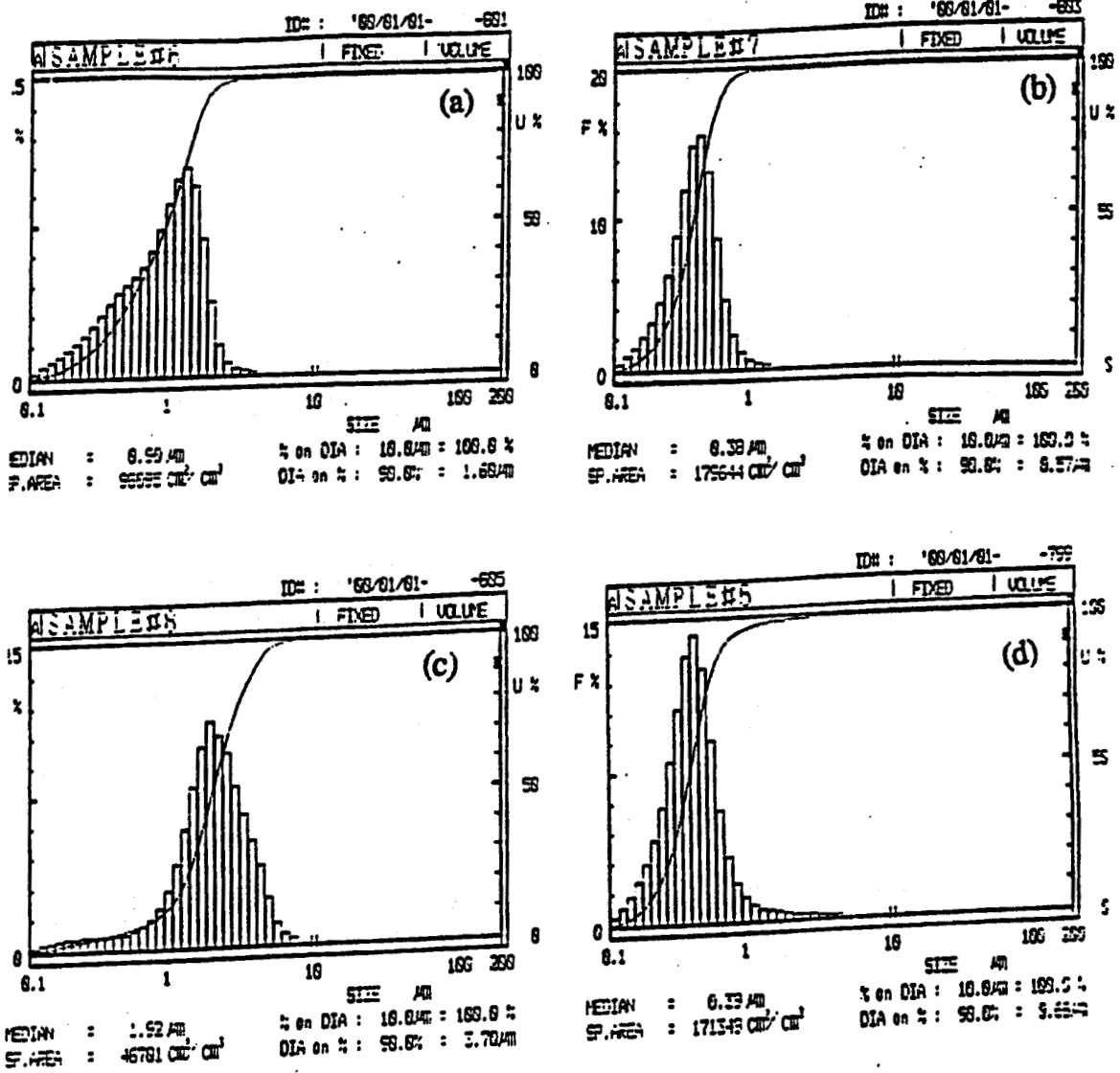


Fig. 3.4-1. The distribution of grain size by liquid sedimentation.

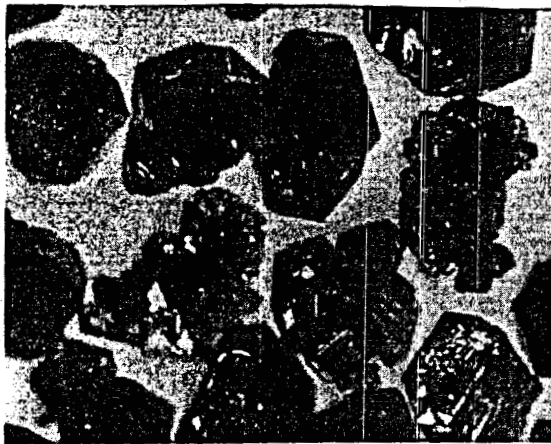


Fig. 3.4-2. Not milled diamond dust with high level of impurities



Fig. 3.4-3. Ellipsoid pure diamond powder

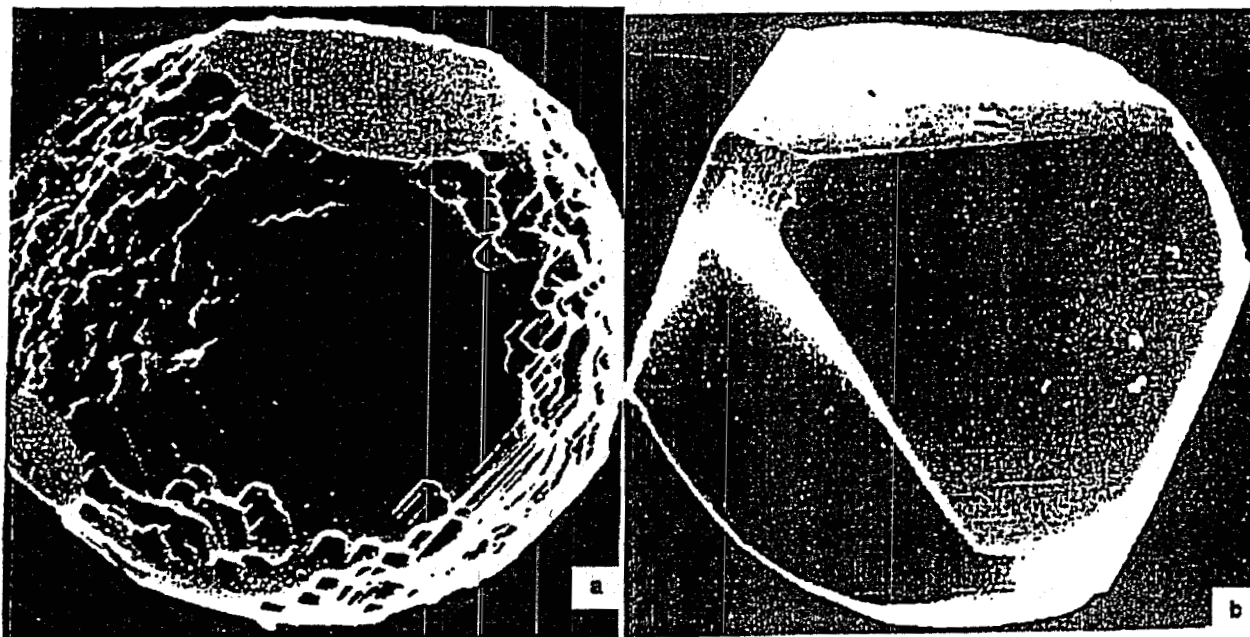


Fig. 3.4-4 and 3.4-5. SEM-images of diamond powder grains for sintering. The grains of powder should be spherically shaped (a). They should have smooth surface (b). The powder must have good compactibility. The quantity of impurities should be low. Fig. 3.4-4: Spherically shaped diamond grains. Fig. 3.4-5: Octahedrally shaped diamond grains with smooth surface.

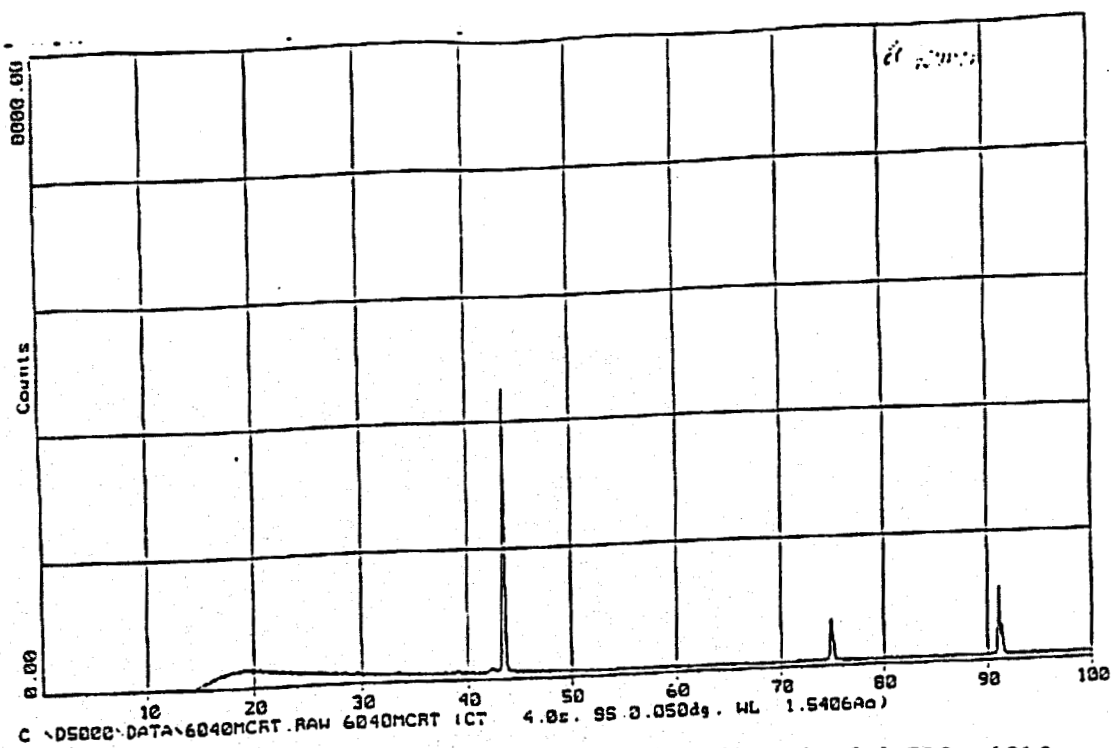


Fig. 3.4-6a. XRD of 40-60 μm diamond powder of good quality (the peaks of $2\theta=75.3$ and 91.3 are resolved).

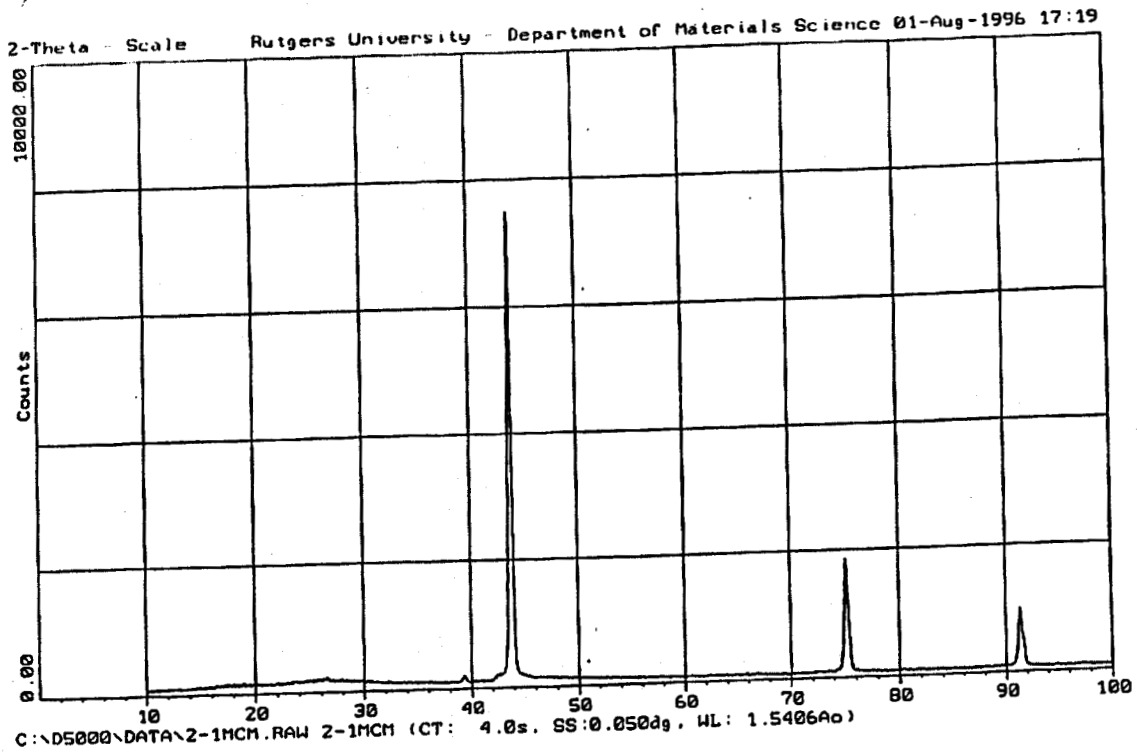


Fig. 3.4-6b. X-Ray pattern of 1-2 μm diamond powder. ($\text{CuK}\alpha$)

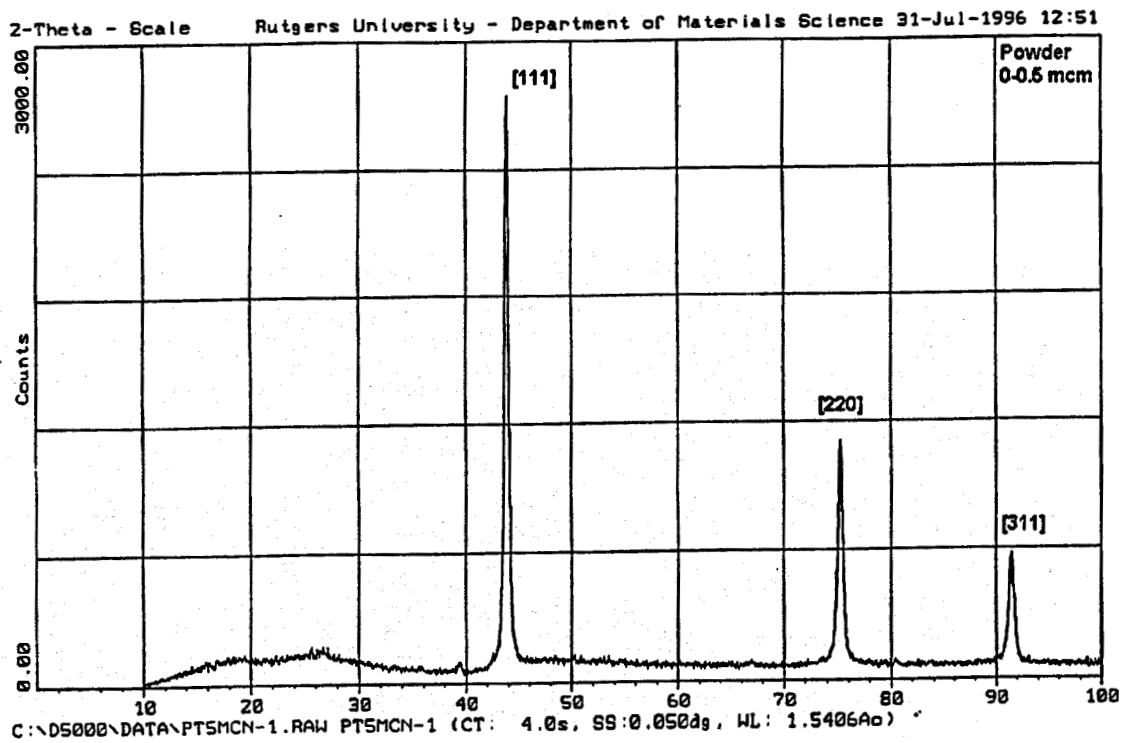


Fig. 3.4-6c. X-Ray pattern of 0.1-0.5 μm diamond powder. ($\text{CuK}\alpha$)

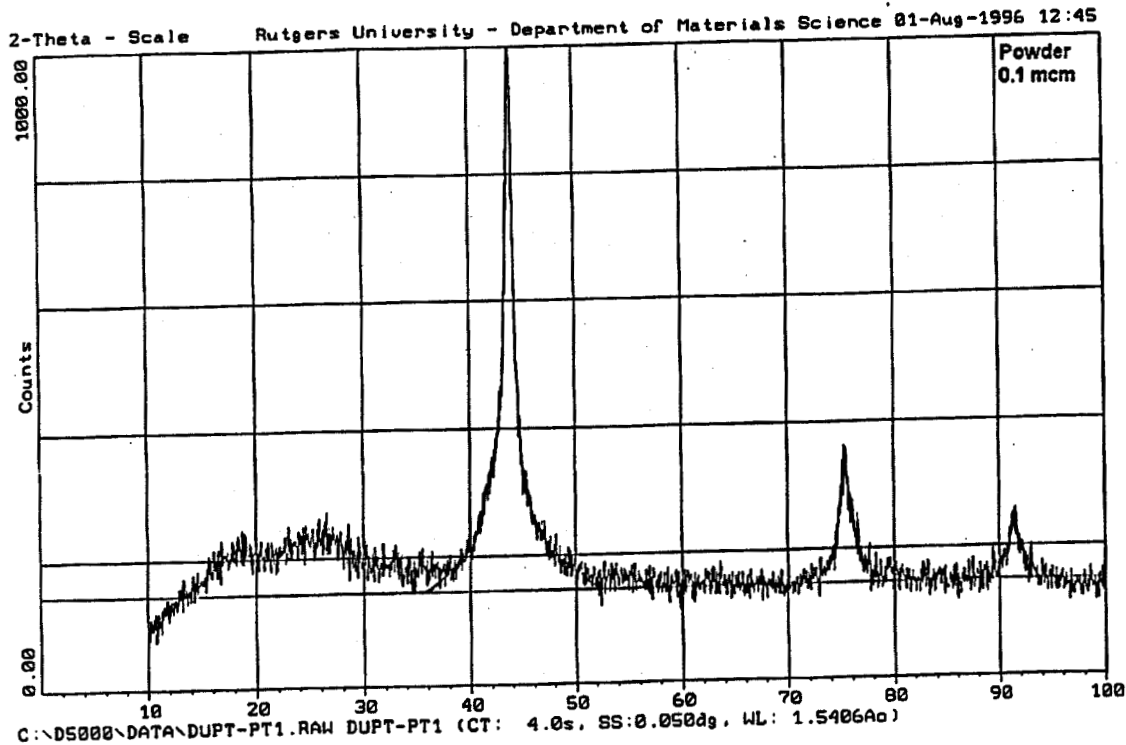


Fig. 3.4-6d. XRD of diamond powder with grains less than 0.1 μm

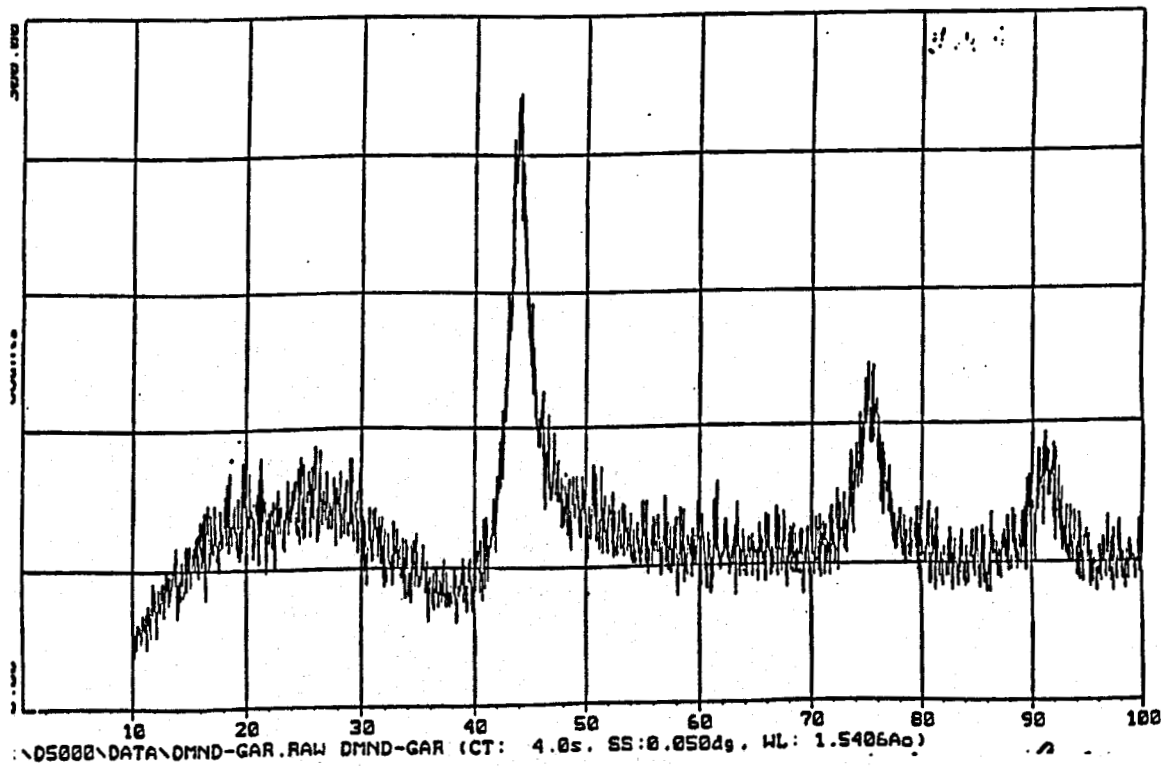


Fig. 3.4-6e. X-Ray pattern of 1-10 nm [7] diamond powder.

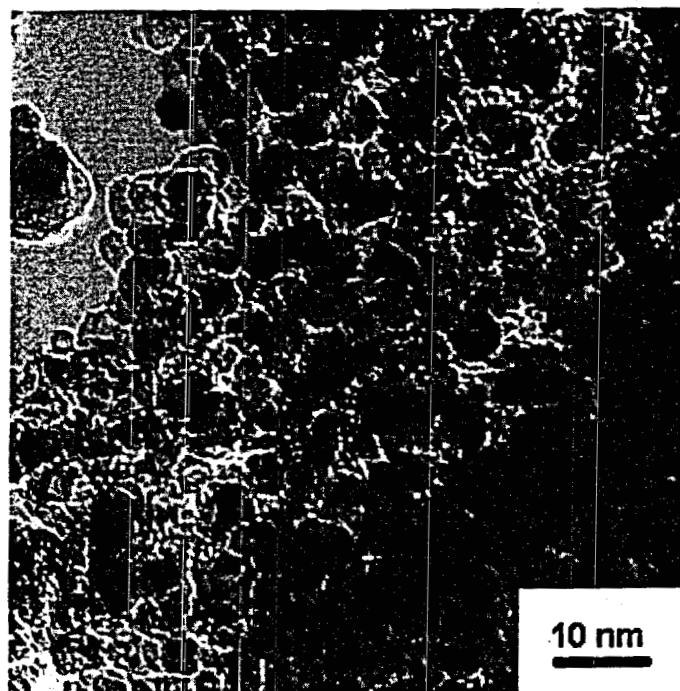


Fig. 3.4-6f. TEM-image of powder with grains of 1-10 nm [7].

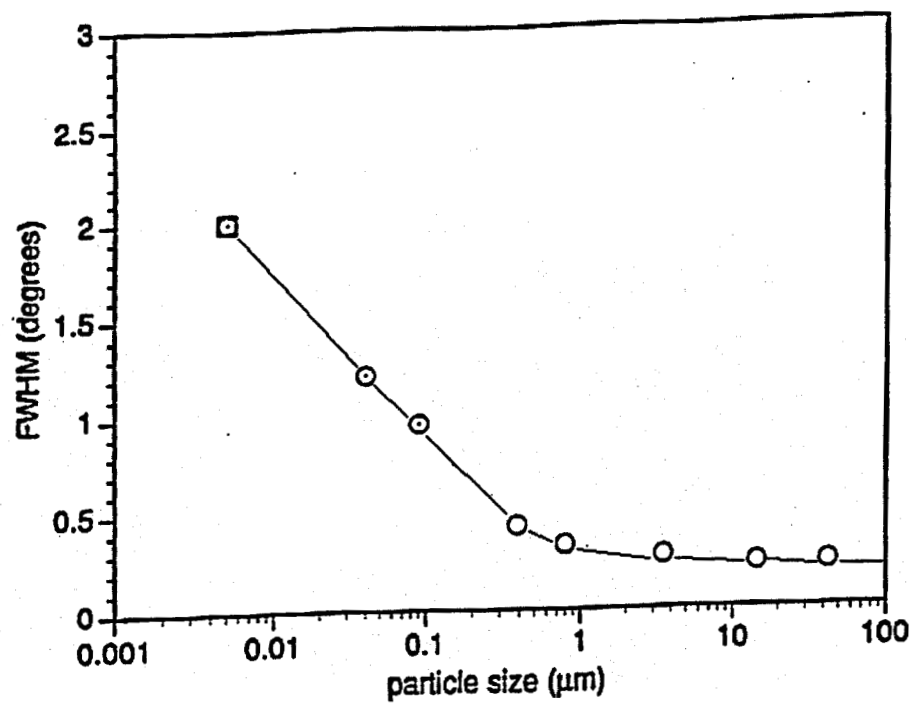


Fig. 3.4-6g. Dependence of XRD peak [111] width (on half-height) in $\text{CuK}\alpha$ on a size of diamond grains.

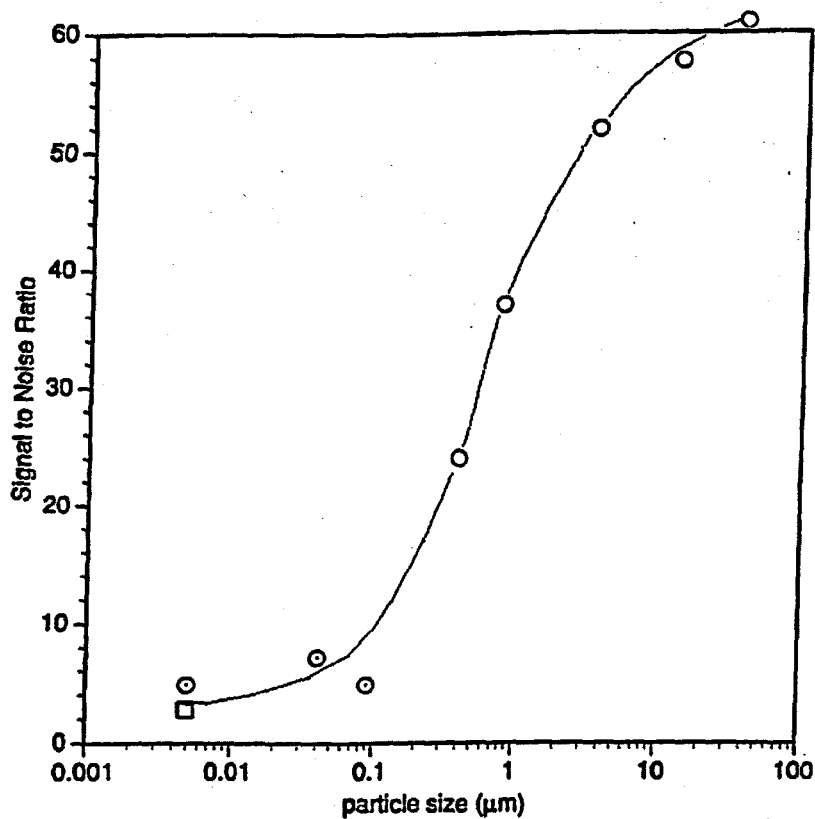


Fig. 3.4-6h. Dependence of signal to noise ratio for XRD [111] peaks in CuK_{α} on size of diamond grains.

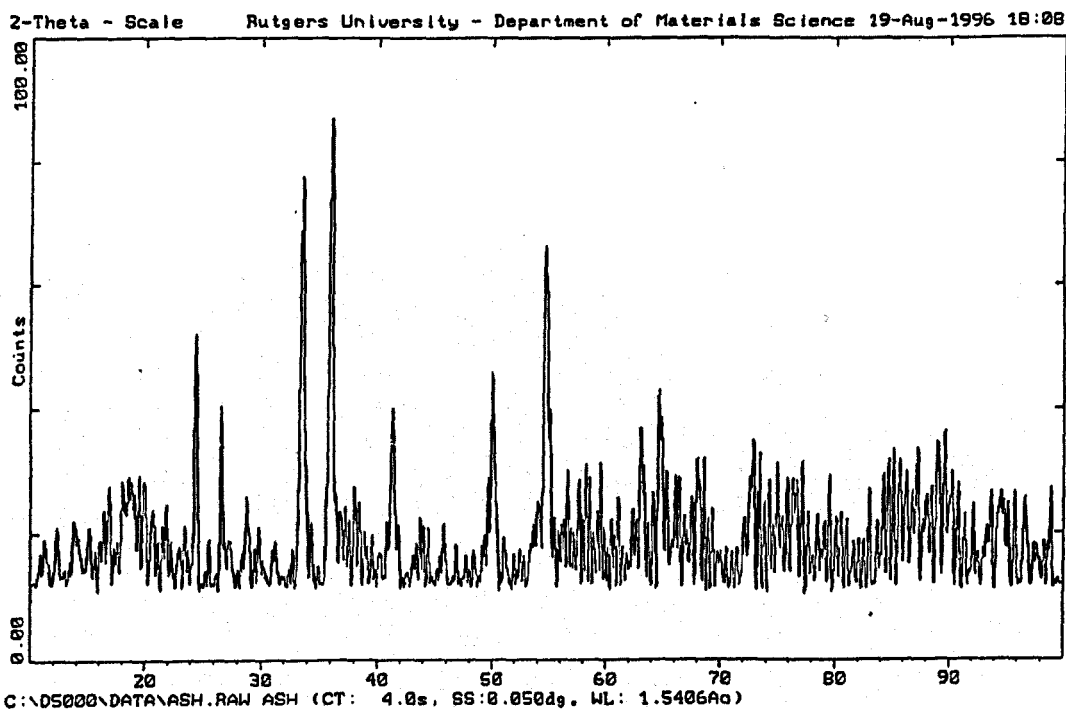


Fig. 3.4-7a. XRD of ash of diamond powder with grains of 1-10 nm.

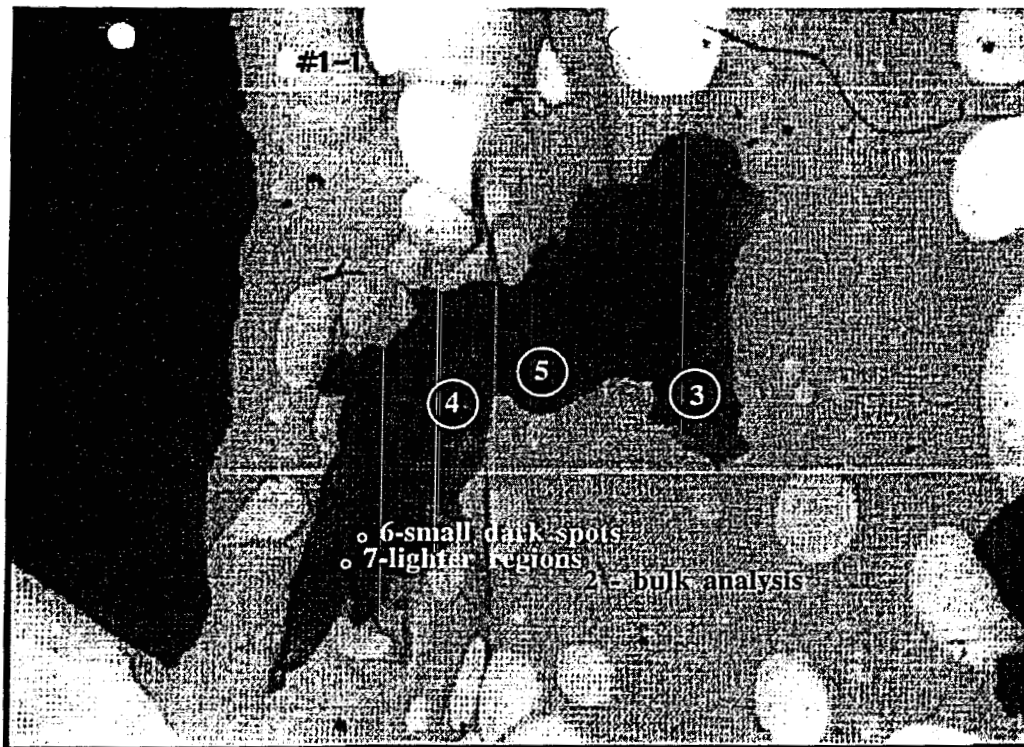


Fig. 3.4-7b. The grain of ash of pure diamond powder (without Ni, Fe, Co) on a sample holder (copper holder plus carbon film) in electron microscope prepared for element X-Ray energy dispersive analysis. This powder has extremely small ash residue after burning out of carbon. Fig. 3.4-7c. The same, b

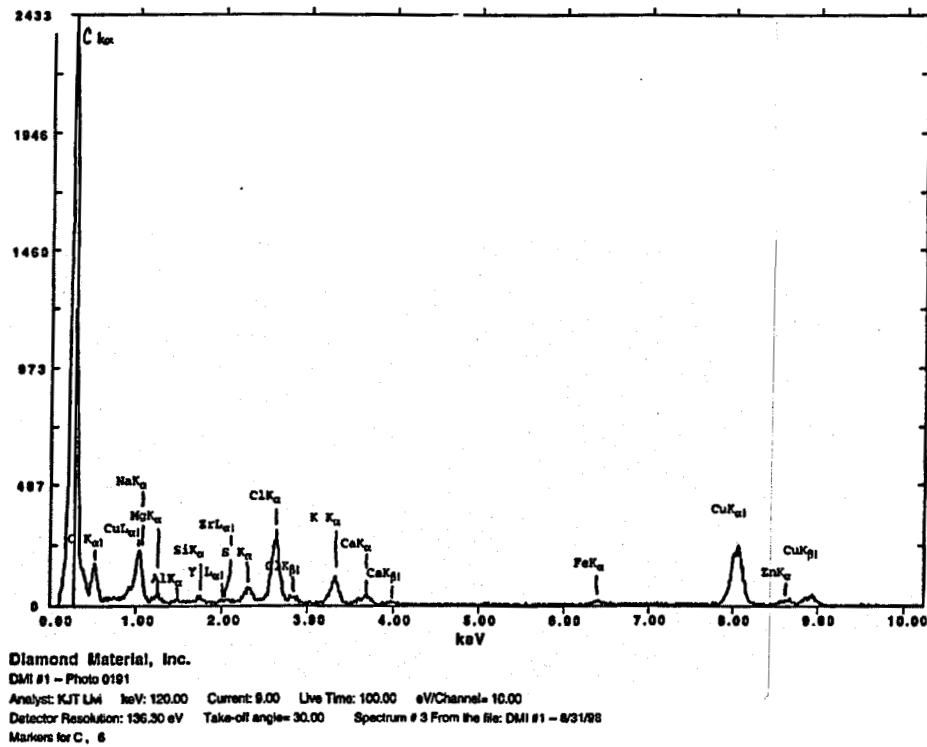
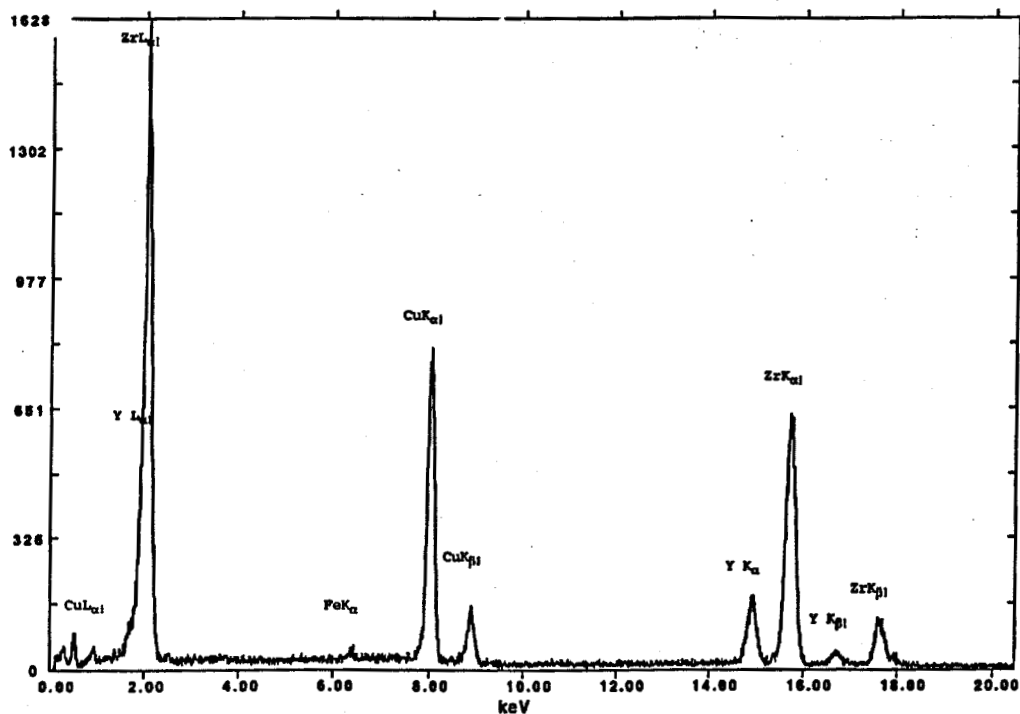


Fig. 3.4-7c. X-ray energy dispersive pattern for spot No. 3 of diamond ash grain shown in Fig. 3.4-7b.



Diamond Material, Inc.

DMI #1 - Photo 0190

Analyst: KJT LMI keV: 120.00 Current: 9.00 Live Time: 100.00 eV/Channel= 10.00

Detector Resolution: 136.30 eV Take-off angle= 30.00 Spectrum # 1 From the file: DMI #1 - 8/31/98

Fig. 3.4-7d. X-ray energy dispersive pattern for bulk analysis of diamond ash grain from fig. 3.4-7b. Carbon and copper peaks might appear from holder. The device does not show hydrogen, helium, lithium, beryllium or boron.

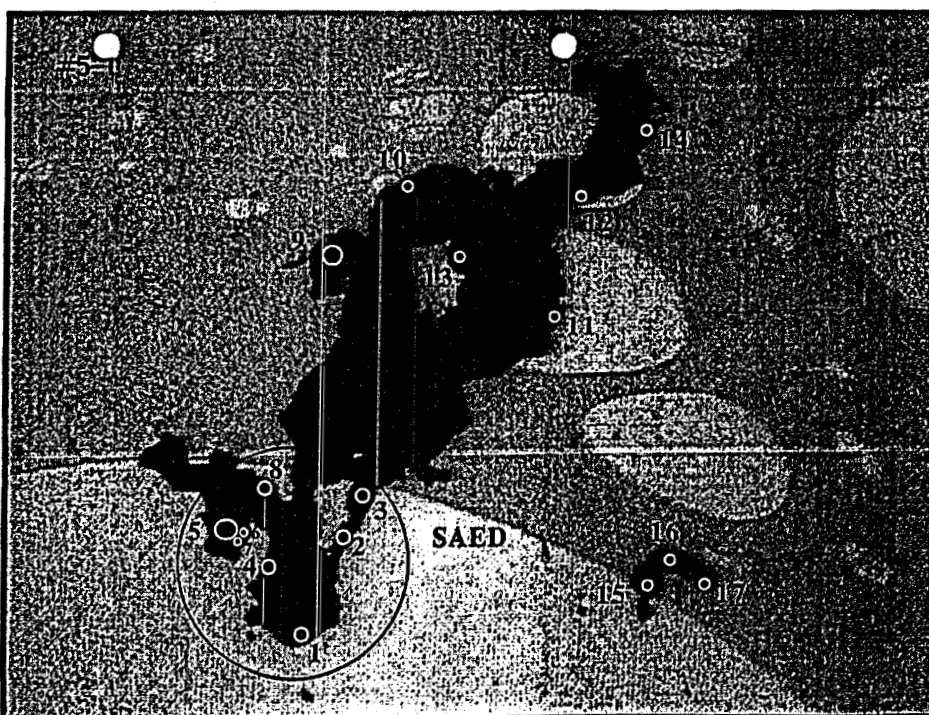
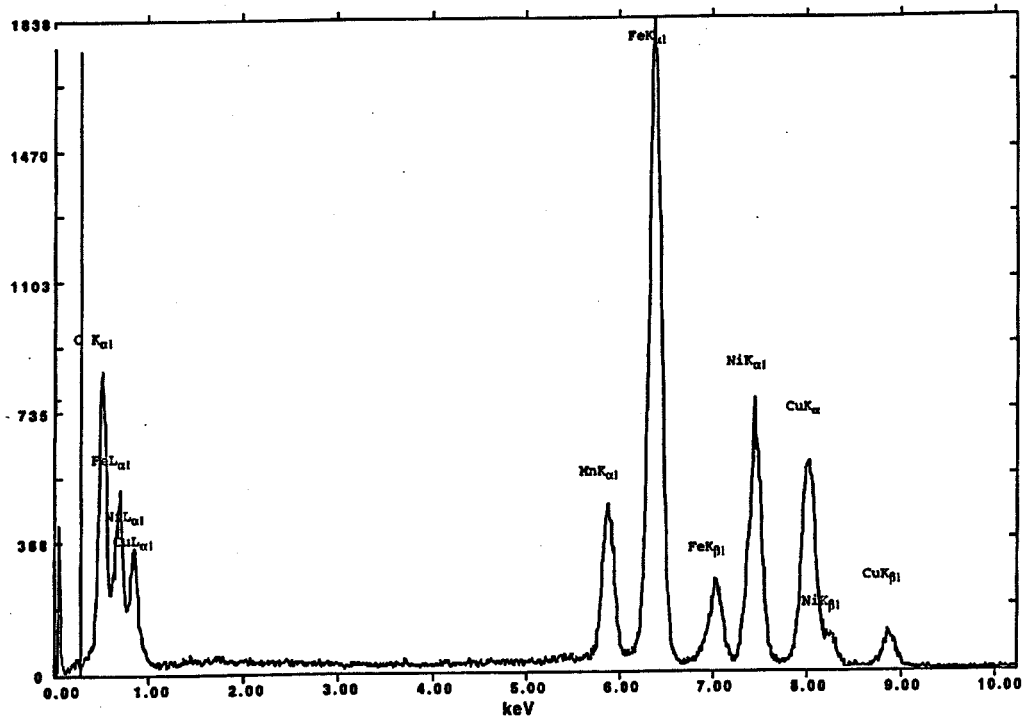
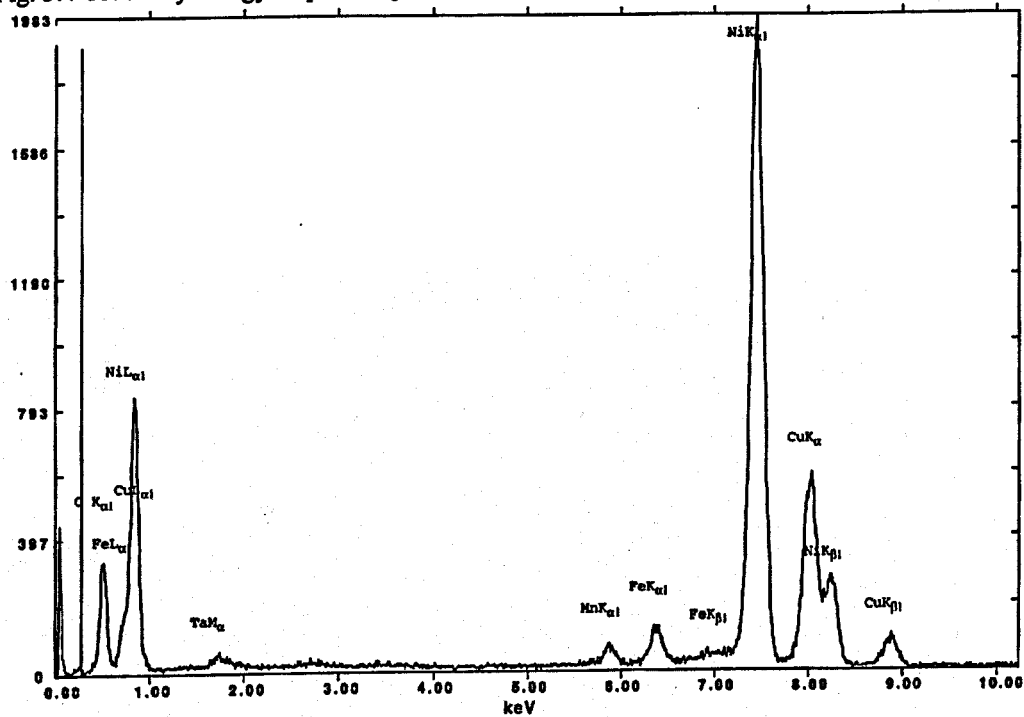


Fig. 3.4-8a. The grain of ash of diamond powder with detectable quantity of Ni, Fe, Co impurities, prepared for X-Ray energy dispersive analysis on a sample holder in electron microscope.



Diamond Material, Inc.
DMI #5 photo 281
Analyst: KJT LVI keV: 120.00 Current: 9.00 Live Time: 47.00 eV/Channel= 10.00
Detector Resolution: 136.30 eV Take-off angle= 30.00 Spectrum # 1 From the file: DMI #5 - 8/31/98
Markers for C, 6

Fig. 3.4-8b. X-ray energy dispersive pattern for spot No. 1 of diamond powder ash shown in fig. 3.4-8a.



Diamond Material, Inc.
DMI #5 photo 281
Analyst: KJT LVI keV: 120.00 Current: 9.00 Live Time: 50.10 eV/Channel= 10.00
Detector Resolution: 136.30 eV Take-off angle= 30.00 Spectrum # 2 From the file: DMI #5 - 8/31/98
Markers for C, 6

Fig. 3.4-8c. X-ray energy dispersive pattern for spot No. 2 of diamond powder ash shown in Fig. 3.4-8a.

Numerous methods have been applied to study mechanical properties, microstructure and cutter applications of BPCD:

1. Wearing of diamond by SiC wheel (fig.3.4-9). This method shows very quickly the quality of every sample. The device is very simple. It is the electronic balance and grinder equipped with silicon carbide wheel.
2. Hardness measuring of WC/Co parts and diamonds. The hardness of samples has been measured on Mohs scale, Rockwell scale and Vickers scale. We adduce just Vickers scale data in this Report. The data for sintered fine-structured WC/Co parts (hardness, density and fracture strength) was obtained partially by Rutgers' students with help of Rutgers equipment.
3. Toughness measuring of WC/Co parts and diamonds. Cylindrical samples has been ground and polished. The fracture strength at compression was measured with help of "Instron". The samples were destroyed between WC/Co anvils, supported by steel rings. Thin copper foil was located between anvils and sample surface. The sample was inserted into rubber ring to prevent flying fragments apart.
4. Thermalstability (fig.3.4-10) in argon and in air (fig.3.4-11). It has been measured by evaluation of fracture strength after heating up to 1200⁰C in argon that corresponds to the temperature of brazing. The thermalstability in air has been measured by long term heat treatment at temperature up to 600⁰C (this is a temperature range where the diamond oxidation rate is still negligibly small). It has been also measured by machining of heated granite logs (up to 400⁰C) by diamond cutters.
5. Oxidation of diamonds in air at 500-1200⁰C range (fig.3.4-12).
6. Wearing of granite by WC/Co and diamond cutters. This study has been accomplished at Kansas State University with help of equipment described lower.
7. Microstructure study with help of SEM (fig.3.4-13) This study clearly shows that compressed diamond grains plastically flow at temperature greater than 1200⁰C, remarkably decreasing porosity. The density increases in this temperature range. The grains sinter together through self-diffusion of carbon atoms. This diffusion occur quickly enough at temperature greater than 1800⁰C. The SEM-image shows very clearly how boundaries between grains disappear and quantity of pores impetuously decreases. Meanwhile the toughness and wear resistance tremendously increase. It is not too easy to make such SEM-images. The diamond surface should be polished extremely well. Proper chemical treatment should be provided for all samples after polishing. The surface should be coated by very thin conducting layer. Since the diamond has extremely high electrical resistivity, the surface could be charged by electrical beam at once. Charged surface will reflect on-coming electrons and picture will quickly disappear. High resolution SEM-imaging of diamond takes a lot of time and funds. Although that photopicture do not look really great, it is a challenge to get it! The X-Ray diffraction pattern of BPCD (fig.3.4-14) shows that it is a diamond. The intensity of peak that might belong to graphite is very small. It could be a graphite on a surface of grains within pores. The pressure and stresses on such surfaces are not high enough to prevent the graphitization of diamond at high temperature.

Table 3.4-1. Some properties of BPCD

Density ρ (g/cm ³)	Strength (GPa) σ_{fst}	Load force on a grain 0.5 ct;(ton)	Thermal Stability* σ_T/σ_o	Thermal Conductivity W/(mK)	Resistivity Ω .cm	Abrasive Wear ** mg/min	Hardness H_v (GPa)
3.1-3.5	3.8-4.2	1.0-1.1	1200C without changes	300-600	$>10^{+12}$	1-2	75

*Holding in argon for 30 min.

**The weight loss after wearing by SiC-wheel at linear speed of 1700 m/min and load force of 10-20 N.

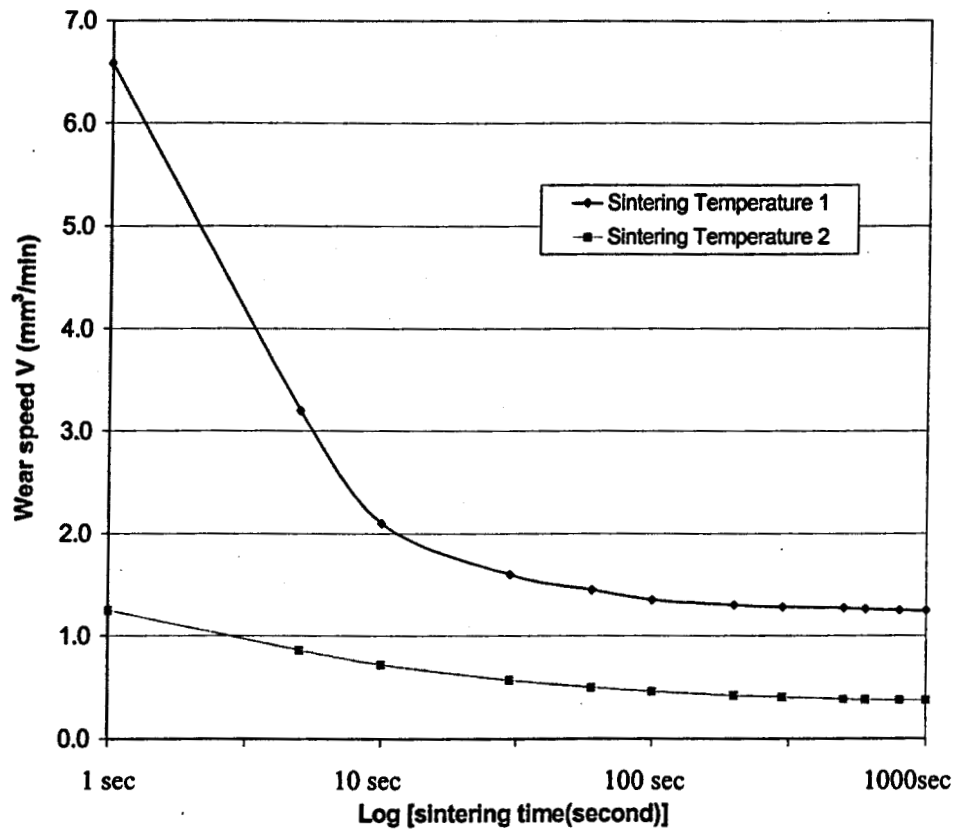


Fig. 3.4-9. Dependence of wear speed (v) of binderless diamond compacts on duration of sintering; (wearing by SiC grinding wheel).

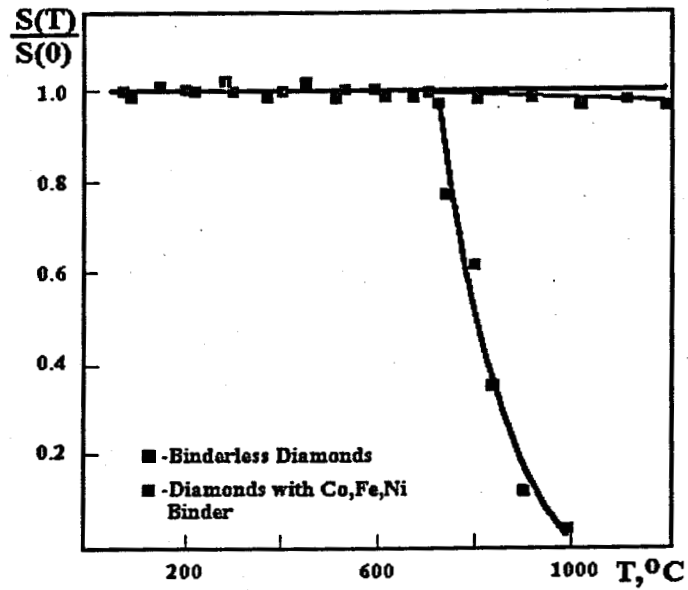


Fig. 3.4-10. Dependence of Compressive Strength $S(T)$ on Temperature in Inert Gas for Binderless Diamonds and Diamonds with admixtures of Co, Fe, Ni.

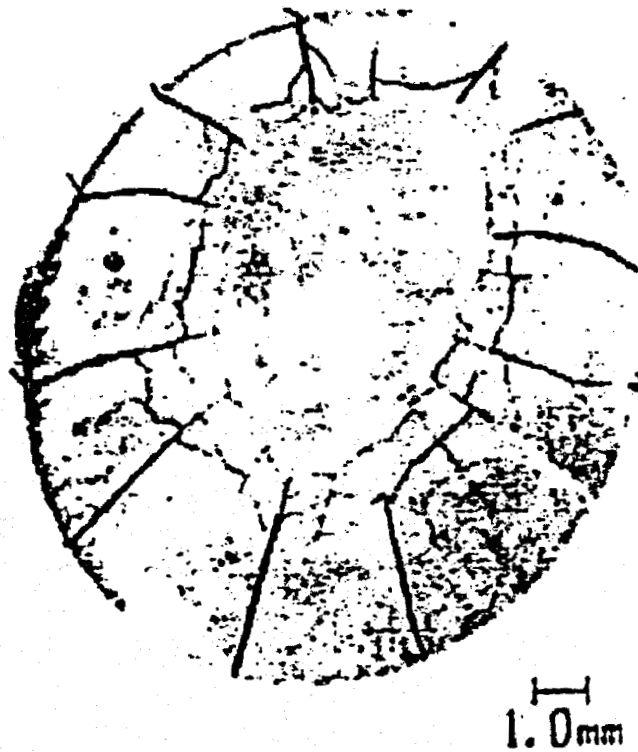


Fig. 3.4-11. Fracture pattern for a fine-grained drill blank heated for a long time. The diamond table spalled off the carbide substrate. [11] BPCD does not crack like this.

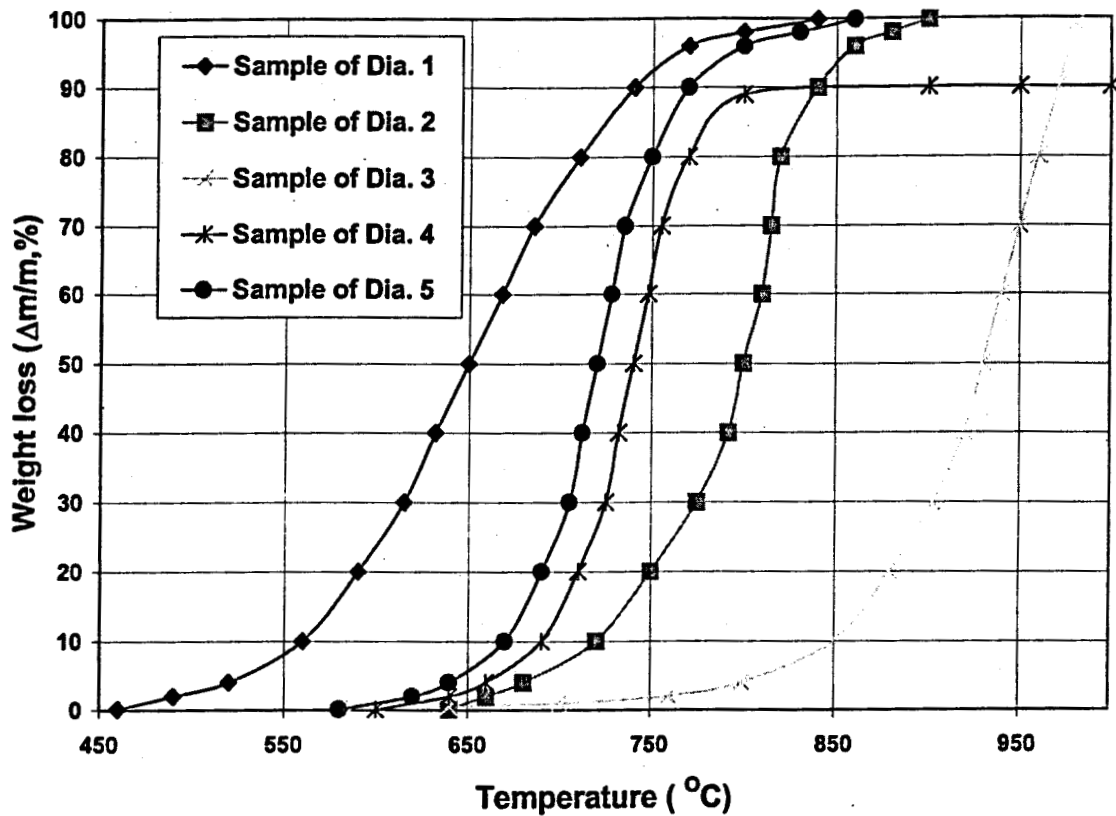


Fig. 3.4-12. Oxidation of diamond powders and BPCD in air.

No. 1—powder 0-1 μm ; No. 2—powder 10-40 μm ; No. 3—powder 500-630 μm ; No. 4—triphasic sponge composite; No. 5—BPCD. Rate of heating is 0.25 $^{\circ}$ /min.

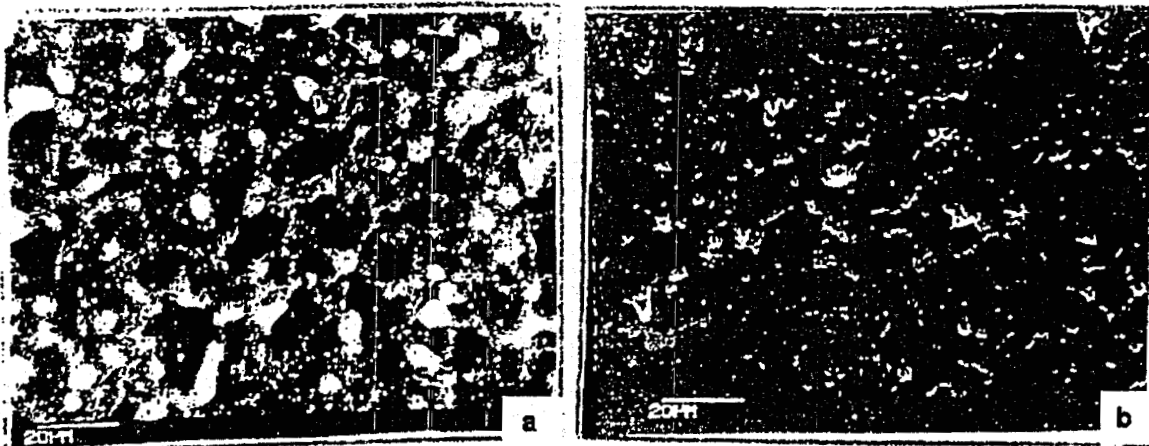


Fig. 3.4-13. SEM-image of BPCD. a) P=8 GPa, T=1200 $^{\circ}\text{C}$, t=80 sec.; b) P=8 GPa, T=1500 $^{\circ}\text{C}$, t=30 sec.

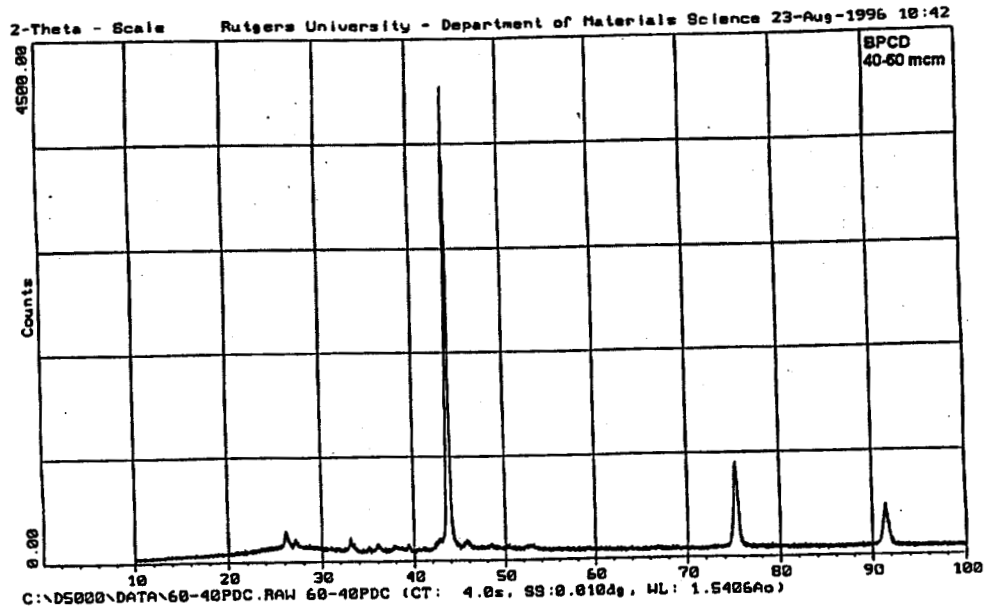


Fig 3.4-14a. XRD of BPCD (40-60 μ m crystallites).

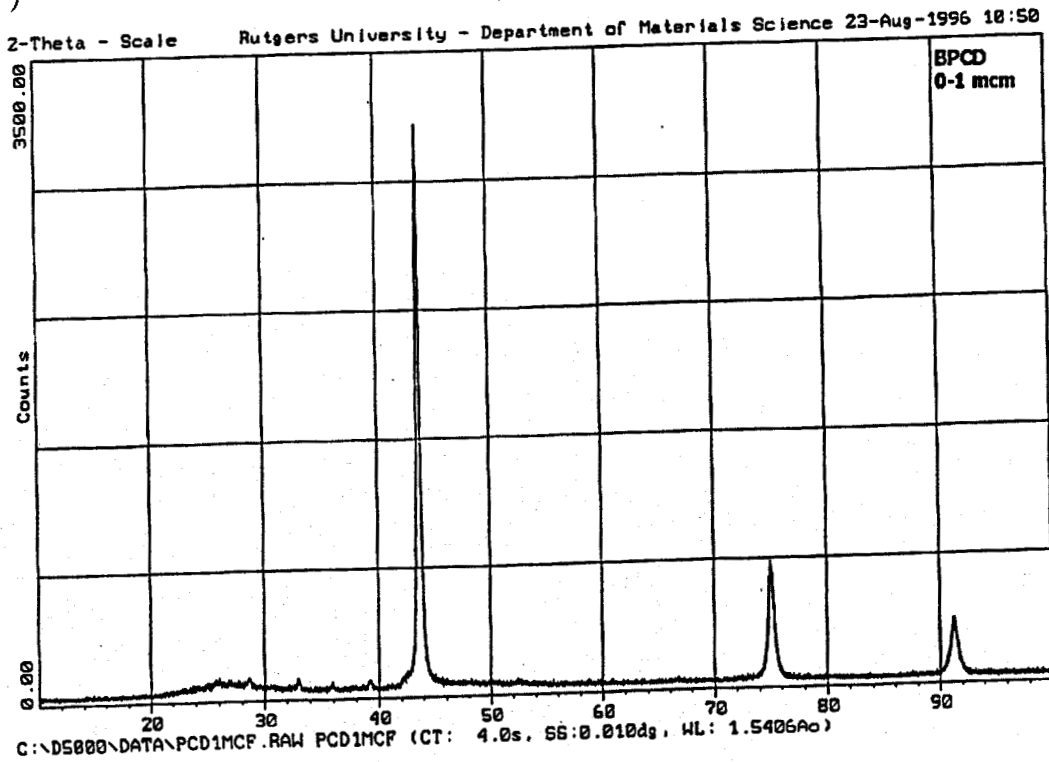


Fig. 3.4-14b XRD of binderless polycrystalline diamond (BPCD) sintered from powder with grains less than 1 μ m (in $\text{CuK}\alpha$).

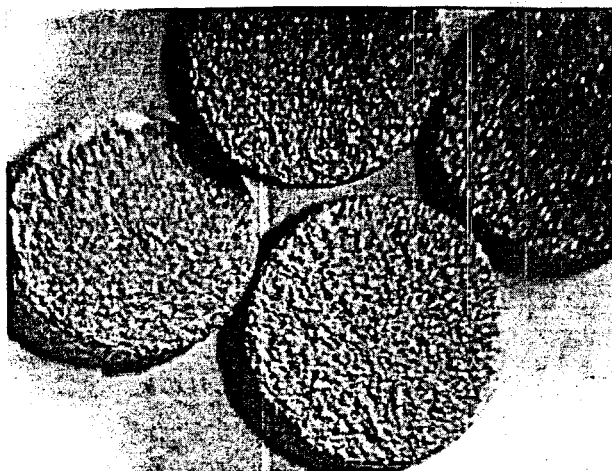


Fig. 3.4-15a. BPCD samples of ϕ 4mm after sintering.

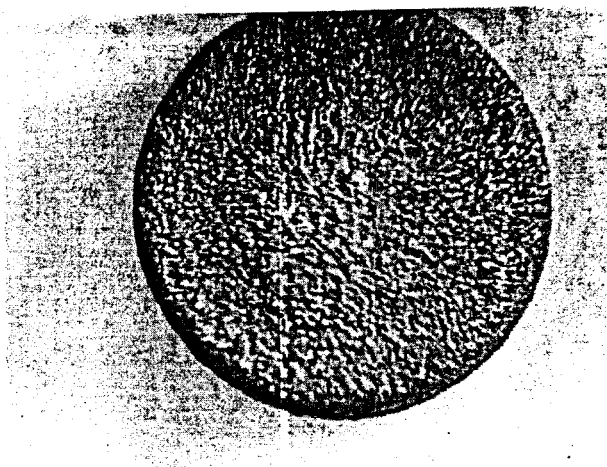


Fig. 3.4-15b. BPCD sample of ϕ 6mm.

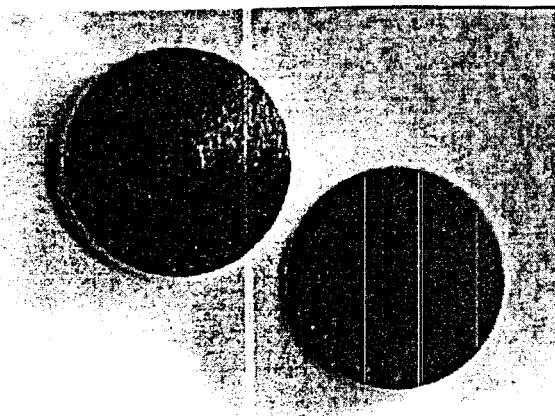


Fig. 3.4-15c. Polished samples of BPCD.

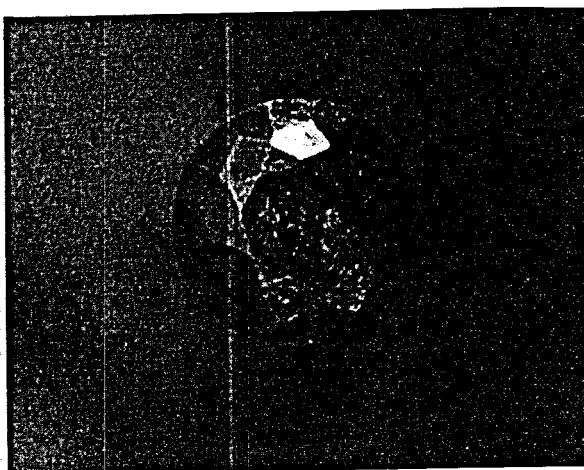


Fig. 3.4-15d. Facetted sample of BPCD. (The faceting is a more difficult operation than for single-crystalline diamond.)

3.5. Testing BPCD samples

The BPCD, PCD, and natural diamond properties that are important for cutter applications are: apparent density, Vickers hardness, Mohs hardness, compressive strength, average strength for crushing a sample with certain characteristic size, impact strength, abrasive wear resistance, and wear resistance in specific applications. When cutting tools are used in air also important is the oxidation rate. This is especially important for smaller grain PCDs, where high surface areas can lead to very significant oxidation rates.

For the current project we considered two very important characteristics: (1) strength in air as a function of temperature; and (2) strength in inert atmosphere as a function of temperature. The first parameter is important for geothermal applications. The second is important for making diamond tools by brazing and other methods.

The prototype of the HPHT system has been developed that permits diamond powder sintering in all size ranges. The compacts are able to machine and wear the stones of all types from soft through medium to hard rocks. The prototype compacts have been sintered and studied. Nevertheless, we have to admit that sintering of nanopowders is still a challenge. First of all, nanopowders are more expensive than powders of micro-ranges. The cleaning, chemical treatment, separation, filtration, agglomeration are all procedures that take more time and more funds than conventional micron sintering with binders. Cleaning must be accomplished much more carefully than treatment of micropowders. The chemical purity of micro-grains is much easier to control. Fig. 3.5.1 shows how surface contamination might depend on grain size. Increasing the ratio of surface-volume atoms leads to new thermodynamic consideration that has technical benefits but cost trade-offs.

The BPCD data are listed in table 3.5.1 and in figures 3.5.1-3.5.10. The methods of NPCD manufacturing will be described below. It is interesting to note that it is possible to manufacture NPCD by a few methods, even with extremely small (1 mm) crystallite sizes. The solid state designed from extremely small crystallites takes on new and unusual properties and demands a different thermodynamic approach. We are planning to apply such compacts for machining of polymeric materials and glasses for optical lenses. There is also project for drilling, machining and digging on Mars, where NPCD will be used with beryllium holders. Beryllium holders are necessary on Mars, since they are 4 time lighter than steel ones, strong enough and provide opportunity to decrease the weight lunched. The density of NPCD is almost the same like for all other BPCD and do not give the weight economy itself, but just on an area, where it might be used instead of WC/Co.

3.5.1 Testing methodology

Well-sharpened and polished diamond cutters can machine any material with high rate and efficiency; nevertheless, the cutters get dull very quickly. Sharpening of diamond cutters is a routine procedure in any machining operation, with the exception of deep well drilling. In a drilling operation, the drill bit must survive as long as possible, since replacement costs are high.

In order to penetrate the rock formation, the effective contact pressure on the cutter should exceed the hardness of the rock. When the contact area is relatively large, the frictional force also becomes large. The resulting frictional heating at the cutting edge therefore increases, which degrades the performance of the cutter. The computerized granite log testing equipment at Kansas State University [9] enables us to study the distribution of load and temperature during the cutting operation. A lathe with strain gauges, thermocouples, analytical-digital converter, and computer is used to evaluate the cutter performance and to improve its design.

For testing machining capabilities, sintered diamond compacts were clamped or press-fitted into a steel holder at room temperature. In order to avoid possible changes in the diamond characteristics, we deliberately avoided brazing. One diamond edge was sharpened and polished for the cutting operation. All samples were operated until they lost at least 50% of their initial weight through wear.

Granite logs about 8.5" diam. x 12" long were worn by diamond cutters at a feed rate of 0.010 in./rev., depth of cut of 0.010", and speed of 359 ft./min. A schematic of the apparatus is shown in Fig. 3.5-1. and photographically in Fig. 3.5-2.

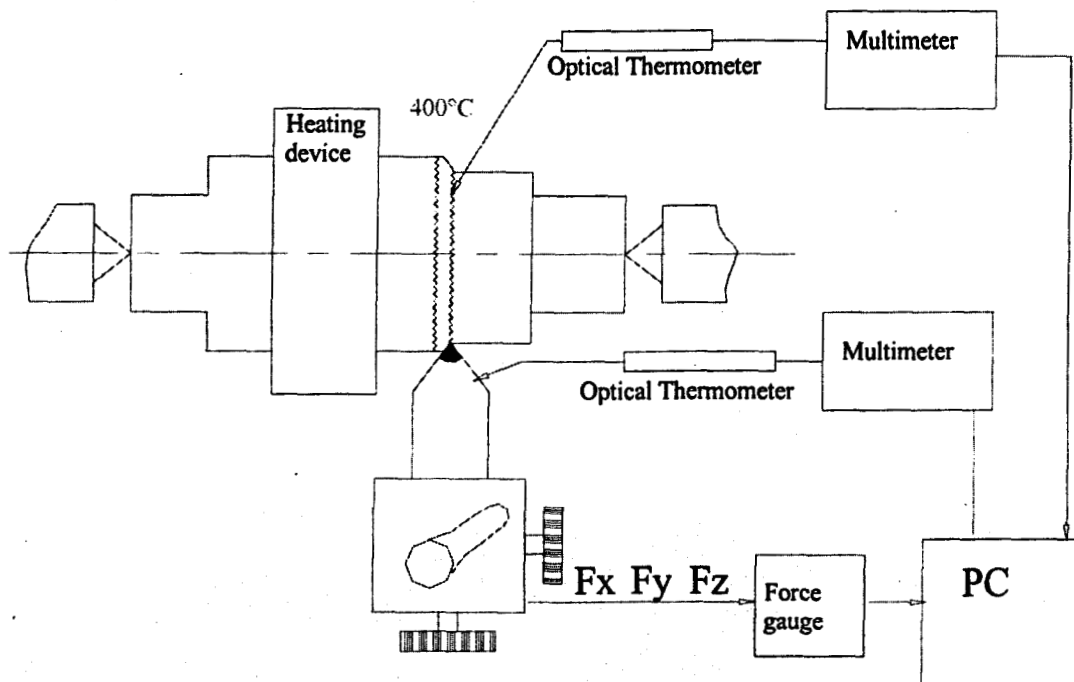


Figure 3.5-1. Schematic of apparatus for granite log wearing by diamond.

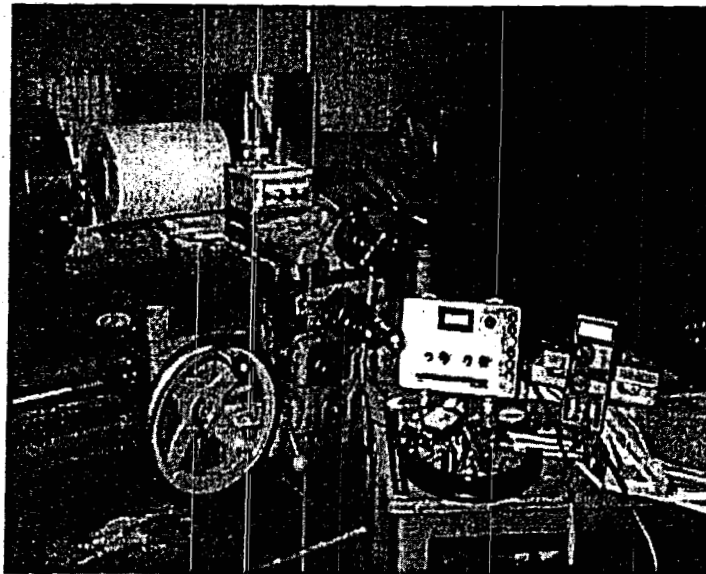


Figure 3.5-2. Photograph of test apparatus.

The experimental set-up consists of a robust numerically controlled lathe, strain gauge dynamometer mounted on the lathe tool post, specially designed tool holder to accommodate the diamond cutter and thermocouples, dial indicators to measure the wear profile of the cutter, a signal conditioning board and an A/D board feeding into a personal computer to acquire running data (forces and temperatures), circulating water cooling system, acetylene torch and optical thermometer. The tool holder containing the cutter and thermocouple was supported on a 3-axis strain gauge dynamometer mounted on the lathe crosshead. The dynamometer was custom built for this purpose by Lebow. The X direction is the normal or radial direction of the rock cylinder, the Y direction is the circumferential or cutting direction, and the Z direction is the side or feed direction towards the tailstock. The Lebow dynamometer was designated for force ranges 0-600 lbs. for X, 0-400 lbs. for Y, and 0-400 lbs. for Z, with an allowance of 50% overload. Cutting forces were sampled at 1-second intervals, and since there was a considerable amount of fluctuation, the forces were plotted using a moving 10-second average. The data acquisition system consists of an 8-channel resistance measurement accessory board (MetraByte EXP-RES), an 8-channel high speed A/D converter, and time/counter interface board (MetraByte DAS-8) compatible with an IBM PC. 'Labtech Notebook' software was used to record the data and to show a graphical display of the running data collected on different channels.

The first set of cuts was done on a granite log that was water-cooled. The circulated water cooled both the log and the cutter. In these experiments, we compared the wear of granite by binderless compacts, by natural single crystal diamond of cubical and octahedral habit, and diamond composite materials with admixture of alloys containing Co, Fe or Ni.

The samples were heated at 100, 200, 300, 400 and 500°C in air for 8 hours. After heat treatment, the wear ratio (WR) was measured again. Binderless diamonds had the same WR, but diamonds with Co, Ni, and Fe admixtures had lower WR. There was no

visible reaction with oxygen or nitrogen at 500°C, but oxidation commenced in air at 600°C.

The second set of cuts was done on a granite log heated to 100°C, 200°C, 300°C and 400°C by torch heating. The log temperature was measured by optical thermometer. As will be shown later, there is no great difference between different diamonds or diamond composites with respect to "dull" wearing of cold granite, provided that the diamonds had no previous heat treatment. In this case, 1 cm³ of diamond can remove about 200,000 cm³ of the hardest granite. Only thermally stable binderless polycrystalline diamond or natural single crystal diamond is suitable for machining hot rock formations without cooling. In addition, thermally stable diamonds are much better at cutting hot rock than cold rock formations.

3.5.2 Testing Results

When the diamond cutter is sharp, it cuts granite very well. Initial wear ratios (WR) for different types of diamond materials are shown in Fig.3.5-3.

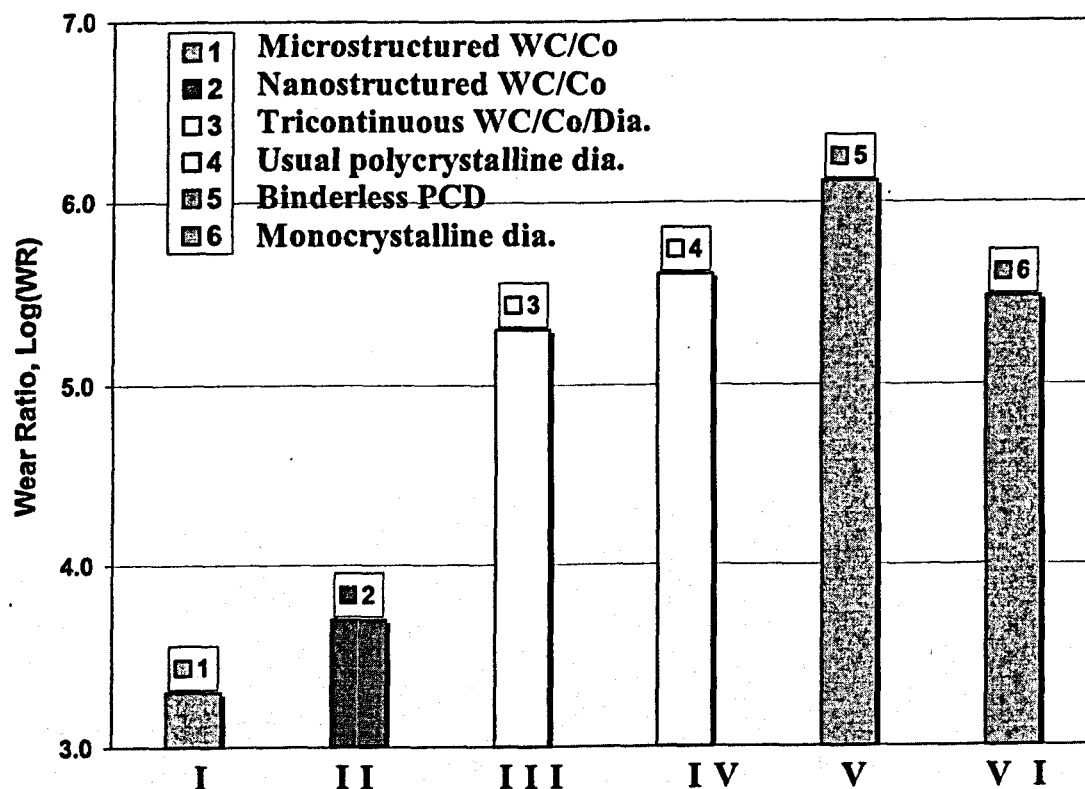


Figure 3.5-3. Wear ratios for diamond materials and hard alloys on granite.

I - Microstructured WC/Co

II - Nanostructured WC/Co

III - WC/Co/diamond sponge composite

IV - Industrial polycrystalline diamond layer on WC/Co substrate

V - Binderless polycrystalline diamond

VI - Natural monocrystalline diamond (2 ct. cube)

Sharp diamond cutters could remove at least 1,300,000 cm³ of granite per 1 cm³ of diamond. Fig.3.5-4 shows the dependence of WR on the number of cuts for the natural single crystal diamond cube cutter. While the corner of the cube remains relatively sharp, it cuts with good WR=1,000,000 – 1,300,000, then the wear ratio stabilizes at the level of WR=189,000. (Fig. 3.5-5, 3.5-6).

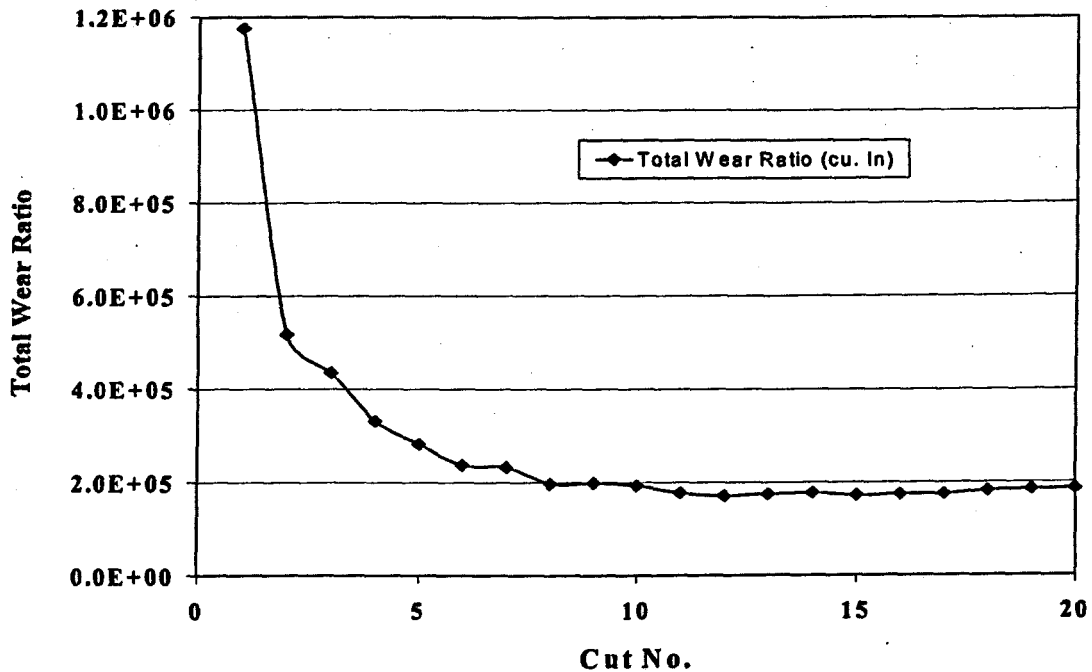


Figure 3.5-4. Plot of total wear ratio vs. number of cuts using a natural single-crystal diamond cutter (cube form, 2 carat weight).

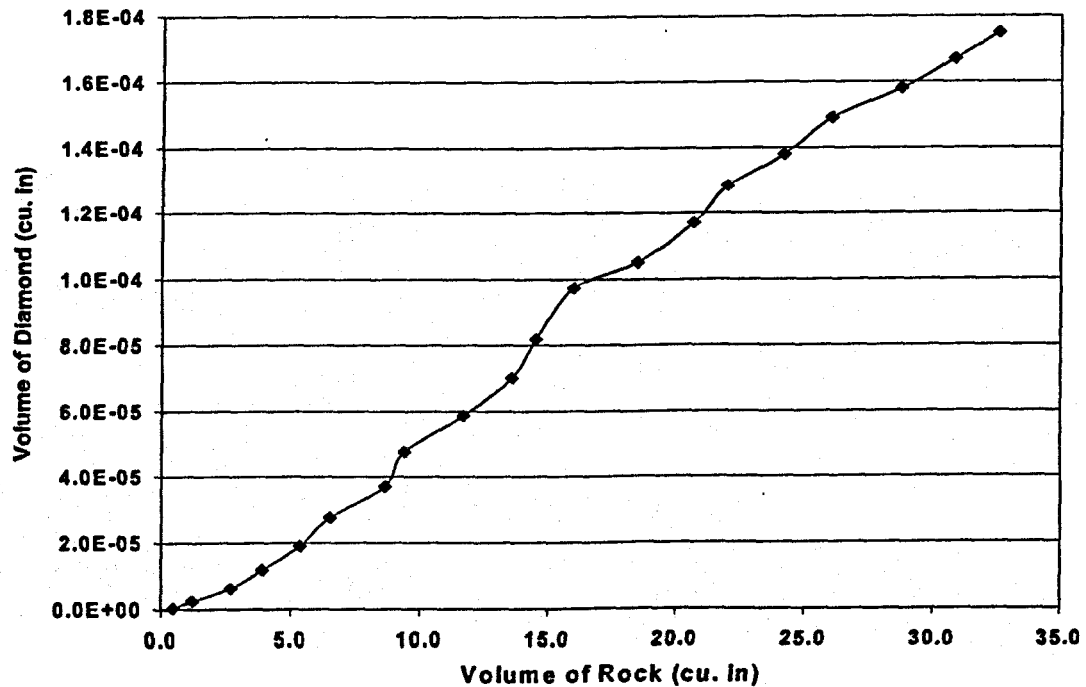


Figure 3.5-5. Wear of granite by a dull cutter of natural single-crystal diamond (cube form, 2 carat weight)

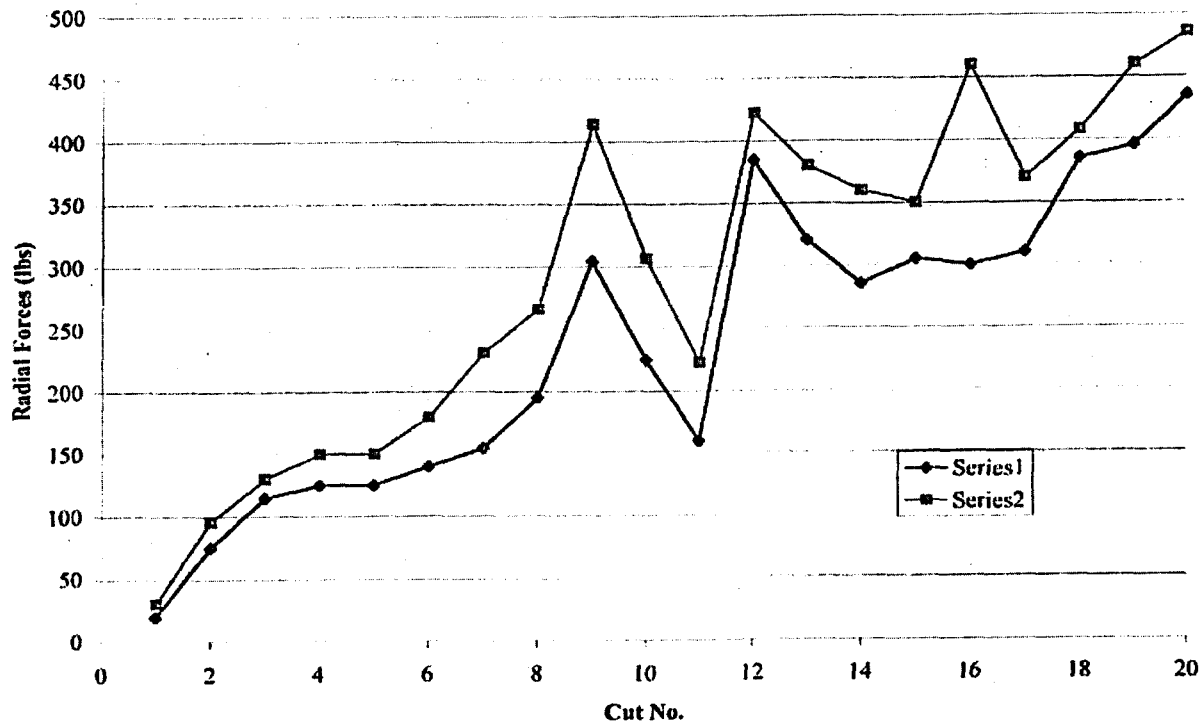


Figure 3.5-6. Dependence of radial force on number of cuts, showing increase due to dulling of the diamond cutter.

For diamond monocrystals the vertex of the octahedral crystal starts cutting granite with a very high WR ratio. This can be explained by the fact that the monocrystal has 100 GPa hardness in this direction when its other directions are significantly softer with hardness of 50 Hpa. The high quality polycrystalline diamond has a uniform 75 GPa hardness. Thus PCD has a great potential as a sharp edge cutter. However, in practical application in cutting granite or other hard stone, the sharp edge will not last long, thus its performance for this application should be evaluated using dull samples.

The radial force F_x , grows from 50 to 500 lbs., as shown in Fig. 3.5-6. All diamond cutters degraded rapidly at 1000°C, due to frictional heating at the cutter rock interface. Binderless polycrystalline diamond cutters withstood short-term heating at 1200°C in argon and could be brazed onto metal holders without loss of strength. In contrast, polycrystalline diamonds with binder phase decomposed at 600°C - 1000°C. [7-9]. The brazing of contaminated diamonds and diamond composites is possible at pressures of 3.0-5.0 GPa (in the region of thermodynamic stability of diamond), which is high enough to suppress diamond decomposition [10]. Transition elements catalyze oxidation and graphitization of diamond in air, whereas binderless phase pure diamond is suitable for drilling rocks up to temperatures of 600°C.

After heat treatment, binderless polycrystalline diamond has the same $WR=215,000$, but diamonds with Co, Ni or Fe binder have 8 times lower WR (see Fig.3.5-7). When the granite log temperature reaches 200°C , the F_x also increases up to a maximum value of $200-300^{\circ}\text{C}$. Above 300°C , F_x decreases and thermally stable diamond machines rock with higher WR .

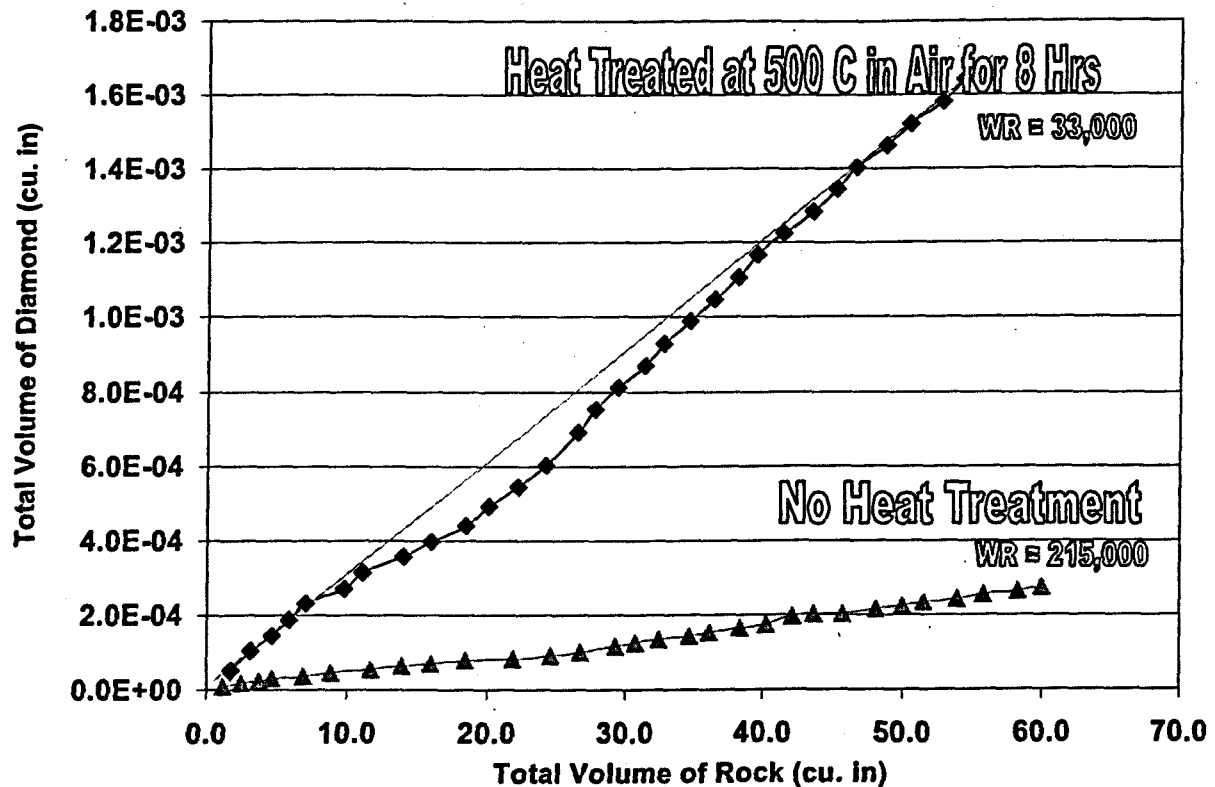


Figure 3.5-7. Wearing of granite by dull cutters of man-made diamonds. $WR=215,000$ for binderless diamond and triphasic composites with cooling water. $WR=33,000$ for triphasic composites after heat-treatment at 500°C in air for 8 hours. WR remains the same for binderless diamonds when heat-treated.

The WR can be increased by heating stone or by cooling diamond. The WR can be tremendously increased in either case, but both procedures are expensive. Any stone can be melted using very low forces near the liquid state, but this takes ten times more energy than mechanical drilling.

3.6. Methods for BPCD and NPCD manufacturing

DMI's prototype equipment allows (as it is designed) the company to manufacture the BPCD and NPCD of ϕ 1-6mm composites and 0.2-2.0 ct weight with given presses, HP apparatus and reaction cells. The Diamond/Carbide/Metal composites and functionally graded composites of ϕ 1-6mm can be produced in the pressure range 7-10 GPa; ϕ 6-8mm can be produced in the pressure range 3-7 GPa, and ϕ 8-13mm can be produced in the pressure range 1-3 GPa.

3.6.1 The principles of polycrystalline diamond materials manufacturing

Polycrystalline diamond materials can be manufactured by HPHT sintering of diamond powders. An idealized structure of compressed powder is shown in fig. 3.6.1-1a. The same structure after high temperature plastic deformation of grains and self-diffusion of carbon atoms is shown in fig.3.6.1-1b. A pressure of $P > 8$ GPa, temperature $T > 1800^{\circ}\text{C}$ and duration $\Delta t > 10$ sec. are necessary for the process of diffusion and acceptable quality of compacts.

Polycrystalline diamond materials can be also produced by HPHT impregnation of metal alloy into compressed diamond powder in a gradient reaction cell (see fig. 3.6.1-2a and 3.6.1-2b). Some boundaries between crystallites will be occupied by metal carbide and the pores will be occupied by metal. The gradient of temperature is needed to realize the sintering of diamond grains and impregnation within one manufacturing cycle. This method can be realized in the pressure range $P = 1-10$ GPa and temperature $T > 1200^{\circ}\text{C}$. Increasing the P,T-parameters will increase the toughness of composites.

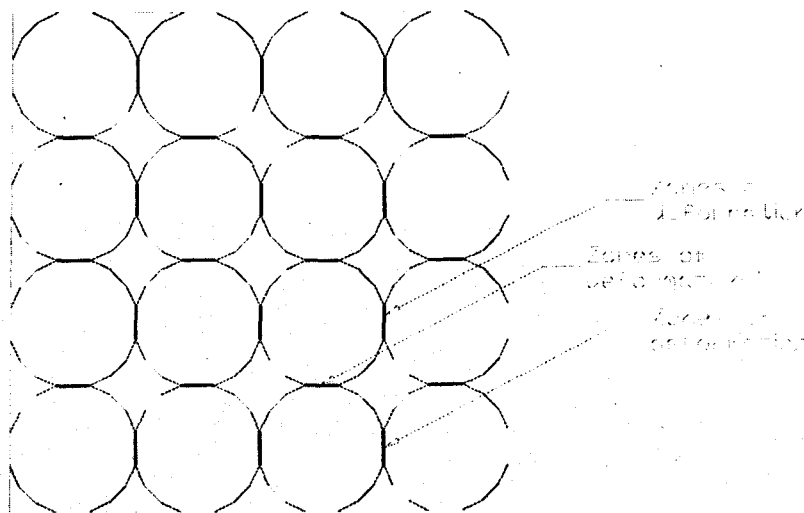


Fig. 3.6.1-1a. Idealized structure of compressed diamond powder

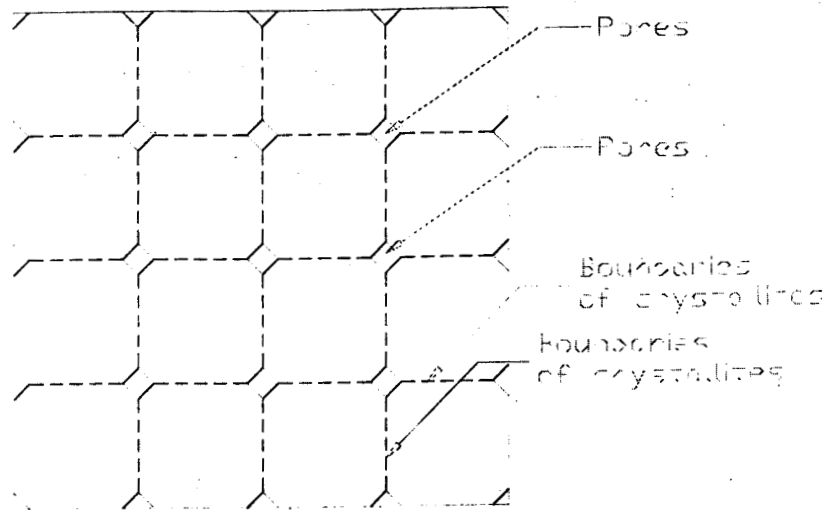


Fig. 3.6.1-1b. The plastic deformation of grains and self-diffusion of carbon atoms structure after high pressure & high temperature.

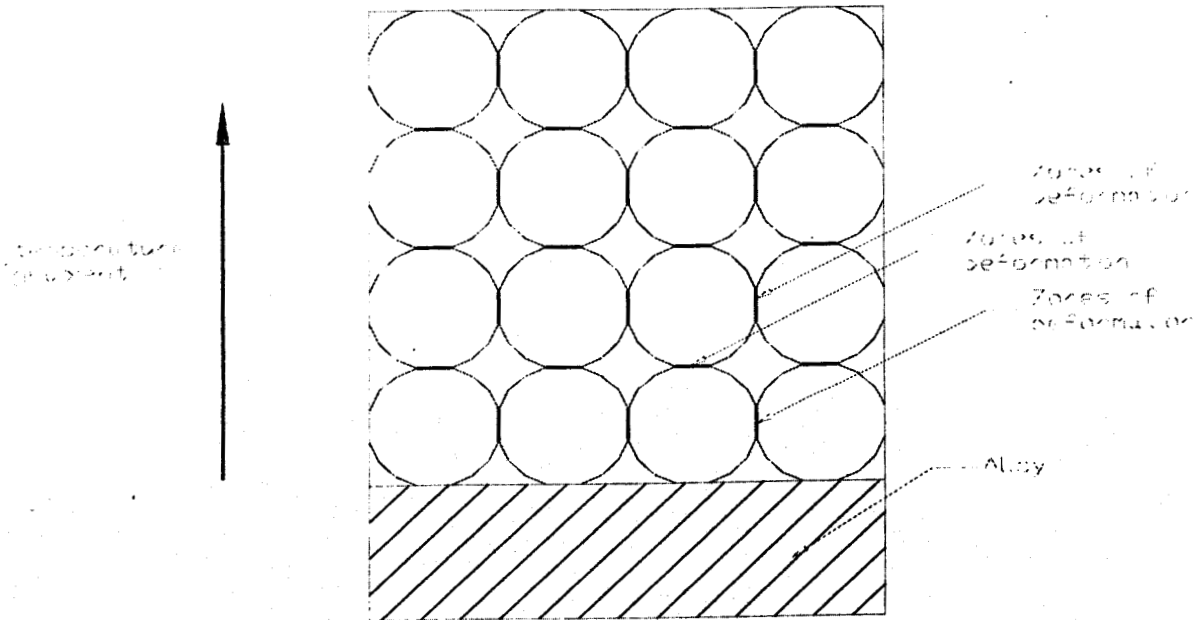


Fig. 3.6.1-2a. Structure of compressed diamond powder in gradient reaction cell with metal alloy before impregnation

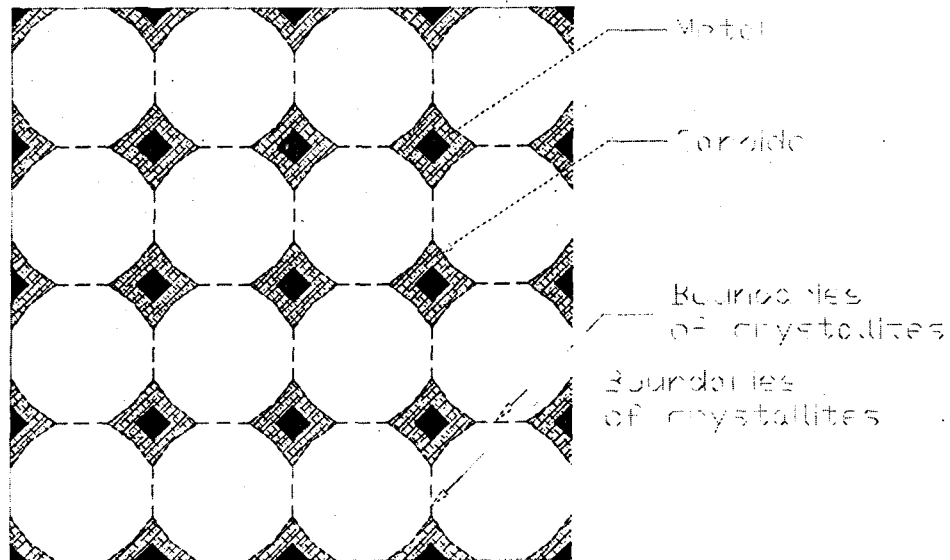


Fig. 3.6.1-2b. Polycrystalline diamond materials produced by HPHT impregnation of metal alloy into compressed diamond powder in gradient reaction cell

Both methods are developed on base of diamond powders. Such manufacturing does not increase the quantity of diamond. It makes a bulk body from powder or increases the size of the bulk body.

There are two methods that increase quantity of diamonds. It is a transformation of non-diamond carbon ceramics into fine structured polycrystalline diamond material in the presence of a metal alloy. In the first method, the metal is located inside a carbon ceramic (fig.3.6.1-3a). In the second method, the metal surrounds the carbon ceramic (fig.3.6.1-3b). The non-diamond carbon might be a graphite ceramic, glassy carbon or fullerene based carbon material. It can be realized at pressure $P > 7$ GPa, $T > 1500^{\circ}\text{C}$ and $\Delta t > 10$ sec. The alloy will penetrate into the pores of the carbon ceramic, transforming non-diamond carbon into polycrystalline diamond and forming carbides on the surfaces of pores. This method works better if the alloy has some quantity of Ni, Fe or Co. An increase in pressure evokes an increase in toughness of the diamond and a decrease in crystallite size.

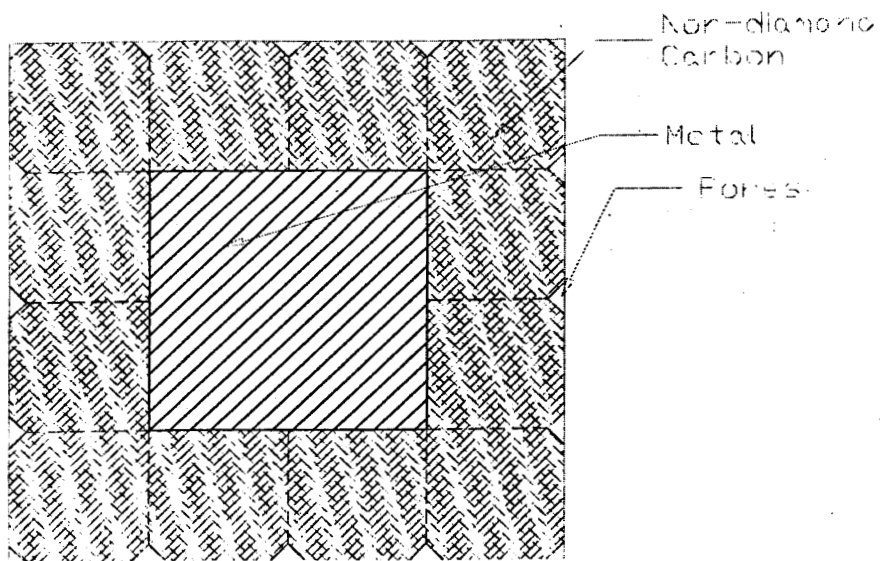


Fig.3.6.1-3a. The metal is located inside carbon ceramic

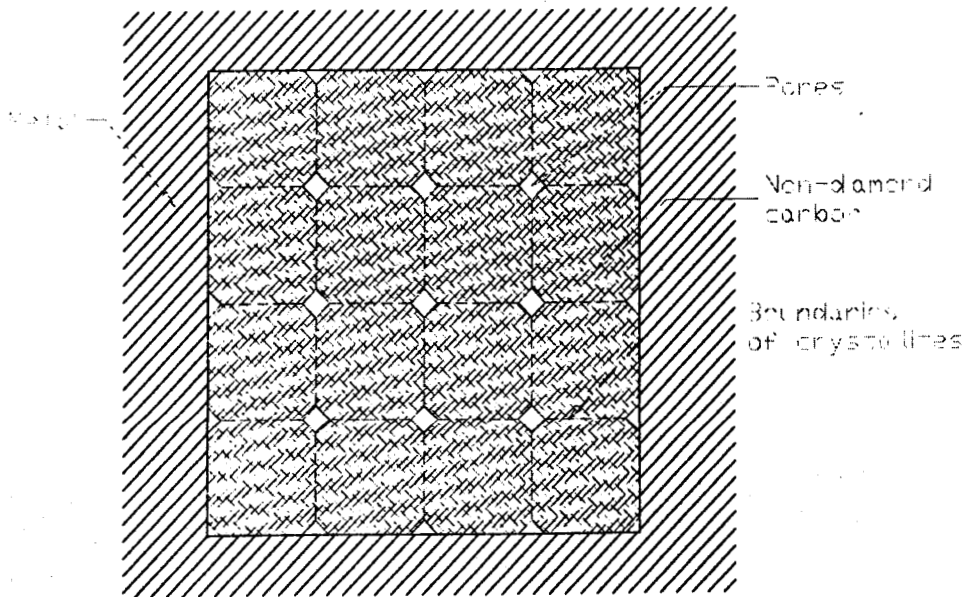


Fig.3.6.1-3b. The metal surrounds carbon ceramic

3.6.2 Automation of BPCD and NPCD manufacturing

The manufacturing of BPCD, NPCD and other polycrystalline diamond materials (fig.3.6.2-1) should be automated. The automation might be organized similar to manufacturing of bullets. Before automation of HPHT sintering of diamond powder, the manufacturing of containers and all parts of reaction cell must be automated (fig.3.6.2-2). Reaction cell should be manufactured by cold pressing of agglomerated powder or CNC. This process is similar to coining of coins. The rate of production will be higher of course, than the rate of sintering. This cold pressing occurs in steel dye at pressure range 0.01-0.1 GPa. It is better to use machined containers from fine-structured limestone. Machined from natural stones the containers have higher quality and increase quality of HPHT sintering at pressure $P > 8.0$ GPa. The parts of reaction cell might be also pressed or machined. Pressed graphite parts are absolutely acceptable and even preferable, since it permits to increase resistivity and voltage of power supply. Nevertheless it is more reasonable to use all machined parts for small-scale production.

TECHNOLOGY FOR THE BINDERLESS POLYCRYSTALLINE DIAMONDS MAKING

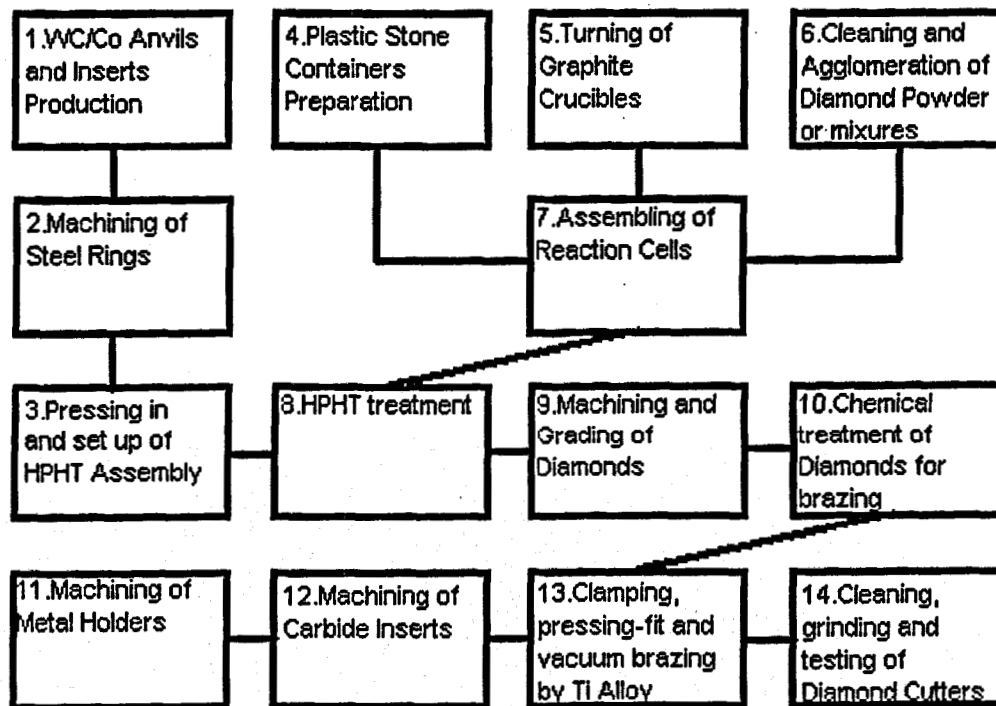


Fig. 3.6.2-1. Manufacturing of diamond materials

PREPARATION OF CONTAINERS FROM PLASTIC STONE Calcite (3), Pyrophyllite (2), Steatite (1)

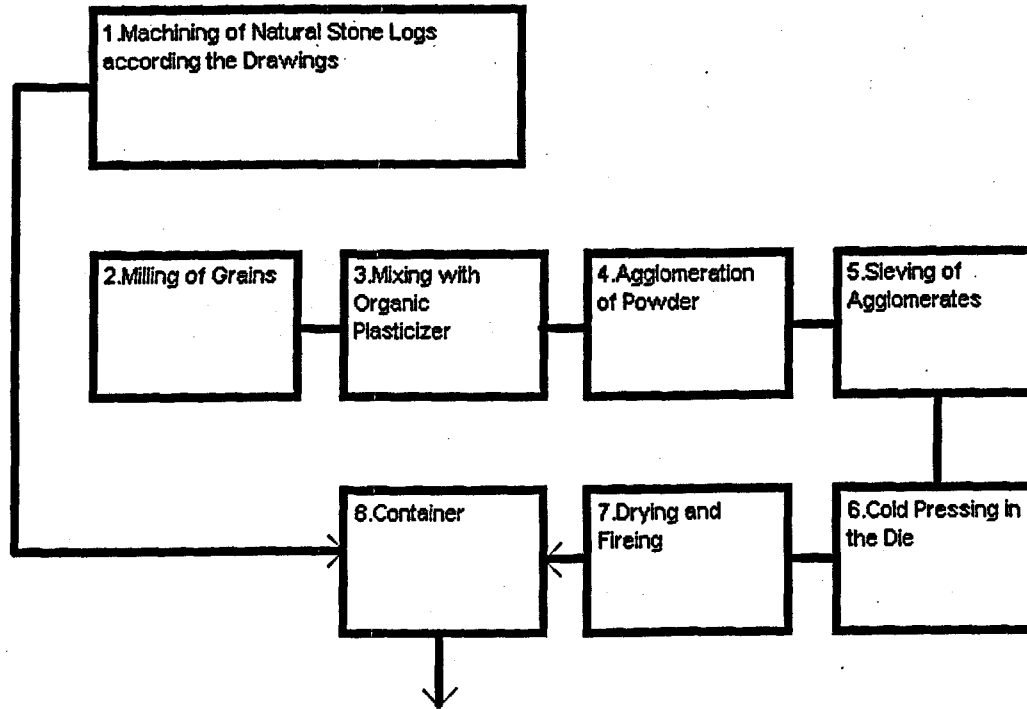


Fig. 3.6.2-2. Manufacturing of plastic stone containers for HPHT system

The HPHT system should be equipped with at least 2 HP apparatus and at least 10 HP chambers (10 pairs of anvils with set of supporting steel rings). They should sequentially be fed into the press, one by one, with a specified interval of time, as shown in fig.3.6.2-3. We will talk below about automation of the HPHT system itself. We must recognize here that the diamond-making process seems easy at first. Nevertheless, it is a very sophisticated process—a lot of technology is involved. Probably it is the most sophisticated process for now. However there are no problems here that could not be solved.

Diamond powder should be prepared from diamond pieces or from diamond dust, as shown in fig.3.6.2-4. The starting powder should be carefully analyzed before application, as was discussed previously in this report. The result of such analysis is shown in table 3.6.2-1. The price of powder should be analyzed and compared very thoroughly. Powder costs have a strong effect on the cost of manufacturing. Usually the chemical treatment and analysis is absolutely necessary, if the powder does not come with proper certification.

HIGH PRESSURE-HIGH TEMPERATURE COMPACTING OF DIAMOND POWDER

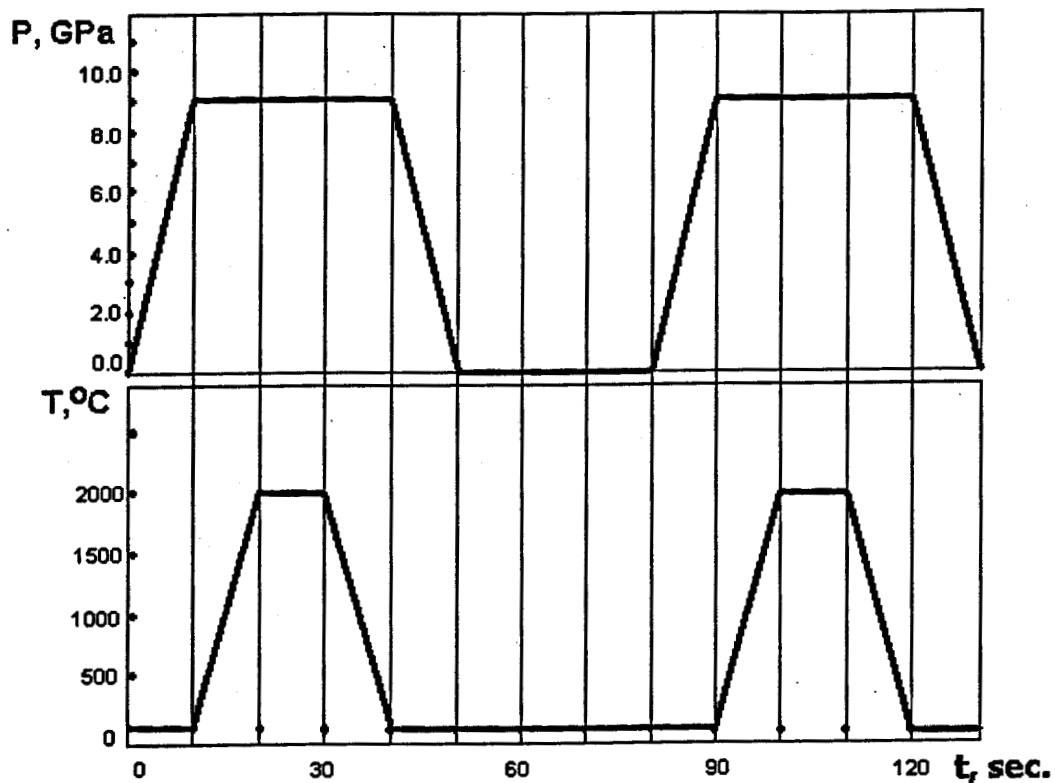


Fig. 3.6.2-3. P-T-t diagram for manufacturing of diamond materials

MAKING OF PURE DIAMOND POWDER

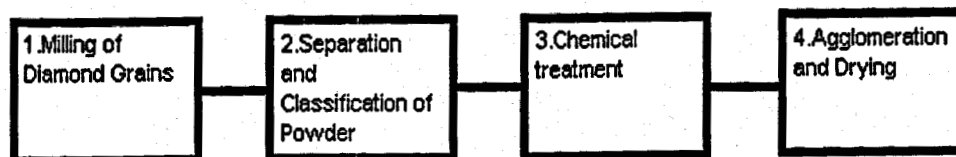


Fig. 3.6.2-4. Preparing of diamond powder for BPCD

Table 3.6.2-1 Analysis of diamond powders

No.	Type of diamond powder and technology	Size of grains (agglomerates) (μm) and color	Size of crystallites \AA	%wt. of contamination	Main elements of contamination	Compactability
1	Dynamic high pressure from graphite; nanostructured, strongly agglomerated	60/40 black	100-1,000	2.0	Cu, Fe, Si, Ca, O	Good
2	Dynamic high pressure from explosive organic compounds, nanopowder weakly agglomerated	5/3 gray	10-100	10.0	O, N, H, Cr, Mn	Bad
3	Static high pressure from hydrocarbons	60/40 white	500,000	0.1	N, H, Si, Ca, O	Good
4	Static low pressure from hydrocarbons	5/3 yellow	50,000	0.1	H, N	Not yet studied
5	Static high pressure, polycrystalline, submicrostructured, milled, strongly agglomerated, from graphite	60/40 black	1,000-10,000	6.0	Ni, Fe, Cr	Good
6	Static high pressure, monocrystalline, from graphite	60/40 yellow 1/0.5 gray	500,000	0.4	Ni, Fe, Mn	Excellent
			5,000-10,000	0.1	Ni, Fe, Mn	Good
7	Static high pressure, monocrystalline, milled from graphite	60/40 green 1/0.5 gray	500,000	0.9	Ni, Mn, Fe	Good
			5,000-10,000	5.2	Ni, Fe, Mn	Good
8	Natural, monocrystalline, milled, from boart	60/40 white 1/0.5 white	500,000	0.1	N, Si, Ca, Zr, O, Y	Excellent
			5,000-10,000	0.2	N, Si, Ca, O	Good
9	Fullerenes from carbon soot, agglomerated	60/40 very black	10	0.1	H, O	Excellent
10	Nanotubes from carbon soot, agglomerated	60/40 very black	10-1,000	20.0	Fe, Ni, H, O	Good
11	Multiwall nanotubes from carbon soot	100/1 black	100-10,000	1	H, O	Very Bad

All hot pressed cylinders (or bodies shaped by another way) should be absolutely equal by weight, size having similar WR and toughness that is hardly possible for natural diamonds. But they all should be faceted and polished into final shape by diamond

3.7 Design of diamond tool with BPCD and NPCD.

We designed and studied some cutting tools with BPCD and NPCD.

3.7.1 Diamond cutter design.

For high rate precision cutting the optimal cutter design is indexable cutter, which allows use of one cutter with out dismounting and sharpening. DMI designed a number of cutting tools. The drawing of one of the cutting tool is shown in Figure 3.7-2. Cutter edges with different geometry are shown in figure 3.7-1. below.

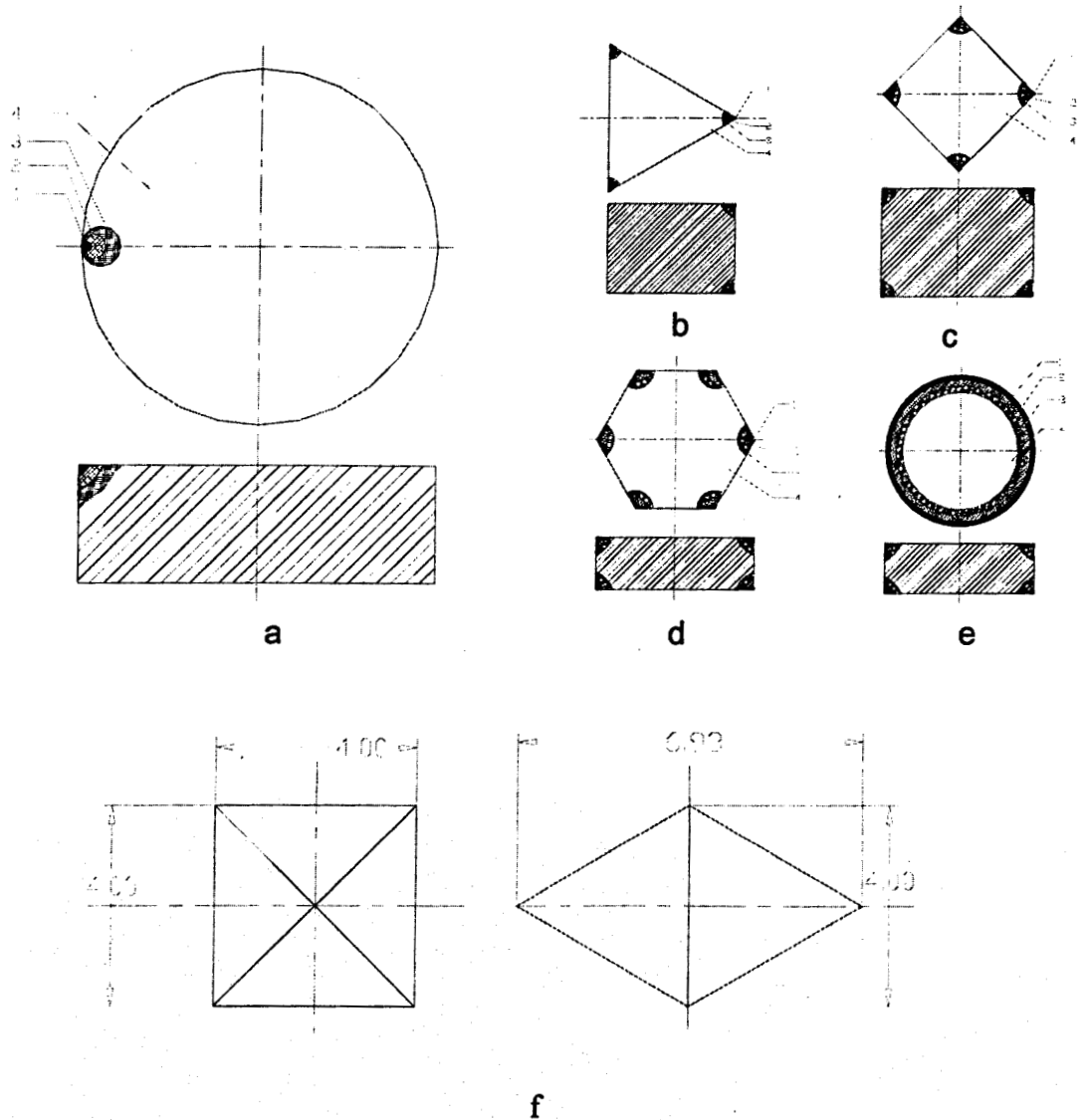


Fig. 3.7-1 Functionally graded indexable cutters: a) round cutter with round insert; b) triangle cutter; c) cubical cutter; d) hexagonal cutter; e) round cutter; f) octahedral cutter.
1-diamond, 2-diamond/metal, 3-4- carbide/metal

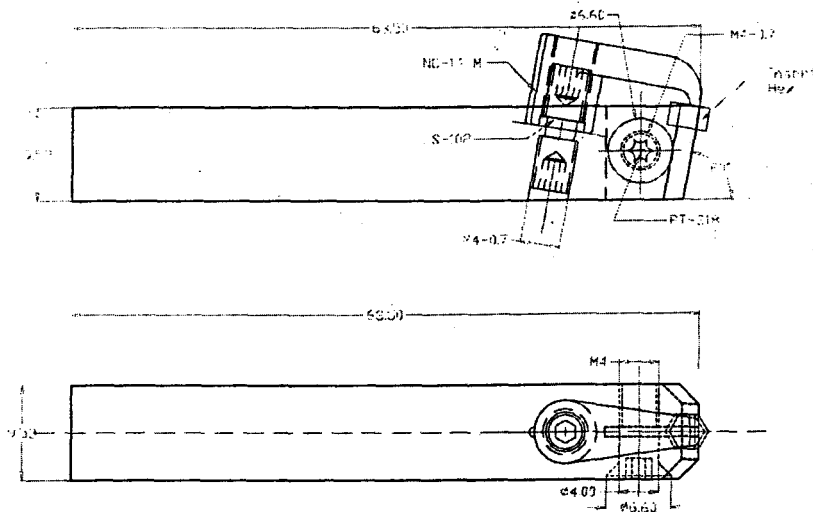


Fig. 3.7-2. The drawing of diamond cutting tool with hexagonal cutter and steel holder

The cost of sharpening and polishing of the diamond cutters is directly proportional to size and number of cutting surfaces. To obtain cutting edges on cylindrically shaped cutter one need to facet and polish three surfaces: top, bottom, and side. Even the number of surfaces is small the cost of producing this type of cutter can be high because of the difficulties related to faceting and polishing a cylindrical edge. Tetrahedral cutter will have six vertexes and five side surfaces (ratio 1.2). The most advantageous configuration in terms of vertex to side surfaces ration is hexagon (1.5) and the worst shape in this octahedral cutter with vertex to side ratio of 0.75. However these are theoretical consideration and practical designs that include a holder and effective angle of sharpening evens up these configurations in terms of available cutting vertices. Small cutters (2.5 mm to 6.0 mm) usually are self-standing. They can be affixed directly to cutter holder brazing or mechanically and do not need additional support. Cutters larger than 6 mm need to be supported by a steel or WC/Co substrate. In this case diamond is brazed in vacuum or at high pressures (1-3 GPa) to the substrate surface. Brazing in vacuum is more cost efficient however it can lead to weakening of the diamond. Thus heating should proceed at high rate with very rapid cooling to shorten the time diamond is exposed to high temperatures. In stead of WC composites we can use TiC/metal and SiC/metal composites which can lead to lighter and less expensive cutters without compromising its quality.

3.7.2 Diamond drill bits.

Steel drill bits can be used for processing metal and soft rock. In Figure 3.7.2-1, we show a typical steel drill bit. Medium hardness stone and concrete can be drilled by the drill bit of the same basic construction as shown in Figure 3.7.2-1; however, they should be equipped with WC/Co inserts, brazed to the cutting edges of the drill bits, as shown in Figure 3.7.2-2. During drilling, the drill bit experiences both impact and shear stresses and material is exposed to impact and abrasive wear.



Fig.3.7.2-1. Standard steel drill

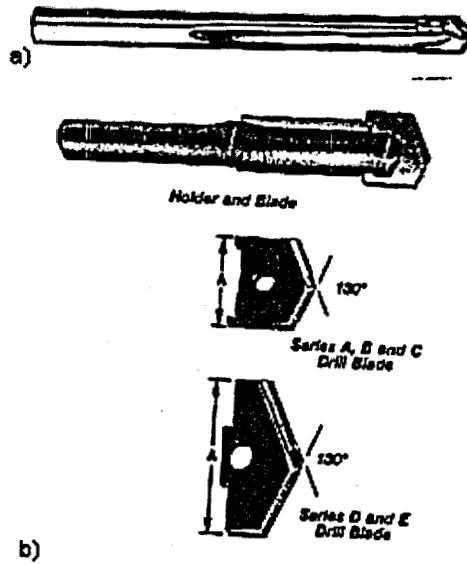


Fig.3.7.2-2. Drills with steel holder and WC/Co cutters

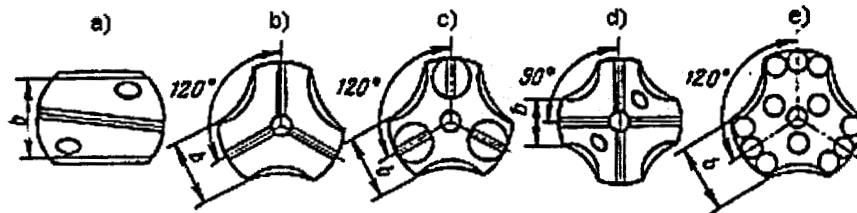


Fig.3.7.2-3. Drag bits for blast-hole drilling

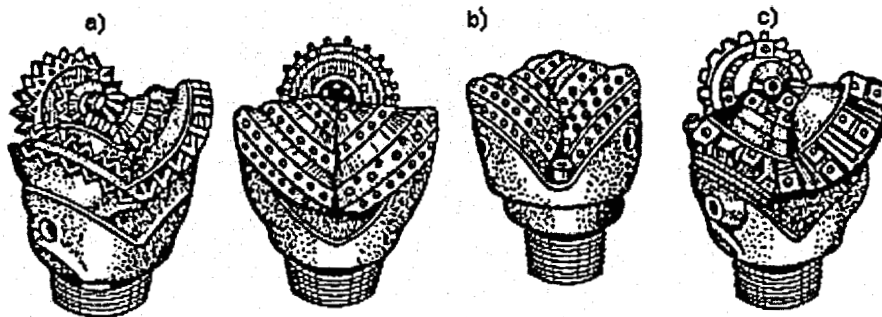


Fig.3.7.2-4. Roller cone bits for blast-hole drilling: a)toothed; b)pined; c)combined.

Processing of hard rock, such as granites, can be achieved with drill bits that are similar in construction to that shown above; however, the cutting edge inserts should be made of diamond materials. It is interesting to note the absence of the standard drill bit in the designs shown in Figure 3.7.2-2, where the cutting edge is made from diamond materials. (Except some CVD coated drill bits have this construction, but they are not used in hard rock drilling). The drill bits for processing of the hard stone will usually have a ring-type construction, with the cutting segments made from metal containing diamond powder. Thus, the cutting process is mainly based on abrasive wear, which is not very efficient. The rotational and impact/rotational drilling is widely used for preparation of holes that are needed for explosives in drilling and excavation for construction. A number of drill bits used for blast-hole drilling are shown in Figure 3.7.2-3. A number of roller cone bit constructions that are used for core and blast-hole drilling are shown in Figure 3.7.2-4. These roller cone drill bits are equipped with insert cutting blades made from WC/Co. Use of roller-cone bits for blast-hole and core drilling is very widespread.

During core drilling, the stone formation is usually penetrated at the ring area of the hole to allow core recovery for analysis of the geological formations. In some instances, the hole is drilled through without core recovery. A schematic of a rig for drilling of geological exploration boreholes is shown in Figure 3.7.2-5. The drilling rig consists of drilling apparatus I, pump II, drilling tower III, engine IV, structure V, drill pipe VI, control system VII, and measuring and analysis equipment VIII.

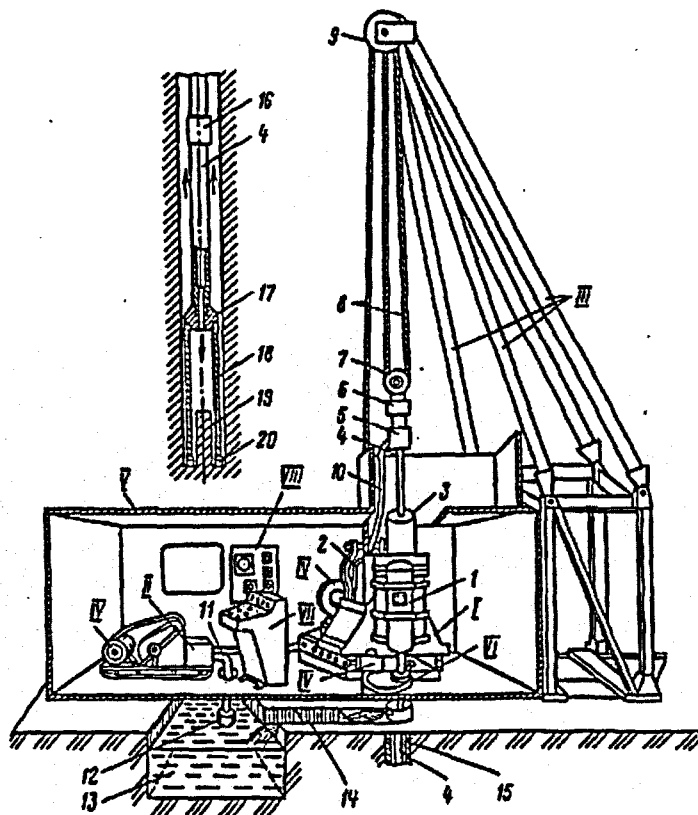


Fig.3.7.2-5 Schematic of rig for drilling of geological exploration boreholes.

Typical core drill bits are shown in Figure 3.7.2-6, and typical chisel bits for drilling without recovery of core samples are shown in Figure 3.7.2-7. Schematics of diamond core drill bits are shown in Figure 3.7.2-8, and in Figure 3.7.2-9, we give an illustration of different core bit designs with "matrix," cutters," and "channel" distribution of diamond cutters. Profiles of possible matrix structures are shown in Figure 3.7.2-10. In figures 3.7.2-11, we show a number of chisel drill bit structures with diamond and WC/Co inserts. In Figure 3.7.2-12, we show four constructions of diamond chisel drill bits with radial, spiral, stepped, and impregnated distribution of diamond inserts.

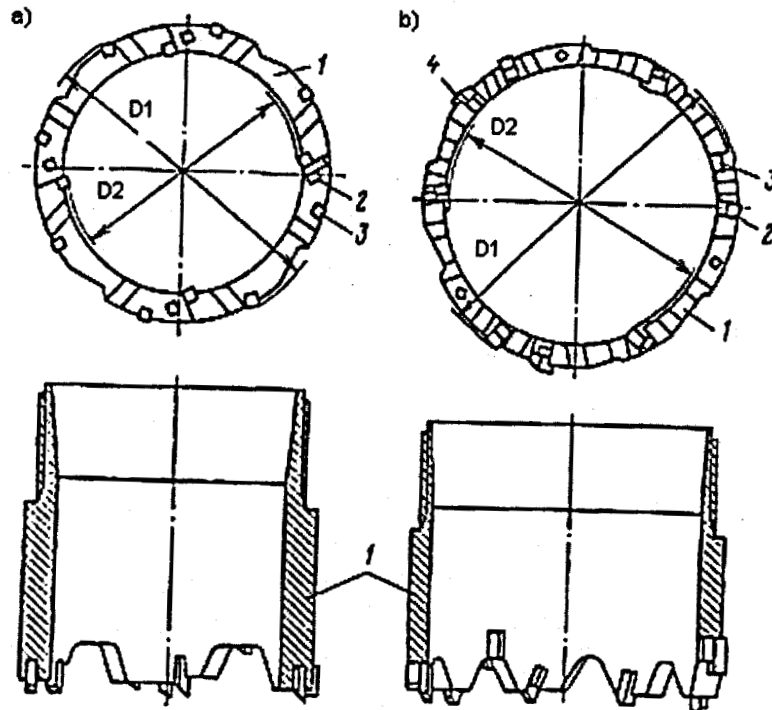


Fig.3.7.2-6. Core drill bits with WC/Co cutters: 1-steel holder; 2-4 cutters.

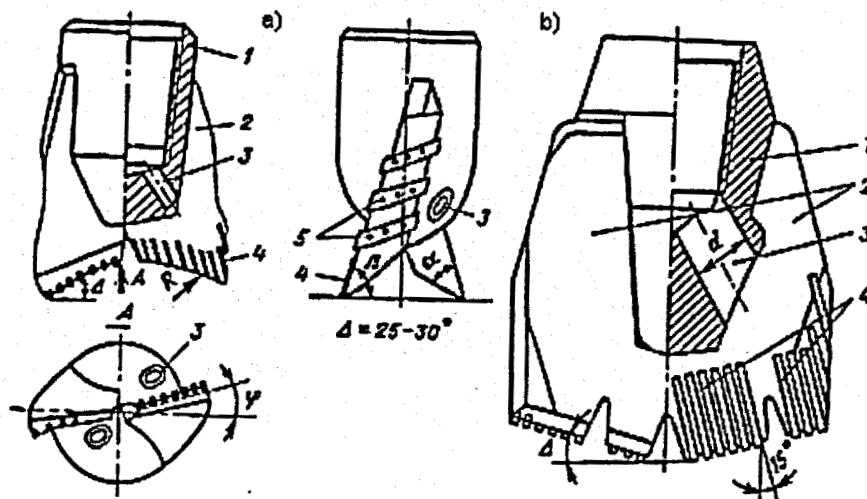


Fig.3.7.2-7. Steel chisel bits with WC/Co cutters for drilling without core sample.

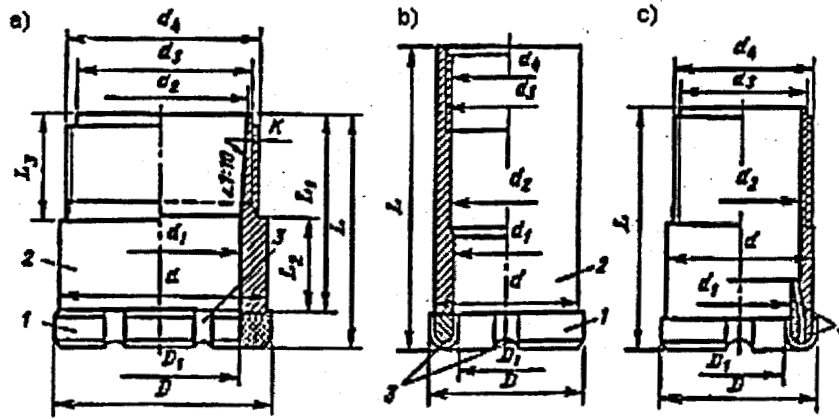


Fig.3.7.2-8. Diamond core drill bits. 1)matrix; 2)steel holder; 3)channels

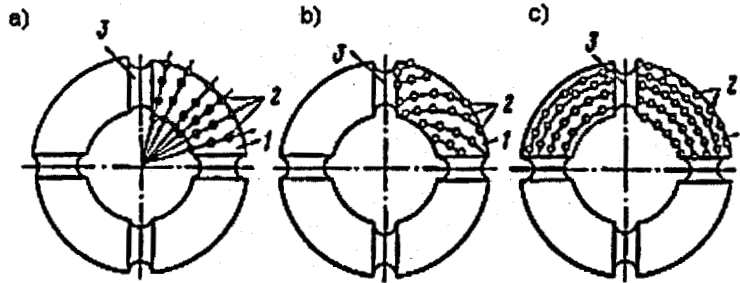


Fig.3.7.2-9. Schematic for location of diamond cutters: 1)matrix; 2)cutters; 3)channels.

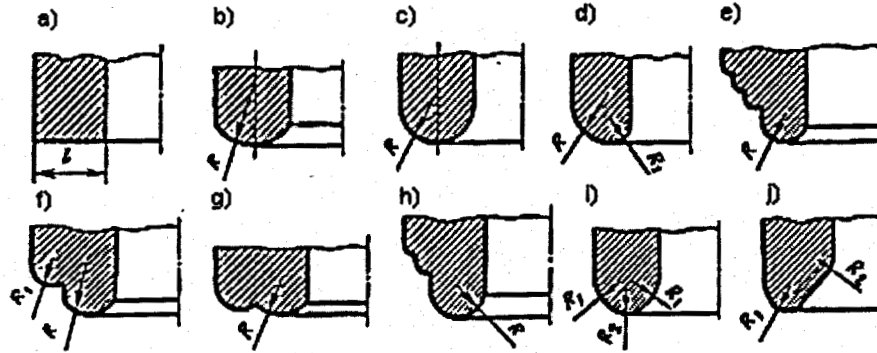


Fig.3.7.2-10. Profile of matrix.

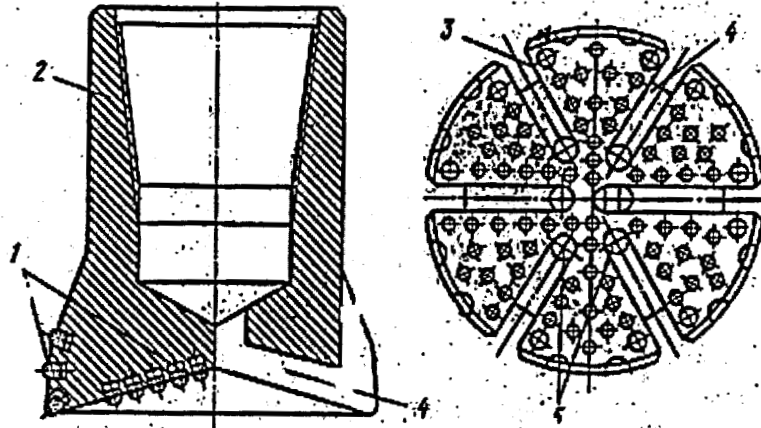


Fig.3.7.2-11a. Chisel drill bit with WC/Co, diamond or diamond/carbide/metal composite inserts. 1)inserts; 2) steel holder; 3)-4) channels; 5)holes.

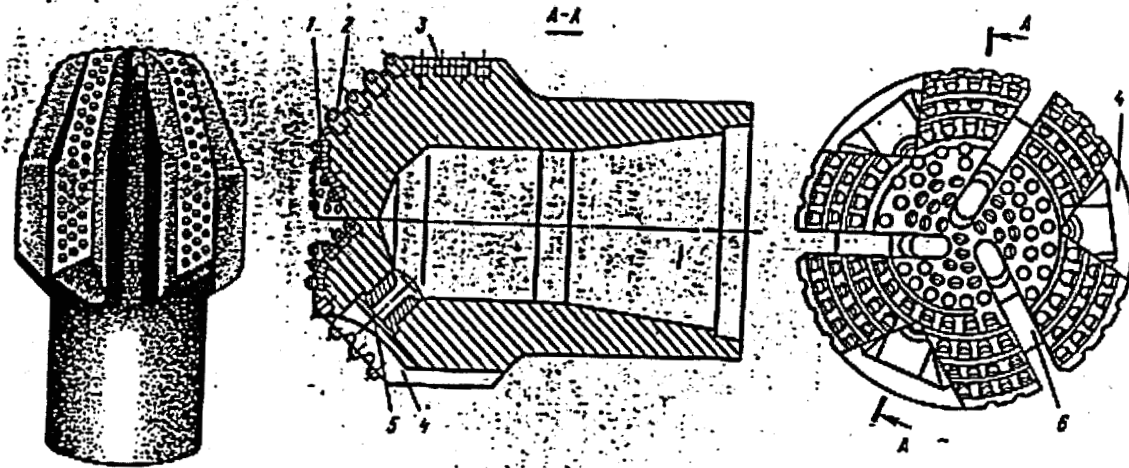


Fig.3.7.2-11b. Chisel drill bit with WC/Co, diamond or diamond/carbide/metal composite inserts. The inserts wear a stone like a dull cutters. 1)-3) inserts; 4)channels; 5)nozzle;

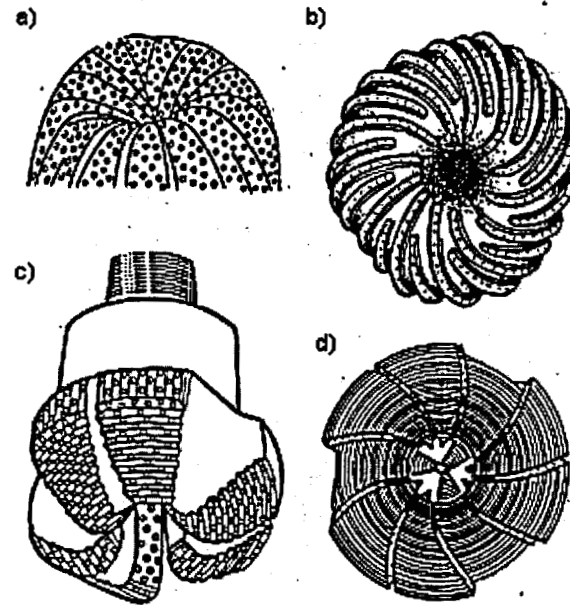


Fig.3.7.2-12. Diamond chisel drill bits: a) radial; b)spiral; c)stepped; d)impregnated.

Hardness and abrasive resistance of the rock formation, cost of the drill bit, and other considerations dictate the choice of drill bit construction. For drill bit manufacturing, natural crystals and carbonados, synthetic PCDs, composites, and diamond powders can be used.

3.8 The idea of self-sharpening cutter.

As it was told earlier, we investigated diamonds in two regimes of cutting (or wearing of samples): like a sharp cutter and like a dull one. The diamond works very well in first case and wears stone with very high WR. It is the best way to use this regime for finishing turning with high precision. We mean here ordinary cutters for turning operations. If the situation is that cutter can be held on a tool-holder by mechanical way, it's best to use an indexable cutter (IC). The holders developed for diamond cutters in an usual American Standard are shown in figures 3.8-1, 3.8-2, 3.8-3, 3.8-4 and 3.8-5. It is cylindrical, triangular, cubical, hexagonal and octahedral IC. It seems that a hexagonal cutter is the most economical. If it is necessary to apply large-sized cutter that hard carbide alloy substrate with cavities are being produced (fig. 3.8-6) and diamond are being brazed into cavities under pressure of 2.5-3.0 GPa by titanium alloy that wets diamond and carbide alloy. Diamond and substrate pass through chemical treatment by boiling perchloric acid before being brazed. (fig. 3.8-7). The cutter is ground by diamond wheel and polished after brazing. In a follow-on project, the first type of cutting tool will be investigated for optical glasses machining (DoD DARPA Project) and the second type of tool will be commercialized in machining of stones, ceramics, composite materials and concrete.

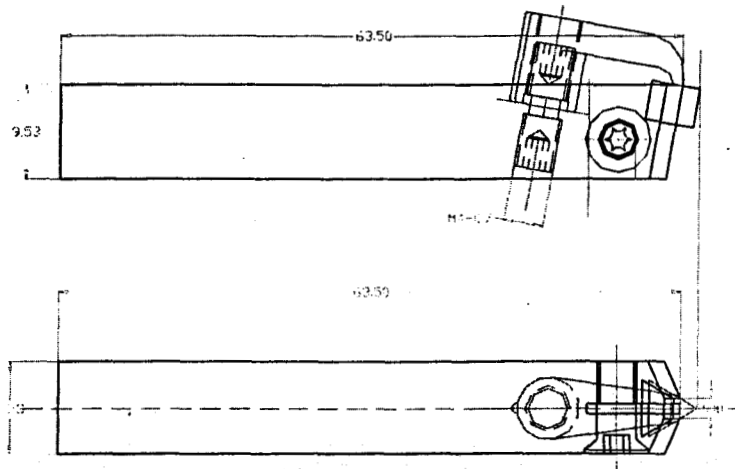


Fig. 3.8-1. The drawing of diamond cutting tool with triangle cutter and steel holder

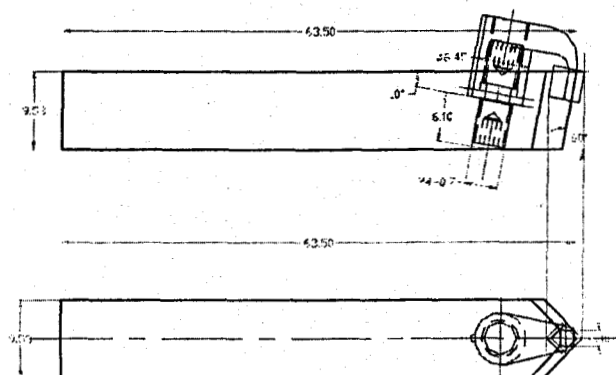


Fig. 3.8-2. The drawing of diamond cutting tool with cubic cutter and steel holder

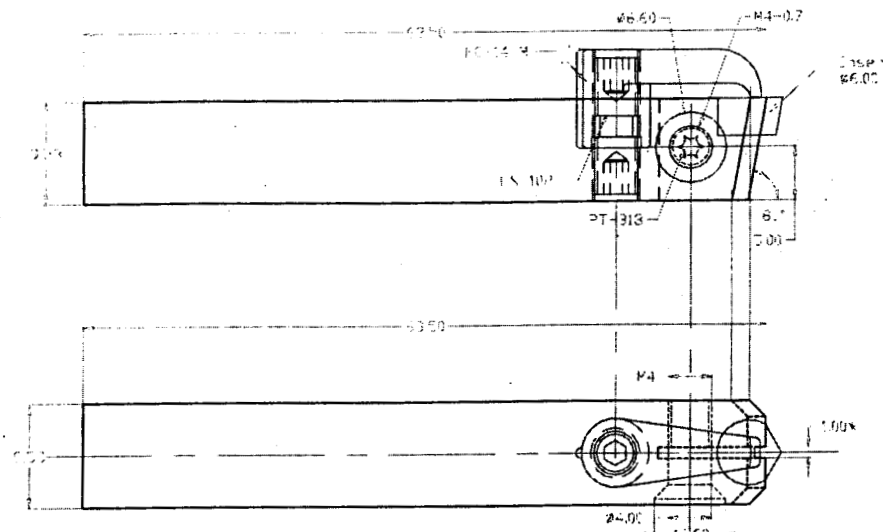


Fig. 3.8-3. The drawing of diamond cutting tool with round cutter and steel holder

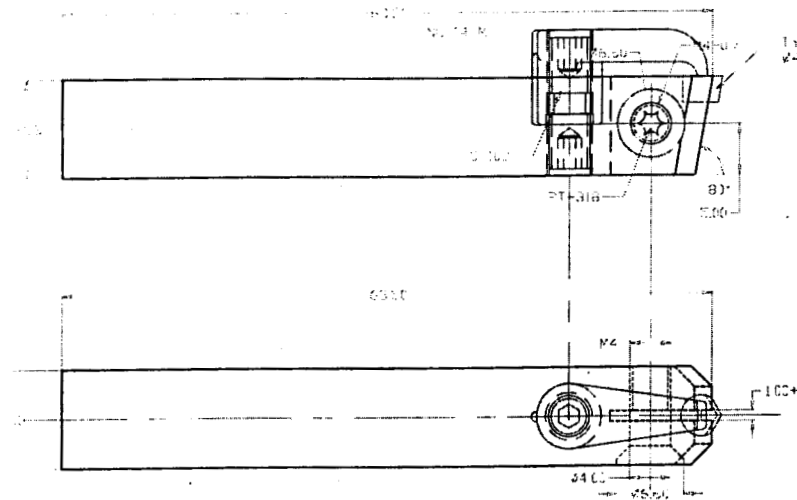


Fig. 3.8-4. The drawing of diamond cutting tool with round cutter of small size and steel holder

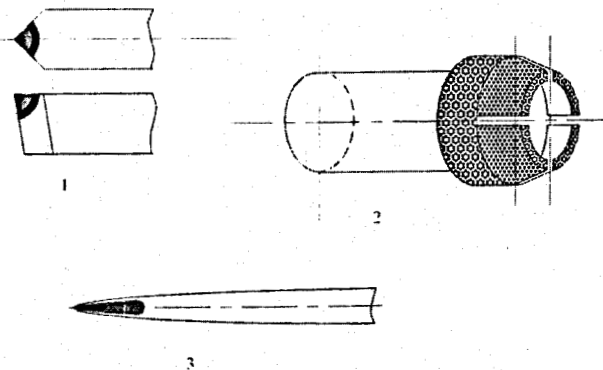


Fig. 3.8-5 The diamond tools are to design for drilling, digging and machining:
1) cutting tool; 2) drilling tool; 3) digging tool.

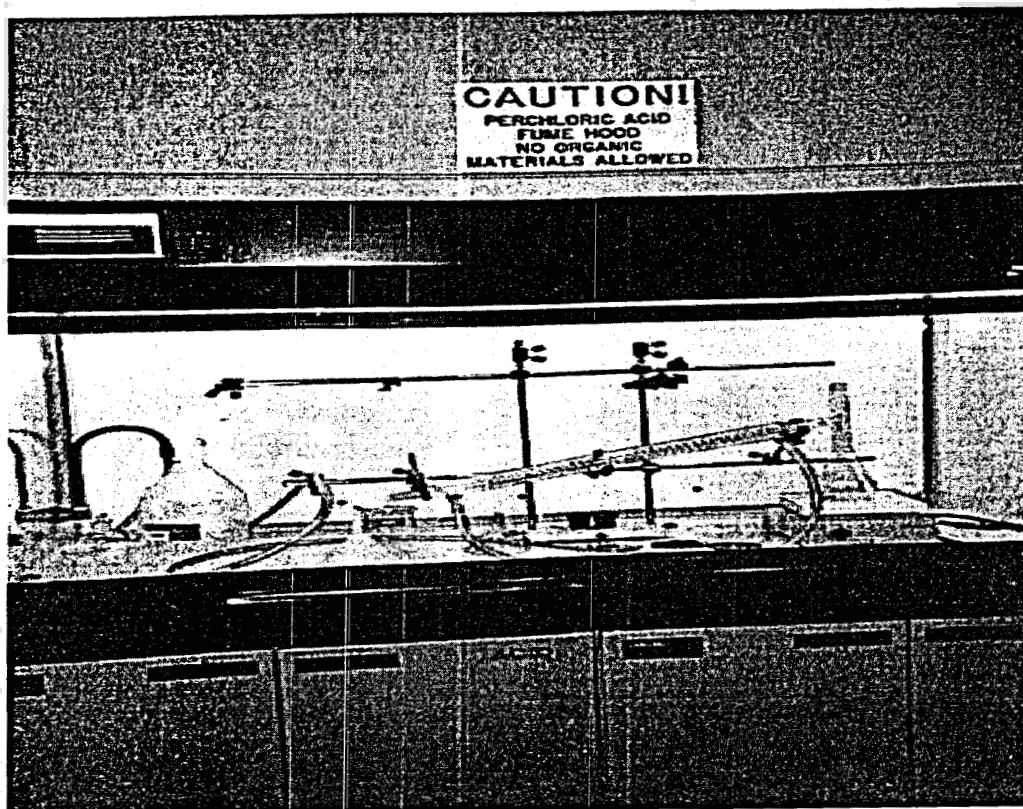
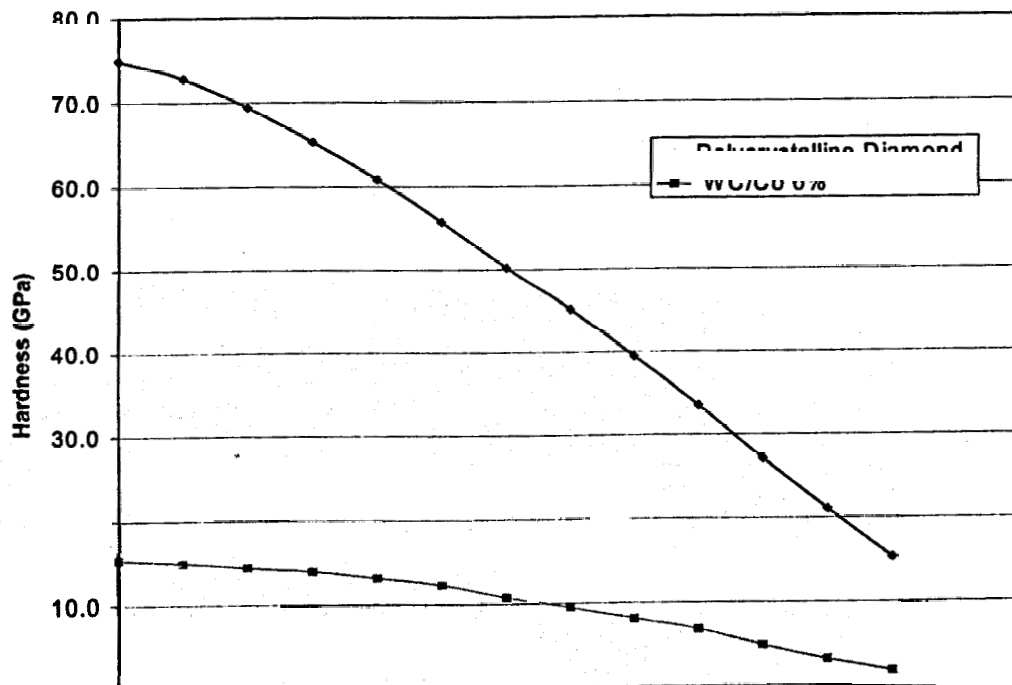


Figure 3.8-6 Cleaning and Separation devices



The study shows that diamond single crystal has maximal hardness in the direction from point to point of octahedron. We mean here not a shape of cutter, but crystallography direction [011]. If some material is being machined by sharp cutter, just last crystallite of PDM is actually working. This crystallite is supported by other crystallites. If this crystallite is oriented in pointed direction, the cutter shows the minimal wear, that is equal to wear of single crystal in this direction. If the speed of machining grows up, the difference induced by temperature of cutter becomes clearly seen (fig. 3.8-8). The thermal conductivity of average quality single crystal is three times higher than the thermal conductivity of the best polycrystalline diamond material (PDM). Therefore, the temperature of mono-crystalline cutting edge is lower than the temperature of PDM's cutting edge. The sample machined is usually very massive and heats up less than the cutter. When the hardness equalizes, the cutter stops to cut and becomes dull. If the machining occurs in air, the edge of cutter burns out from 700°C and higher. If the machining occurs in argon, the cutter could be heated up to 1200°C, but the hardness becomes lower -- even lower than the hardness of corund (alumina) at room temperature. Therefore, it is reasonable to cool down a cutter and heat up machined article. During the facetting and polishing of diamond, during the cutter re-sharpening it is also reasonable to cool down the diamond wheel and heat the diamond up to 1000°C in inert gas. When heated, a diamond can be machined easier using a diamond wheel.

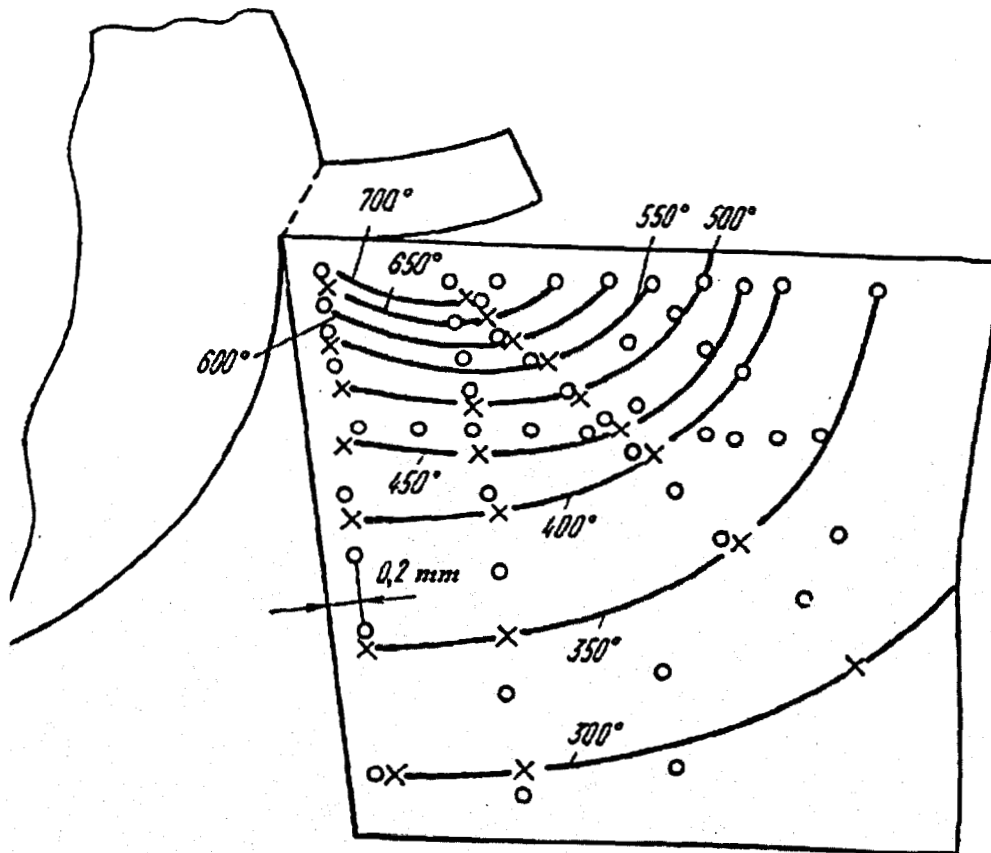


Fig. 3.8-8. Temperature field of cutter for cutting steel. The cutter is made of WC15%TiC6%Co; depth of cut is $t=2.55$ mm; feed is 0.2 mm/rev.; and speed is $v=150$ m/min.

Nevertheless, when the temperature is higher, the time of operational holding should be lower to prevent transformation of the diamond into graphite and an irreversible decrease in hardness and toughness.

The cutters cannot be re-sharpened in drilling tools. Core drill bits are being used for blast hole drilling and for geological exploration drilling. Chisel drill bits are being used for petroleum and geothermal drilling. It is reasonable in this case to wear diamond completely working with one bit as long as possible. It is also more reasonable to use PDM, but not mono crystalline diamond materials (MDM), since a diamond will work like a dull cutter anyway. Diamond wears granite very well if contact area does not exceed $\sim 1 \text{ mm}^2$. The loading onto any diamond is just enough to make the force divided by contact area higher than hardness of rock. The granites have a hardness $5 < H_v < 10$ GPa. If PDM has a shape of cylindrical finger of 0.35 mm diameter, the cross-section is $\sim 0.1 \text{ mm}^2$ and loading will be $\sim 100 \text{ kgf/cutter}$ for hardest granite. If there are ten of such fingers, uniformly distributed on a bit surface, the 1 ton load will be needed. Otherwise the cutters will slide on a surface of rock. The rock will heat and polish the diamonds. The bit will start to work like a bearing. Diamond fingers should rest on hard carbide alloy substrate, otherwise they will "sink" into bit body that is softer than granite. Long and thin diamond finger will not survive such a load, if he will be not supported by chemical bonding with carbide. It could be titanium carbide surrounded by relatively soft metal of body. This is an idea of self-sharpening cutter. Diamond "needle" is surrounded by carbide and carbide is surrounded by metal. The hardness of cutter decreases from cutting point to periphery. The periphery wears more quickly disclosing diamond layer. The loading onto each cutter does not increase, but pressure under the cutter sharp edge stays high enough to penetrate into machined material. Three layers cutter, drill bit and spade that do not dull up are shown in fig. 3.8-5.

4.0 Phase III commercialization plan

Table Phase III Commercialization

Product	←---Sales---→		←---Development---→			Partners	DOE Ph II SBIR Projs	Comments
	Non Federal	Federal	Internal	Non Federal	Federal Non-SBIR			
Binderless Polycrystalline Diamond Compacts. High thermal stability and high wear resistance	136.50 ¹	0	0	0	0	Tempo Technology Corp. (TTC) Hughes Christensen Kansas State Univ. Rutgers Univ Garori Inc. Sandia National Lab Hutchinson Inc.	40979	Development and collaborations continue to build.
Nanophase Polycrystalline Diamond Compacts sintered from fullerene material	0	0	0	0	0	MER Corp. Rutgers Univ. Garori, Inc.	40979	
Triphasic diamond composite suitable for oil and gas drilling	0	0	0	0	173,280	Kansas State Univ. Rutgers Univ. Garori, Inc.	40979	
Diamonite - new carbon material sintered from fullerenes	250.00 ²	0	0	0	349,000 ⁴	Edge Technologies MER Corp Johns Hopkins Univ. Rutgers Univ	40979	DARPA is supporting development of this as a precision cutting tool.
Triphasic diamond composite cutting tools for machining of Al-Si parts	0	0	0	0	100,000 ⁴	Carl's Cutting Edge Garori, Inc. Rutgers Univ. Hutchinson Inc.	40979	NSF is supporting development of this technology
Diamond/Bc ₂ C/Be cutting tools for drilling on Mars	0	0	0	0	70,000 ⁴	Carl's Cutting Edge Rutgers Univ. Garori, Inc	40979	NASA is supporting development of this technology
Functionally Graded Tricontinuous Diamond-WC/Co Compact	0	0	0	5,000	0	Boart Longyear Tempo Technology Corp.		Awaiting further refinement
3 carat sintered Diamond cylinders	63.00 ³	0	0	0	0			
SERVICES								
Study of USA and international diamond market	0	0	0	0	0		40979	
Investigation of USA prices and situation with diamond cutting tools	0	0	0	0	0		40979	

¹ samples sold to Hughes Christensen Company² nanograined polycrystal diamond compact pellets sold to Edge Technologies Inc.³ sold to Micro-Optics Design Corporation⁴ SBIR projects funded by other agencies.

It is well known that polycrystalline diamond compacts (PCDs) serve a very useful function in high rate drilling of soft and medium-tough but abrasive rock formations. However, for hard rock drilling, hard and tough WC/Co cutters remain the workhorse materials in the oil and gas exploration industry. The work performed under this contract clearly demonstrates that binderless PCDs offer advantages in geothermal drilling applications, because of the elimination of the Co binder phase, which is susceptible to hot corrosion. Moreover, concurrent research on nanophase WC/Co and functionally graded WC/Co/diamond presents new opportunities for cutters in drilling. In this new concept, a binderless PCD facing is bonded to a functionally graded triphasic WC/Co/diamond nanocomposite, which should further improve performance of the cutters for two reasons. First, the elimination of a sharp interface between diamond facing and the WC/Co substrate makes the material less susceptible to delamination in service. Second, the presence of the diamond phase in the triphasic material further enhances the wear resistance of the substrate. Thus, in this new design concept for rock cutters, hot corrosion resistance for the diamond facing is combined with superior toughness of the supporting substrate, and enhances the abrasive wear resistance of the cutters, particularly for drag bits, where the wear involves removal of material from the diamond facing *and* its substrate. The situation with respect to roller cone bits is more complicated because most of the wear occurs directly on the diamond facing. Nevertheless, there remains a significant advantage in long-term performance because of the much stronger and more mechanically shock resistant diamond/substrate interface.

For all these reasons, we anticipate rapid commercialization of the new cutter technology into rock drilling applications, including geothermal drilling. At this stage, DMI is engaged in a dialogue with several end-user companies. For example, Smith International sees considerable potential in the functionally graded cutters for all types of drilling, machining, and cutting operations. In other words, it seems that the machine tool industry could benefit just as much from this new class of cutter materials as the drilling industry. In order to explore this new dimension of applications more thoroughly, we have also entered into discussions with established machine tool companies. A good example of the utility of the new cutter technology is its use in high speed machining operations, particularly for machining of fiber-reinforced composites, where abrasive wear is a serious problem.

Although progress has been made on the *nanophase* WC/Co/diamond composite materials, it seems that this might be too big a step-out beyond today's technology. On the other hand, this same material with *microphase* structures could be readily adapted to the needs of the drilling industry. Accordingly, we have set the latter as our primary objective in the near term, and the former as a follow-up technology.

5.0 References

1. P.W. Bridgman, *Scientific American*, Nov. 1955, p. 42.
2. H.T. Hall, U.S. Patent No. 2,941,248, 1960, "High Temperature-High Pressure Apparatus."
3. L.F. Vereshchagin et al., U.S. Patent No. 3,746,484, 1960, "Apparatus for Achieving High Pressure and High Temperature."
4. O.A. Voronov, "High Pressure Apparatus of Cylindrical Type," *Inst. For High Pressure Physics Report*, p. 1-25, Joint Scientific and Technical Information Center of the USSR, No. 0035462, 1985 (in Russian).
5. O.A. Voronov, "Diamond Compacts," *Diamond Materials*, Electrochemical Society, PV93-17, p. 1018-1025, 1993.
6. B.H. Kear, L.E. McCandlish, "Chemical Processing and Properties of Nanostructured WC-Co Materials," *Nanostructured Materials*, v. 3, p. 19-30, 1993.
7. S. Eidelman, A. Altshuler, "Synthesis of Nanoscale Materials using Detonation of Solid Explosives," *Nanostructured Materials*, V.3, p. 31-41, 1993.
8. O.A. Voronov, "Diamond Ceramics Produced at High Pressure," *Report for SAIC*, 1995, p. 1-87.
9. F.C. Apple, C.C. Wilson, "Experimental Measurement of Forces, Temperatures and Wear of Polycrystalline Diamond Cutters in Orthogonal Rock Cutting," *Final Report for NSF*, Grant No. CBT-8819165, 1991.
10. G.A. Voronin, "The Toughness of Diamond Crystals in Large Temperature Range," Ph.D. thesis, *Inst. For Superhard Materials*, Kiev, 1984, p. 1-209 (in Russian).
11. R.L. Mehan, L.E. Hibbs, "Thermal Degradation of Sintered Diamond Compacts," *J. Mat. Sci.*, v. 24, p. 942-950, 1989.

6.0 Publications, Reports and Patent Applications during this Project.

1. B.H. Kear, R.K. Sadangi, L.E. McCandlish, O.A. Voronov, "Triphasic Composite and Method for making Same," Intn'l Application No. PCT/US98/05849, 25.03.97.
2. G.S. Tompa, O.A. Voronov, "Diamonite Polymeric Material Compacts of Soot, Fullerenes, Nanotubes, and Related Materials," Provisional Application No. 60/100,078; 09/14/98.
3. O.A. Voronov, "Supercell for Achieving High Static Pressure and Temperature in a Relatively Large Volume," Provisional Application in process, 06/20/00.
4. O.A. Voronov, G.S. Tompa, B.H. Kear, W.E. Mayo, S-C. Liao, R.K. Sadangi, K.J.T. Livi, R.O. Loutfy, "High Pressure High Temperature Consolidation of Carbon Nanotubes for Structural and Other Applications," Report DMI-41023-FINAL for US Army Aviation & Missile Command, DoD DARPA, 58 pages, 1998.
5. O.A. Voronov (PI), "Development and Testing of Functionally Graded Triphasic (WC-Co-diamond) Compacts-FGTC," Final Report No. 681190 for National Advanced Drilling and Excavation Technologies Program," 1999, p. 1-57.
6. O.A. Voronov, G.S. Tompa, B.H. Kear, R.K. Sadangi, C.C. Wilson, "Tricontinuous Diamond/WC/Co Cutting Tools for High Rate High Precision Machining of Nonferrous materials, Composites, and Ceramics," Final Report No. 9860480 for NSF, 1999, p. 1-27.
7. O.A. Voronov, G.S. Tompa, P. Yan, D. O'Brien, A. Ghavami, B. Baxter, "Nanophase Fullerene/Nanotube-Beryllium Composite Cutters for Drilling on Mars," Report DMI-41042-FINAL for NASA, 2000, p. 1-31.
8. The NADET News: "NADET Advanced Drilling Projects Enter 2nd Round," v. 5, No. 1, 1998.
9. R.K. Sadangi, O.A. Voronov, G.S. Tompa, B.H. Kear, "Spuerhard Nanophase Materials for Rock Drilling Applications," p. 5-39, 5-47 in Proc. Geothermal Program, Review XV, "The Role of Research in the Changing World of Energy Supply," U.S. Dept. of Energy, DOE/EE-0139, 1997.
10. R.K. Sadangi, O.A. Voronov, G.S. Tompa, B.H. Kear, S.-C. Liao, C.C. Wilson, J. Yorston, "Functionally Graded WC-Co-Diamond Composites," MRS Fall Meeting, Abstract, 1997.
11. R.K. Sadangi, O.A. Voronov, B.H. Kear, "WC-Co-Diamond Nano-Composites," Nanostructured Materials, v. 12, p. 1031-1034, 1999.
12. O.A. Voronov, G.S. Tompa, B.H. Kear, K.J. Livi, R.O. Loutfy, "High Pressure Compaction and Sintering of Carbon Nanopowders," Proceedings of 47th Sagamore Conference on Nanostructured Materials (on CD), 23-26 August, 1999, Easton, MD.
13. O. Voronov, G. Tompa, B. Kear, W. Mayo, S. Liao, R. Loutfy, K. Livi, "On the High Pressure Consolidation of C₆₀," MRS 1998 Fall Meeting, Boston, MA.
14. G.S. Tompa, O.A. Voronov, B.H. Kear, K.J.T. Livi, W.E. Mayo, "Nanotube and Fullerene Derived Super-Tough, Super-Hard Materials," The Knowledge Foundation Meeting on Carbon Nanotubes, April 22-23, 1999, Washington, DC.
15. O.A. Voronov, G.S. Tompa, B.H. Kear, R.K. Sadangi, C.C. Wilson, "Functionally Graded Triphasic WC/Co/Diamond Composites," Abstract No. 808; V. 99-2 Meeting Abstracts, The 1999 Joint Intl. Meeting of The Electrochemical Society, Hawaii, October 17-22, 1999.
16. O.A. Voronov, G.S. Tompa, B.H. Kear, C.C. Wilson, "Binderless Polycrystalline Diamonds for Geothermal Drilling," Abstract No. 809; V. 99-2 Meeting Abstracts, The 1999 Joint Intl. Meeting of The Electrochemical Society, Hawaii, October 17-22, 1999.
17. O.A. Voronov, G.S. Tompa, B.H. Kear, K.J. Livi, R.O. Loutfy, W.E. Mayo, "High Pressure Sintering of Fullerene Soot," Abstract No. 1457, V. 99-2 Meeting Abstracts, The 1999 Joint Intl. Meeting of The Electrochemical Society, Hawaii, October 17-22, 1999.

18. O.A. Voronov, G.S. Tompa, B.H. Kear, S.-C. Liao, K.J. Livi, W.E. Mayo, "High Pressure Polymerization of Single-Wall Nanotubes," Abstract No. 1507; V. 99-2 Meeting Abstracts, The 1999 Joint Intl. Meeting of The Electrochemical Society, Hawaii, October 17-22, 1999.
19. O.A. Voronov, G.S. Tompa, B.H. Kear, R.K. Sadangi, C.C. Wilson, "Functionally Graded Triphasic WC/Co/Diamond Composites," Diamond Materials VI, 2000, will be published.
20. O.A. Voronov, G.S. Tompa, B.H. Kear, C.C. Wilson, "Binderless Polycrystalline Diamonds for Geothermal Drilling," Diamond Materials VI, 2000 will be published.

7.0 Appendix

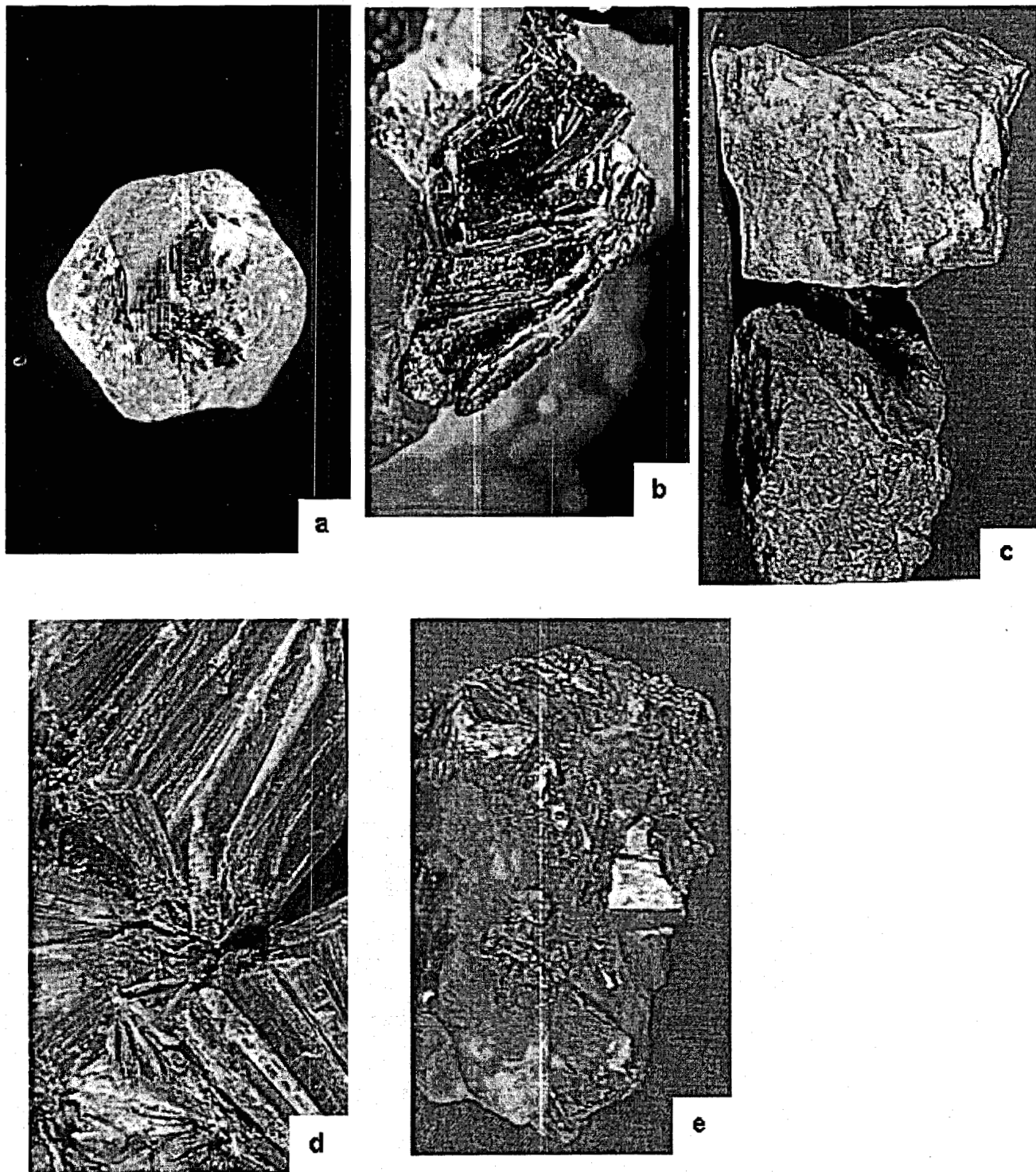


Fig. 7-1. The minerals that DMI used in this Project. a) diamond, b) graphite, c) limestone, d) pyrophyllite, e) talc. Limestone, pyrophyllite and talc have been used for making containers and reaction cells.

Table 7.1 Lava-stone properties

PROPERTIES	FIRED (760°C)	UNFIRED
MELTING POINT	3200° F.	X
MAX OPERATING TEMP	2100° F. (1148°C)	1000° F. (538°C)
CONTINUOUS SERVICE TEMP	2100° F.	X
COLOR	PINK	X
HARDNESS (MOHS SCALE)	6	1-2
SPECIFIC GRAVITY	2.3	2.4
VOLUME	11.75 #/IN ³	X
DENSITY (#/IN ³)	0.083	0.098
WATER ABSORPTION (%)	2.5	X
POROSITY (%)	2.3	2.6
THERMAL EXPANSION PER °F x 10 ⁻⁶	2.9	2.5
TENSILE STRENGTH	3000	X
COMPRESSIVE STRENGTH (PSI)	25,000	12,000
FLEXURAL STRENGTH (PSI)	10,000	4,500
DIELECTRIC STRENGTH (VOLTS/MIL)	100	80
POWER FACTOR	.01	X
LOSS FACTOR AT 1MHZ	.053	.06
DIELECTRIC CONSTANT AT 1MHZ	5.3	5.8
THERMAL CONDUCTIVITY BTU/HR/ FT ² /F/INCH	8.0	11.0
VOLUME RESISTIVITY	10 ¹⁴ Ohm cm	X
SOFTENING TEMP	1600° C 2912° F	X
LINEAR COEFFICIENT OF THERMAL EXPANSION	25° C-100° C	2.9 x 10 ⁻⁶
	25° C-600° C	3.6 x 10 ⁻⁶
TE VALUE	700	X

Table 7.2 Thermal transformations of Lava-stone (pyrofillite) at ambient pressure

	Burn Temperature (°C)						
	Unburned	200	400	600	800	1000	1200
Apparent Density (g/cm ³)	2.641	2.593	2.585	2.408	2.35	2.34	2.47
Color	Dark gray	Slightly less dark gray	Slightly less dark gray	Light gray	Gray-white	beige	Gray-brown
Hardness (Mohs Scale)	2	2	2	2	2	5	6

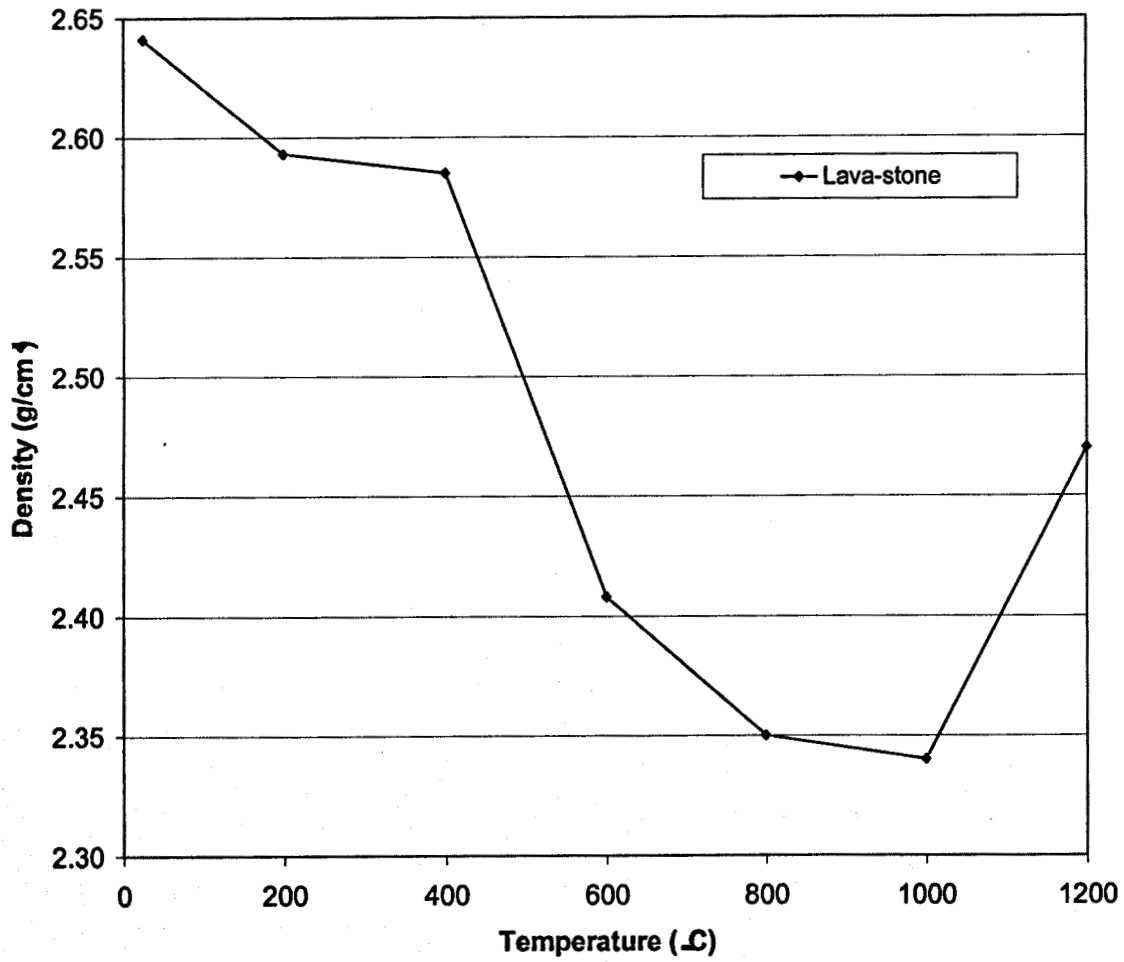


Fig. 7-2 Grade A Lava-stone rod's density varies with temperature under ambient pressure

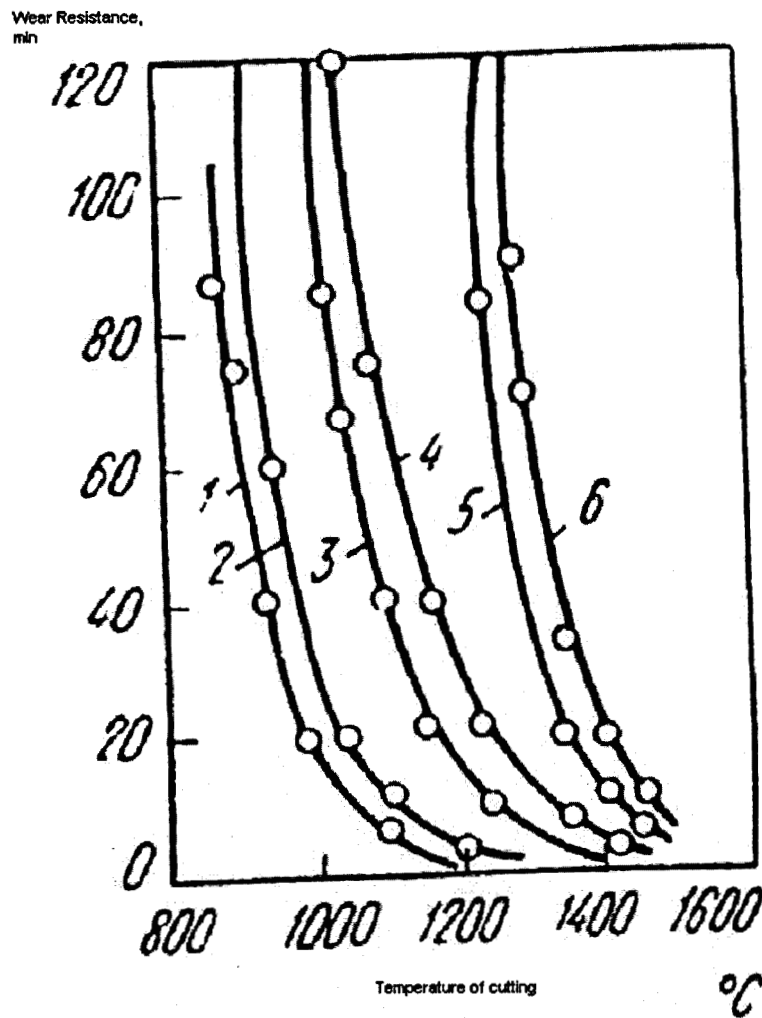


Fig. 7-3. Dependence of wear resistance of
1.WC6%Co;2.WC8%Co;3.WC5%TiC10%Co;4.WC15%TiC6%Co;5.WC30%TiC4%Co;
6.WC60%TiC6%Co
On temperature of cutting edge for cutting of Steel40 with depth of cut of 2 mm and feed of 0.2
mm/rev.

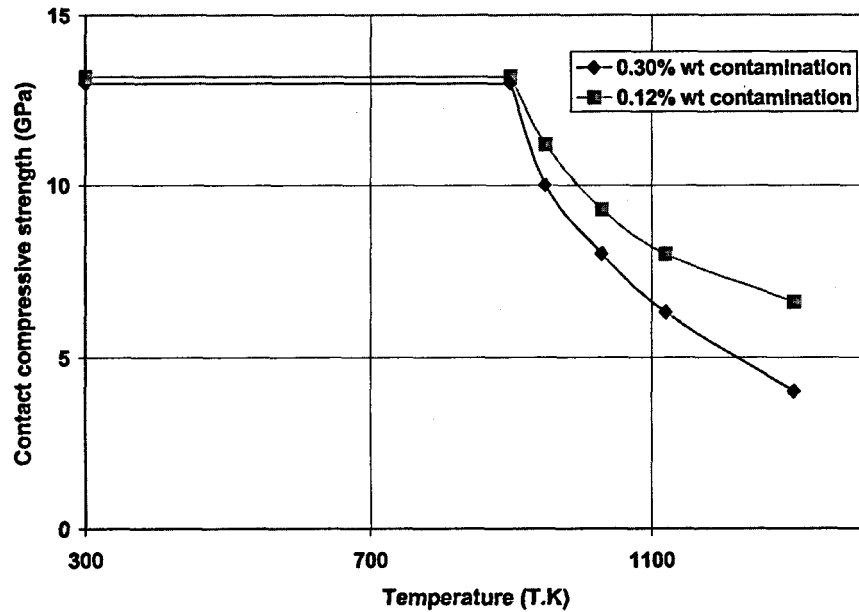


Fig. 7-4a. Toughness of the best synthetic industrial diamond single crystals as a function of temperature, single crystals are octahedrons of 500 μm size, obtained with the help of Fe-Ni-Co alloy. The quantity of nano-contamination is: 1-3: 0.30wt.%; 2-4: 0.12wt.%.

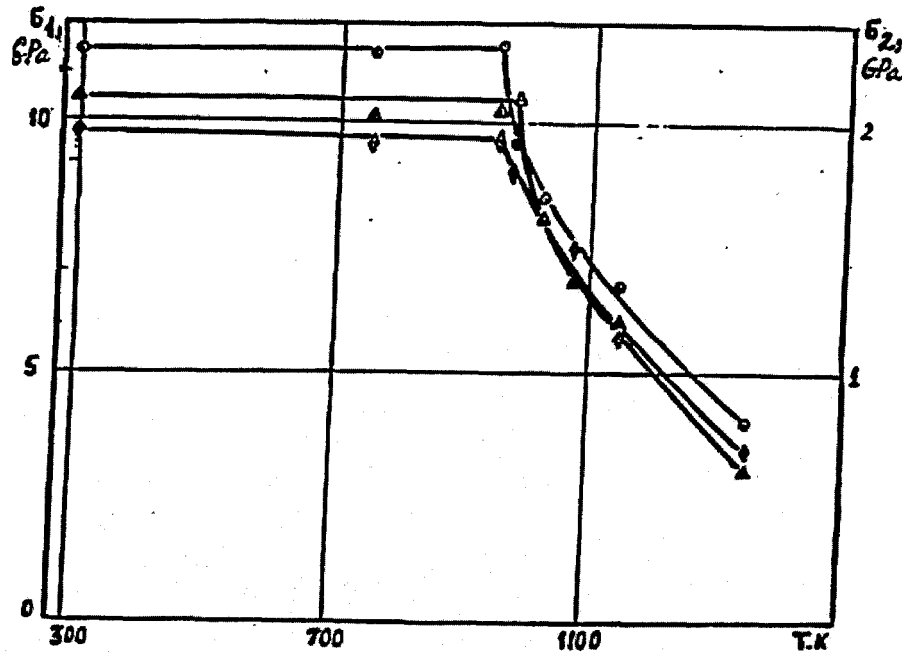


Fig. 7-4b. Dependence of contact compressive strength (σ_1) (Z-axis component) and equivalent compressive strength (σ_2) (combination of Z,Y,X-axis components) on temperature in inert gas for synthetic diamond single crystals. Single crystals are octahedrons with size of 500 μm , obtained with help of metal alloys:

1- Fe-Ni-C; 2- Fe-Co-C; 3- Ni-Mn-C.

This is the grains of the best industrial synthetic diamond powder, contaminated by nano admixtures of Ni, Fe, Co.

The quantity of admixtures is less than 0.5% wt.

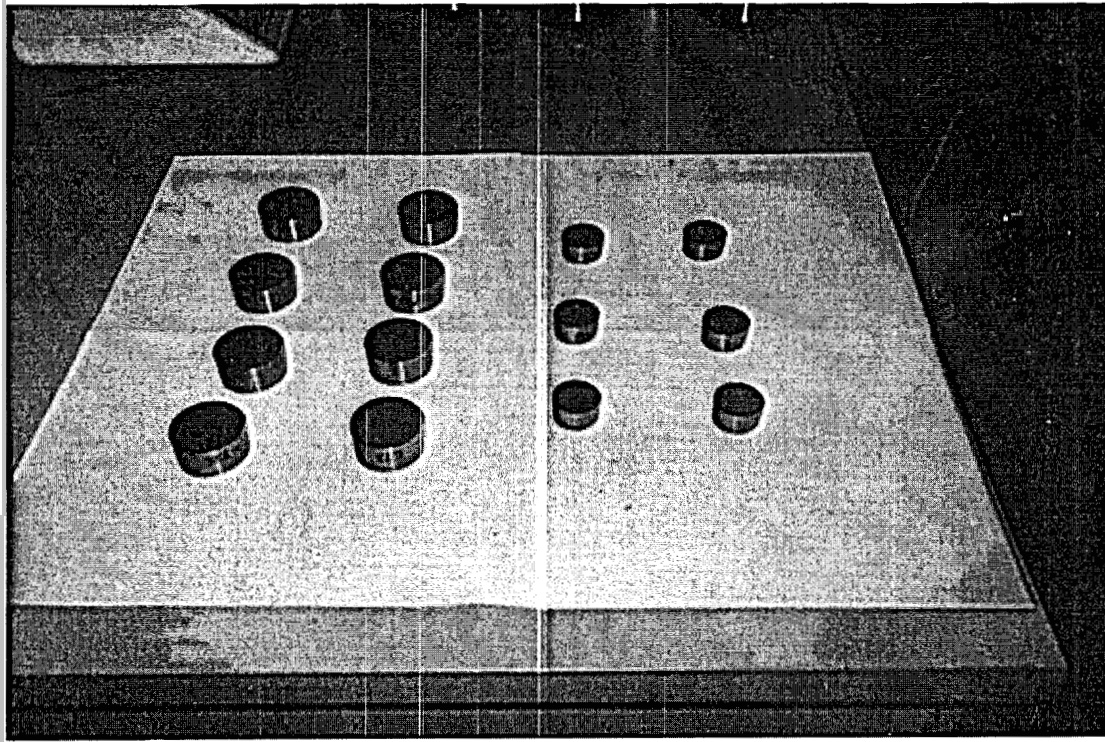


Fig. 7-5. Sintered samples of fine-structured WC/Co10%wt. These cylindrical samples were sintered by students of RSU, ground by diamond wheels and prepared for fracture strength study in compression and dependence of those on volume.

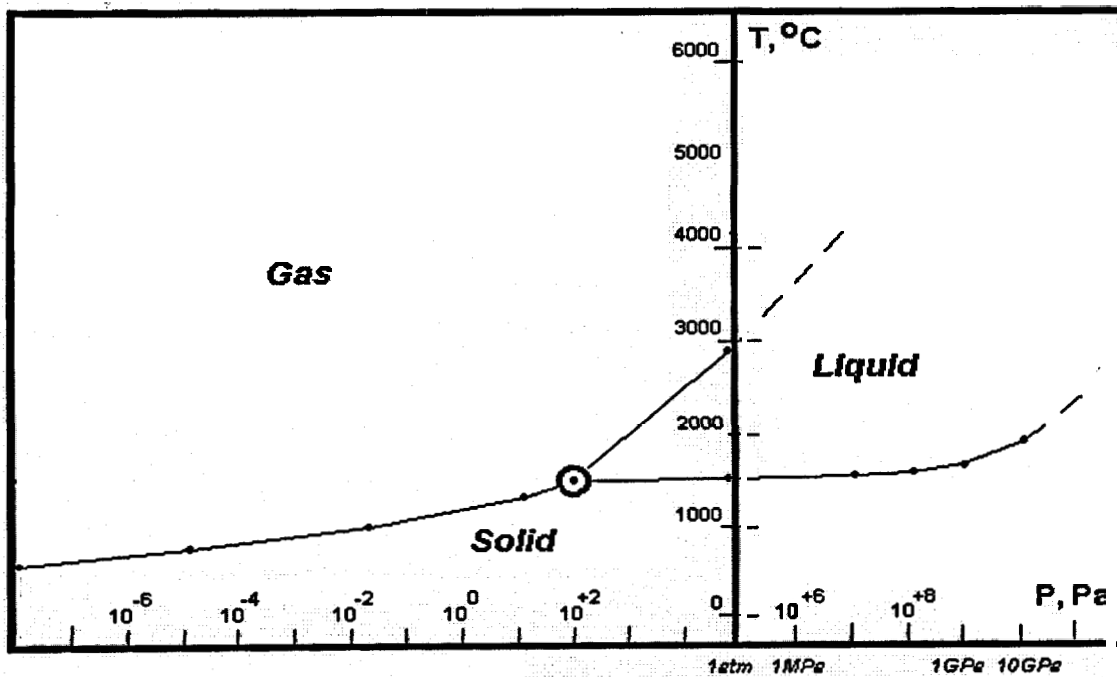


Fig. 7-6. The temperature-pressure (T-lgP) phase diagram of cobalt.